Identification Technique of Mechanism-Based Constitutive Model for Cast Iron under Thermo-Mechanical Loads

Dissertation
zur Erlangung des akademischen Grades

Doktoringenieur
(Dr.-Ing.)

von M.Sc. Mykola Ievdokymov
geb. am 10.09.1985 in Izvarino, Ukraine
genehmigt durch die Fakultät für Maschinenbau
der Otto-von-Guericke-Universität Magdeburg

Gutachter:
Prof. Dr.-Ing.habil. Holm Altenbach
Jun.-Prof. Dr.-Ing. Manja Krüger
Dr.-Ing.habil. Claus Oberste-Brandenburg

Promotionskolloquium am 5.05.2015

Contents

List of Symbols

Abbreviations

CT	Creep test	TMF	Thermo-mechanical fatigue
LCF	Low-cycle fatigue	TT	Tensile test

Operators

$(\cdot)^T$	transpose operator	d	differentiation operator
$\boldsymbol{\nabla}$	$\boldsymbol{\nabla}_{(\cdot)} = \frac{\mathrm{d}}{\mathrm{d}(\cdot)_i}\boldsymbol{e}_i$	∂	partial derivative
$\cdot$	scalar product	sgn	signum operator
$\cdot\cdot$	double scalar product	$\times$	vector product
det	determinant	tr	trace of tensor

General

$\overline{\boldsymbol{s}}$	deviatoric part of active stress tensor	α_T	thermal expansion coefficient
		$\overline{\boldsymbol{\sigma}}$	active stress tensor
$\alpha_\mathrm{i}^\mathrm{H}$, $\alpha_\mathrm{i}^\mathrm{L}$, T_*^i	parameters of $R_\mathrm{i}(T)$	$\overline{\sigma}$	active stress (uniaxial case)
$\alpha_\mathrm{s}^\mathrm{H}$, $\alpha_\mathrm{s}^\mathrm{L}$, T_*^s	parameters of $R_\mathrm{s}(T)$	$\overline{\sigma}_\mathrm{vM}$	von Mises equivalent of active stress tensor
α_D	parameters of $D(T)$		

β backstress (uniaxial case)

$\boldsymbol{\gamma}$ body forces

$\boldsymbol{C}$ right Cauchy-Green deformation tensor

$\boldsymbol{E}$ Green-Lagrangian strain tensor

$\boldsymbol{p}$ vector of material parameters

$\beta_*(T,\boldsymbol{\sigma})$ backstress saturation function

$\boldsymbol{\alpha}$ backstress tensor

$\boldsymbol{\beta}$ deviatoric part of backstress tensor

β_{vM} von Mises equivalent of $\boldsymbol{\beta}$

$\boldsymbol{e}_i$ basis vectors

χ numerical stabilization coefficient

$\boldsymbol{x}$ actual configuration

$\boldsymbol{F}$ deformation gradient

$\boldsymbol{u}$ displacements vector

$\dot{\varepsilon}^{\mathrm{p}}_{\mathrm{n}}$ normalizing factor for inelastic strain rate

$\dot{\omega}_{\mathrm{c}}$ creep damage rate

$\dot{\omega}_{\mathrm{f}}$ fatigue damage rate

$\dot{\boldsymbol{\varepsilon}}^{\mathrm{p}}$ inelastic strain rate tensor

$\dot{\varepsilon}^{\mathrm{p}}$ plastic strain rate (uniaxial case)

$\dot{\varepsilon}^{\mathrm{p}}_{\mathrm{i}}$ initial inelastic strain rate

$\dot{\varepsilon}^{\mathrm{p}}_{\mathrm{s}}$ steady inelastic strain rate

$\dot{\varepsilon}^{\mathrm{p}}_{\mathrm{vM}}$ von Mises equivalent of inelastic strain rate

ϵ_{br}, a_ε, b_ε, c_ε parameters of $\varepsilon^{\mathrm{p}}_*(T,\boldsymbol{\sigma})$

$\boldsymbol{\varepsilon}^{\mathrm{el}}$ elastic strain tensor

$\varepsilon^{\mathrm{el}}$ elastic strain (uniaxial case)

κ stiffness degradation function

λ, μ Lamé's parameters

$\mathbb{P}$ unbounded space of material parameters $\boldsymbol{p}$

$\mathfrak{C}$ creep damage state function

$\mathfrak{F}$ fatigue damage rate state function

μ_{a}, μ_{b} parameters of $\mu_{\mathrm{h}}(T)$

$\mu_{\mathrm{h}}(T)$ hardening rate function

ν Poisson's ratio

ω continuum damage

$\boldsymbol{\varepsilon}^{\mathrm{p}}$ inelastic strain tensor

ε^{p} plastic strain (uniaxial case)

$\varepsilon^{\mathrm{p}}_*$ inelastic rupture strain

$\varepsilon^{\mathrm{p}}_I$, $\varepsilon^{\mathrm{p}}_{II}$, $\varepsilon^{\mathrm{p}}_{III}$ principal values of $\boldsymbol{\varepsilon}^{\mathrm{p}}$

$\boldsymbol{X}$ reference configuration

ρ mass density

σ stress (uniaxial case)

σ_{A} amplitude of stress

σ_{n} normalizing factor for stress

σ_{f} fracture strength

σ_{u} tensile strength

σ_I, σ_{II}, σ_{III} principal values of $\boldsymbol{\sigma}$

$\boldsymbol{\varepsilon}$ strain tensor

$\varepsilon_{\mathrm{eq}}$ equivalent of total strain (4.26)

$\boldsymbol{\sigma}$ Cauchy stress tensor

$\boldsymbol{s}$ deviatory part of $\boldsymbol{\sigma}$

σ_{vM} von Mises equivalent of stress tensor $\boldsymbol{\sigma}$

T absolute temperature

T_{m} melting temperature

$\boldsymbol{\varepsilon}^{\mathrm{th}}$ thermal strain tensor

$\boldsymbol{I}$ unity tensor

ε strain (uniaxial case)

ε^{m} mechanical part of strain (uniaxial case)

$\varepsilon_{\mathrm{n}}^{\mathrm{p}}$ normalizing factor for inelastic strain

ε_{A} amplitude of strain

ε_{n} normalizing factor for strain

$\vartheta(\dot{\boldsymbol{\varepsilon}}^{\mathrm{p}})$ binary mixture function used in F

ϑ_{a}, ϑ_{b} parameters of $\vartheta(\dot{\boldsymbol{\varepsilon}}^{\mathrm{p}})$

ξ Gauß function

A_{i}, B_{i}, n_{i} parameters of $f_{\mathrm{i}}(\sigma)$

A_{s}, B_{s}, n_{s} parameters of $f_{\mathrm{s}}(\sigma)$

$D(T)$ temperature response function in $\varepsilon_{*}^{\mathrm{p}}(T,\boldsymbol{\sigma})$

E Young's modulus

E_{a}, E_{b} parameters of $E(T)$

$F(\dot{\omega}_{\mathrm{c}},\dot{\omega}_{\mathrm{f}})$ creep-fatigue interaction function

$f\left(\overline{\sigma}_{\mathrm{vM}}\right)$ stress response function

H_{c}, Y, H_{f} tension/compression influence functions

J_1, J_2, J_3 invariants of $\boldsymbol{\sigma}$

l parameter of function $r(\omega)$

N cycle number

n temperature independent material parameter of $\mathfrak{F}$

N^{*} normalizing factor for number of cycles

N_{A} number of cycles to rupture

Q activation energy

$r(\omega)$ accumulated damage response function

$R(T)$ temperature response function

R_{i}, f_i response functions temperature and stress in $\dot{\varepsilon}_{\mathrm{i}}^{\mathrm{p}}$

R_{s}, f_s response functions temperature and stress in $\dot{\varepsilon}_{\mathrm{s}}^{\mathrm{p}}$

R_{a} gas constant

R_{p02} offset yield strength

S temperature dependent material parameter of $\mathfrak{F}$

s_{a}, s_{b} parameters of $S(T)$

$S_{\boldsymbol{\sigma}}$, $S_{\boldsymbol{\varepsilon}^{\mathrm{p}}}$ tensile/compressive stress/strain mode functions

W creep potential

Chapter 1

ψ	continuity of material

Chapter 2

$\boldsymbol{f_n}$	force
$\boldsymbol{F}_B$	resultant force
$\boldsymbol{I}_B$	linear momentum
$\boldsymbol{R}$	rotational part of $\boldsymbol{F}$
$\boldsymbol{T}_B$	resultant torque
$\boldsymbol{U}$	left stretch tensor
$\boldsymbol{V}$	right stretch tensor
$l(\boldsymbol{x})$	curve in actual configuration
$L(\boldsymbol{X})$	curve in reference configuration
$\Delta\Omega$	infinitesimal area
$\boldsymbol{\phi}_t$	deformation map function
$\boldsymbol{n}$	normal vector
Ω	cutting plane
ψ	elastic strain potential
$\boldsymbol{t}$	vector, tangent to $l(\boldsymbol{x})$
$\boldsymbol{T}$	vector, tangent to $L(\boldsymbol{X})$
$\boldsymbol{\tau}$	Cauchy traction vector
B	sub-domain of continuum
c_h	material parameter Eq. 2.43
L_B	angular momentum
m	mass
M_B	mass of sub-domain B
P	point of continuum
S	sub-domain of continuum
V	volume

Chapter 3

$\boldsymbol{c}$	constitutive model
$\boldsymbol{d}$	experimental data
$\boldsymbol{w}$	synaptic weights of neurons
$\boldsymbol{y}_\mathrm{out}$	output of neural network
γ	regularization parameter

Chapter 5

α	scale factor of transformation $T(\boldsymbol{p})$
η	convergency criteria
$\mathbb{P}_*$	bounded space of parameters
$\mathfrak{E}$	complete set of experimental data

$\mathfrak{E}_1, \mathfrak{E}_2$	sub-sets of complete experimental data $\mathfrak{E}$	ξ^i	value of Gauß function for i^{th} set of experimental data
$p^i_{\max}$	upper bound of i^{th} parameter	e^i	i^{th} set of experimental data
$p^i_{\min}$	lower bound of i^{th} parameter	k	logarithmic damage rate
$\boldsymbol{\theta}^i$	scale factor of transformation $T(\boldsymbol{p})$	s^i	simulation of material behavior at loads corresponding to i^{th} set of experimental data
$\widetilde{\boldsymbol{p}}$	updated parameters		
$\widetilde{\xi}$	modified Gauß function	$T(\boldsymbol{p})$	parameters transition function
$\widetilde{k}$	parameter of $\widetilde{\xi}$	w	weight factor

CHAPTER

1 Introduction

The prediction of the lifetime of mechanical designs is a challenging task in mechanical engineering. The accurate estimation of risks and providing the warranty on the mechanical components is a problem taking place mainly in the industry, e.g. in the manufacturing of engines, turbines, heat exchangers, etc. The importance of this problem is strongly related to the income of the manufacturer, which is one of reasons for their interest. Besides the mercantile reasons, the safety is also a very significant factor, which, however, is also related to the excessive expenditures in case of accidents, e.g. failures of turbines with destruction of turbine housing[1], an explosion of engine in the vehicle, etc.

The field of the highest interest is represented by the structural components of power plants, chemical reactors, heat engines, pipework systems, turbines, etc. It is induced by high prices and safety requirements to components. Mainly, the mentioned cases are related to a high temperature and mechanical loading conditions. The operating of a component at temperatures $T > 0.3\,T_{\mathrm{m}}$ (T_{m} is a melting temperature) induces the evolution of strains over time even at a constant load. Such strains are referred to as *creep strains* [27, 50]. Thereby, another important factor affecting the material behavior is time. The task of mechanical engineering within the above-mentioned case of the operation conditions is the modeling of time-dependent changes of stress and strain states until the failure of the component.

The overlay of cyclic mechanical and thermal loads leads to the deterioration of a material referred to as *thermo-mechanical fatigue*. The above-

[1] Sayano-Shushenskaya hydroelectric power station accident occurred on 17 August 2009. 9 of 10 turbines were destroyed, 75 people have died.

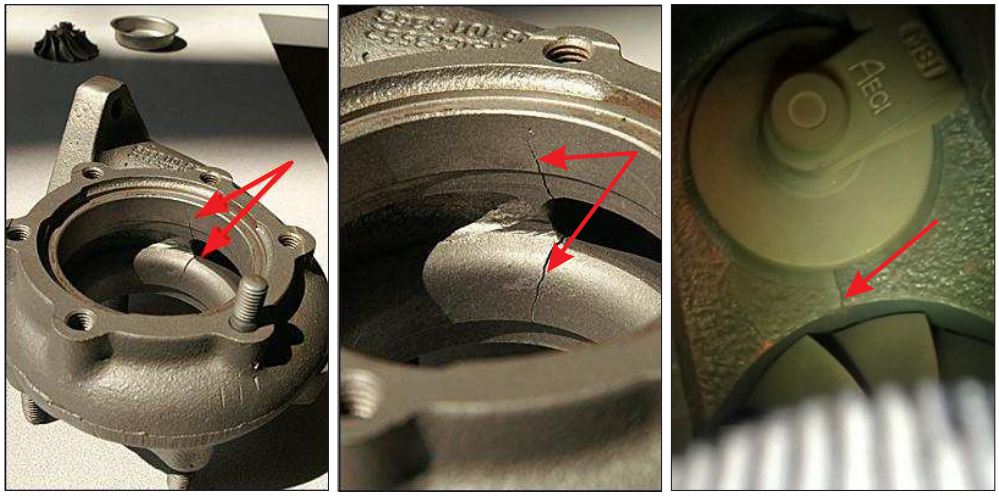

(a) **(b)** **(c)**

Figure 1.1: Failures of turbine housings induced by thermo-mechanical fatigue: **(a)** and **(b)** turbine housings used in Porsche 924T engine (taken from www.rennlist.com/forums), **(c)** turbine housing of Garrett GT3071R turbo charger compressor turbine (taken from www.uksaabs.co.uk/UKS)

mentioned loading conditions are typical for steam and gas turbines and leads to the nucleation and fast growth of cracks on a component's surface. Figure 1.1 shows the typical failure of the turbine housings induced by thermo-mechanical fatigue. There are several mechanisms affecting the thermo-mechanical fatigue [78, 90]: creep and creep damage [25, 32, 50], damaging induced by oxidation [54], and fatigue damage [32, 46].

The creep mechanics were intensively developed mainly in the middle of the 19^{th} century. The particular problems of the creep mechanics, e.g. the modeling of the behavior of specific structural components and the solution of non-linear initial-boundary value problems, became trivial in mechanical engineering since the works of Odqvist [58], Odqvist and Hult [60], Hult [24], and Rabotnov [76]. Beginning from 1970s creep problems of mechanics have been significantly investigated, the concepts of hardening/recovery and creep damage were introduced [10, 28, 38], the thermodynamic approach for the formulation of constitutive equations was developed [31, 79]. The recently published book of Naumenko and Altenbach [50] includes sophisticated approaches for solution of creep problems for general cases and particular structural components.

At the initial stage of development of the damage mechanics, the damage was classified as the deterioration of the material taking place directly before

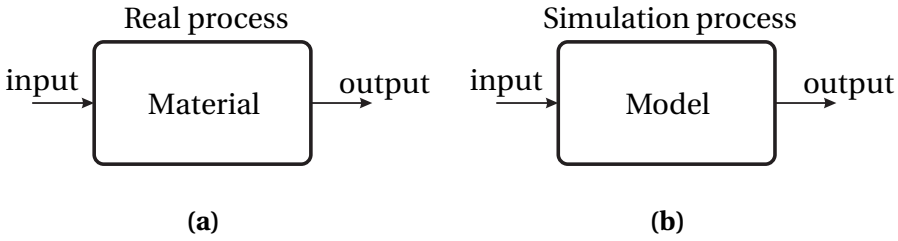

Figure 1.2: Behavior of material: **(a)** real process, **(b)** simulation process

the failure, i.e. damage was introduced as a generalized resultant characteristic. At the same time the failure was described by the categories "yes" or "no". The pioneers, who have introduced the variable representing progressive deterioration of material before the rupture, were Palmgren [63], Miner [45], and Robinson [77]. The development of the creep damage concept was proceeded by Kachanov [25], who has introduced the internal variable ϑ, called "continuity", representing the fraction of undamaged material in the mechanical part. Later, the introduced "continuity" variable has received the thermodynamical meaning through the relation with the damage variable $\omega = 1 - \vartheta$, which is still used in modern mechanics. The failure of material at cyclic loads, referred to as *fatigue damage*, was described independently by Manson and Coffin by means of a famous empirical law, nowadays called *Manson-Coffin law* [41]. This approach has successfully been used upto now for the application at strict loading conditions. For the next 40 years, the fatigue damage concept has significantly been developed and became as well the part of continuum damage mechanics [30, 46]. This concept has been constructs the fatigue damage law in the standard time scale, that leads to known challenges with the time-consumption of algorithm. However, despite the mentioned problems with time-consumption, the approaches of continuum damage mechanics allow us to take into account the complete history of loads.

On the other hand, the development of new industrial products is often related to the application of new materials (e.g. newest cast irons and steels with inclusions, composites, nano-materials, etc.), which requires the solution of the identification problem in order to formulate the constitutive model representing their behavior. Thereby, an experimental testing of a material, a phenomenological modeling of the observed processes and identification problem are always coming together while the formulation of the constitutive model. The structure of the material identification problem is shown in Fig. 1.2. Within this scheme, the material is represented through some block transforming the input parameters (e.g. mechanical and thermal loads) into

the output parameters (e.g. displacements, deformations, stresses, etc.). The aim of the identification is to replace the real process by a mathematical model with the saving of similar correspondence between input and output characteristics of the process [16, 56, 57]. The formulation of the constitutive model is mainly based on the available experimental data and on the requirements to the constitutive model, and always is a time-consuming problem for the advanced constitutive models. Unfortunately, the application of a neural networks [23, 88] or a numerical optimization for the determination of the material parameters [5, 13] for the formulated constitutive model makes the identification the challenging task, and, in some situations, non-realistic for its solution within the framework of the mechanical engineering department of an industrial company. The required time for the development of the product is normally very limited by economic factors, which demotivates mechanical engineers to apply the newest materials for the development of the design. The challenges related to the analysis of the experimental data, the control of the data's accuracy and human factors, together with the requirement of a short development time, finally lead to the situation, that the application of new material with high potential for the development is completely degraded by the implementation complexities.

Aims and tasks

The aim of the current work is to develop a generalized strategy for the formulation of mechanisms-based constitutive models, which include elasticity, inelastic properties, creep and fatigue damage processes, and are unified for a wide range of the operational conditions. The work is focused on the development of an identification strategy for the narrow class of cast irons used in the structural components and subjected to thermo-mechanical loading conditions which are a standard situation in turbines, pipe systems, heat exchangers, etc. The low amount of knowledge about the structure of the constitutive model and the shape of the response functions used by this model are challenges of the generalized identification. Therefore, within the current work, the identification is designed in a way, that each step considers the certain phenomenological mechanism representing the behavior of the material.

The unification of the constitutive model for application in a wide range of loading conditions necessarily leads to the complication of the model, and, therefore, to an increase of time required for the formulation of a constitutive model. The proper way to reduce the complexity of the identification problem is the consideration of the mechanisms taking place in the material during the

operation. For instance, the elastic material properties can be considered independently from the rest of the experimental data. Additionally, the experimental data for inelastic strain rates can be considered independently from the hardening/softening or damage processes. On the other hand, the identification of the kinematic hardening does not require the information about the damaging of the material, etc. The partition of the constitutive model onto mechanism-based constituents allows to significantly reduce the dimension of the identification problem.

Unfortunately, the processes taking place in the material behavior under some loads are not always observed in explicit form, and, therefore, can not be identified by a decomposition of the constitutive model on the mechanism-based constituents. Within the above-mentioned case, the identification of hidden processes requires to work with the full dimension of the constitutive model, which is time-consuming and, often, not possible, if the structure of the constitutive model is not known. However, the experimental data can be decomposed, according to the assumed phenomenological structure of the constitutive model, onto constituents which may represent such processes as hardening/softening or damage in an explicit form. Unfortunately, there is a disadvantage of the above-mentioned approach related to the reduction of accuracy of the estimated data. This problem is induced by a multiplicative effect of processing on the error taking place in the experimental data. Therefore, its application is justified only in situations, in which a preliminary estimation of the constitutive model is performed.

The application of approaches mentioned above allows to significantly simplify the identification of new cast irons and steels for mechanical engineers. Within the current work, we developed the step-by-step identification strategy in order to illuminate the above-mentioned problems.

Of course, the development of the unified identification strategy requires the experimental data for certain material. Within the framework of the current work, the identification strategy is presented on base of GJV cast iron with vermicular graphite inclusions. However, during the development of identification approaches given in this work the experimental data for the GJS (D5-S) cast iron have been also used. Thereby, major target material of the current work are the heat resistant cast irons with graphite inclusions.

The current thesis is structured as follows:

- Chapter 2 is focused on the consideration of the basic set of governing equations, which are necessary for the formulation of mechanical balance principles, a basic sketch of the constitutive model for the description of the elastic and inelastic material behavior and damaging process.

The relations presented within this chapter are mainly given for generalized continuum with coverage of some particular features belonging to cast irons.

- Within the Chapt. 3, the existing techniques available for solving of the identification problem are presented, and a generalized strategy of the identification is discussed. This chapter also includes the experimental data for GJV cast iron used for the representation of the identification steps.

- Chapter 4 presents the initial step of the identification process. This part is referred to as *primary identification* and is mainly focused on the determination of the structure of the constitutive model and a preliminary estimation of the material parameters. The primary identification is based on the simplest identification approaches such as trial approach and hand-fitting, described in Chapt. 3. Within the framework of current chapter, the identification is performed mainly based on the experimental data from creep and tensile tests.

- Within the Chapt. 5, the optimization-based identification approach is considered. This part of research is focused on the formulation of a flexible and unified identification algorithm for the solution of the parameters identification problem. Within the current chapter, the approaches for the calibration of the constitutive model, reduction of the simulation time, and multi-threading techniques are considered.

- Chapter 6 is focused on the verification of the resulting constitutive model. This part is subjected to the estimation of the quality of the identified constitutive model, its accuracy of the prediction of the inelastic behavior and the lifetime of material. Furthermore, the accuracy of the additional approaches used within the current work is checked.

- Chapter 7 finalizes current thesis with summary, list of the restrictions for the application of developed methods and outlook.

The primary identification of the fatigue damage model requires to analyse the stress response of the material during the low-cyclic fatigue test.

CHAPTER

2 Basic equations

2.1 General remarks

The application of materials in modern mechanical engineering requires the detailed consideration of phenomena and processes, which take place in these materials. Within the framework of current research, cast irons can get mechanical deformations as a result of applied temperature fields and external mechanical loads. In general the interest of industrial engineering is more focused on the risk analysis, which takes into account the instant strength as well as the durability of design.

Proper risk analysis must consider the dominant phenomenon, which takes place in the material during the exploitation of the mechanical design, as well as structural properties of the material. Within a small representative volume of a material, the distribution of graphite inclusions in space and the distribution of their sizes is random [66, 85]. Therefore, cast iron can be simulated as an isotropic one. The phenomenological modeling in the particular case of cast irons is normally based on the small displacements and the material's isotropy assumptions [26, 31, 50].

The operation conditions in the case of application of the material in turbine housing can be characterized by high temperatures about $T_{\mathrm{m}}/3$ values and higher, cyclic thermal and mechanical loads and by the presence of steady regimes at the different temperatures. Within the framework of current class of materials, risk analysis must consider elasticity, plasticity, creep and creep-fatigue damage interaction.

This chapter contains basic equations which describe the elastic material behavior, creep, damage and its influence on the basic material properties.

The kinematic equations are derived under the assumption of small displacements. The plasticity is considered from the position of fast rate-dependent material behavior, which is included in creep models through consideration of exponential regimes in inelastic strain rates. The continuous fatigue damage model is formulated in a general time scale in order to represent the material behavior for complicated loading cycles with non-regular holdings.

2.2 Kinematics

2.2.1 Deformation map

The current section provides the fundamental principles and definitions which are used for the description of the body motion. The starting point is the consideration of the transformation of the state of continuum sub-domain B from a *reference configuration* with position $\boldsymbol{X}$ of some point P into a *actual configuration* of transformed continuum sub-domain S with position $\boldsymbol{x}$ of the same point P (Fig. 2.1).

Given displacement vector $\boldsymbol{u}$ is characterizing the position change of point P during the transformation of the body from reference state B to the actual state S:

$$\boldsymbol{u} = \boldsymbol{x} - \boldsymbol{X}$$

The vector function $\boldsymbol{\phi}_t$ of vector argument $\boldsymbol{X}$ is referred to as *deformation map*:

$$\boldsymbol{x} = \boldsymbol{\phi}_t(\boldsymbol{X}) \Rightarrow \boldsymbol{\phi}_t(\boldsymbol{X}) = \boldsymbol{X} + \boldsymbol{u}$$

The deformation map function describes the movement of all particles of sub-domain B, and, consequently, its transformation to sub-domain S.

2.2.2 Deformation gradient

A deformation gradient is applied for the analysis of the deformed state of the body. The deformation gradient $\boldsymbol{F}$ is the derivative of the actual configuration vector $\boldsymbol{x}$ with respect to reference configuration vector $\boldsymbol{X}$:

$$\boldsymbol{F} = \frac{\mathrm{d}\boldsymbol{x}}{\mathrm{d}\boldsymbol{X}} \equiv \nabla_X \boldsymbol{\phi}_t(\boldsymbol{X}) \equiv \boldsymbol{I} + \frac{\mathrm{d}\boldsymbol{u}}{\mathrm{d}\boldsymbol{X}} \equiv \boldsymbol{I} + \nabla_X \boldsymbol{u},$$

where $\boldsymbol{I}$ is the second-order unit tensor. In fact, the deformation gradient $\boldsymbol{F}$ maps tangent vector $\boldsymbol{T}$ of curve $L(\boldsymbol{X})$ of reference configuration B into tangent vector $\boldsymbol{t}$ of curve $l(\boldsymbol{x})$ of actual configuration S: $\boldsymbol{t} = \boldsymbol{F} \cdot \boldsymbol{T}$.

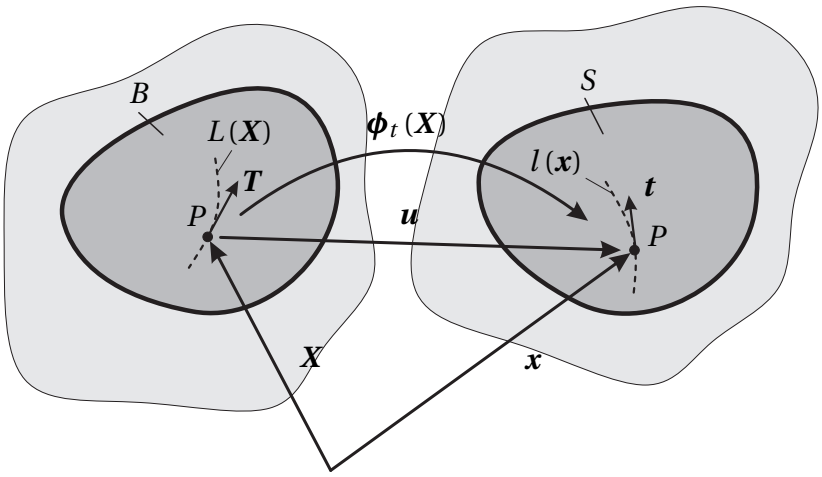

Figure 2.1: Displacements and deformation map

Applying of the polar decomposition theorem of a second order tensor [50, 65] to the deformation gradient $\boldsymbol{F}$, one can decompose $\boldsymbol{F}$ into the product of two second order tensors [83] as follows:

$$\boldsymbol{F} = \boldsymbol{R} \cdot \boldsymbol{U} = \boldsymbol{V} \cdot \boldsymbol{R}, \tag{2.1}$$

where tensor $\boldsymbol{R}$ is an orthogonal tensor ($\boldsymbol{R}^T = \boldsymbol{R}^{-1}$ and $\det \boldsymbol{R} = 1$). Tensor $\boldsymbol{R}$ contains the rotational part of deformations. $\boldsymbol{U}$ and $\boldsymbol{V}$ are *right* and *left stretch tensors*, respectively. $\boldsymbol{U}$ and $\boldsymbol{V}$ are positively defined symmetric tensors.

2.2.3 Concept of strain

The right Cauchy-Green deformation tensor is the rotation-independent measure of deformations, which is most popular for the use in mechanical engineering. This tensor was introduced by George Green[1] as follows:

$$\boldsymbol{C} = \boldsymbol{F}^T \cdot \boldsymbol{F} = \boldsymbol{U}^2 \tag{2.2}$$

In particular, engineers use the concept of strain, which evaluates how displacement differs locally from a rigid body displacement [33]. One of such strains is *the Green-Lagrangian strain tensor* [34, 35], defined as follows:

$$\boldsymbol{E} = \frac{1}{2}(\boldsymbol{C} - \boldsymbol{I}) \equiv \frac{1}{2}\left[(\nabla_{\boldsymbol{X}} \boldsymbol{u})^T + \nabla_{\boldsymbol{X}} \boldsymbol{u} + (\nabla_{\boldsymbol{X}} \boldsymbol{u})^T \cdot \nabla_{\boldsymbol{X}} \boldsymbol{u}\right] \tag{2.3}$$

[1] George Green (14 July 1793 - 31 May 1841) was a British mathematical physicist. In his essay "An Essay on the Application of Mathematical Analysis to the Theories of Electricity and Magnetism" he introduced several important concepts, among them a theorem similar to the modern Green's theorem, the idea of potential functions as currently used in physics, and the concept of what is now called Green's functions.

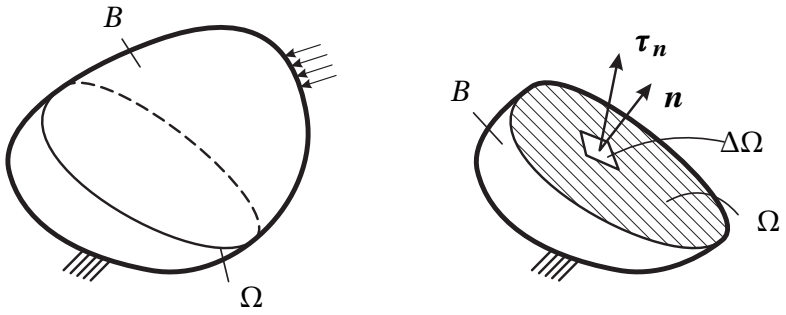

Figure 2.2: Euler's cut principle: **(a)** initial configuration of solid body, **(b)** cutted body balanced by forces

2.3 Mechanical balance principles

The differential equations based on the integral balances of physical quantities describe the state of continuum. For any representative volume of the continuum the balances of mass, momentum, angular momentum and energy hold true [4]. This section focused on the consideration of those balances.

2.3.1 Concept of stress

In the particular case of metals, the deformation of the solid body at the macrolevel is represented as the distortion of a crystal lattice at the nanoscale. The displacement of the atoms from the equilibrium positions, which can be reached only at zero absolute temperature, conduct atomic acting forces tending to return the lattice into an equilibrium position. The summation of all atomic forces at the macroscale is called internal forces [64].

Let us consider the body with an applied system of loads and boundary conditions (Fig. 2.2). The state of the mechanical system is characterized by equilibrium between a multiple number of internal forces and external loads (Fig. 2.2a). According to the cutting principle, the arbitrary part of solid can be replaced by the force, which acts in each point of the cutting surface Ω [34, 64]. The influence of the removed part on the mechanical system is compensated by the surface traction vector $\boldsymbol{\tau}_{\boldsymbol{n}}$ in each point of Ω with normal vector $\boldsymbol{n}$ (Fig. 2.2b). The resulting force $\boldsymbol{f}_{\boldsymbol{n}}$ acting on the infinitesimal area $\Delta\Omega$ with normal $\boldsymbol{n}$ is the following:

$$\boldsymbol{f}_{\boldsymbol{n}} = \boldsymbol{\tau}_{\boldsymbol{n}} \Delta\Omega \tag{2.4}$$

The traction vector $\boldsymbol{\tau_n}$ is called *Cauchy*[1] *traction vector* and depends on the normal $\boldsymbol{n}$ and differs for each point of a cross-section. The Cauchy traction vector $\boldsymbol{\tau_n}$ can be represented by the linear function of the normal $\boldsymbol{n}$ and the second-order tensor:

$$\boldsymbol{\tau_n} = \boldsymbol{\sigma} \cdot \boldsymbol{n}, \tag{2.5}$$

where $\boldsymbol{\sigma}$ is the second-order *Cauchy stress tensor*. Within the used formulation, the Cauchy stress tensor $\boldsymbol{\sigma}$ represents the stress state of the solid, independent from the choice of the cutting plane Ω and normal $\boldsymbol{n}$. The presented definition of the stress was first given by Cauchy and often referenced as *true stress*.

2.3.2 Balance of mass

The starting point for the derivation of material independent continuum equations is the definition of mass density:

$$\rho = \lim_{\Delta V \to 0} \frac{\Delta m}{\Delta V}, \tag{2.6}$$

where V and m are the volume and the mass of the continuum. In the general case, mass density may differ for each point of the continuum: $\rho = \rho(\boldsymbol{X})$.

The mass M_B of continuum sub-domain B for the mentioned mass density $\rho(\boldsymbol{X})$ is defined in (2.8). The balance of mass is based on the statement that in the absence of mass supply, production or transport, the mass M_B does not change:

$$\begin{aligned} M_B &= \int_B \rho(\boldsymbol{X}, t)\, \mathrm{d}V, \\ \frac{\mathrm{d}}{\mathrm{d}t} M_B &= 0 \end{aligned} \tag{2.7}$$

[1] Augustin-Louis Cauchy (21 August 1789 - 23 May 1857) was a French mathematician, the pioneer of mathematical analysis and founder of complex analysis. As a perfect mathematician, Cauchy had a strong influence on the development of mathematical physics.

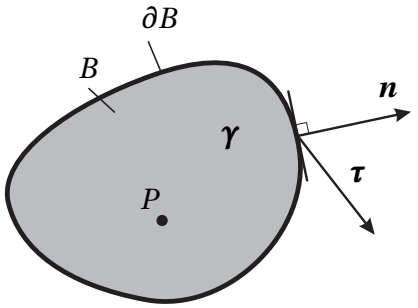

Figure 2.3: Surface and body forces acting on continuum sub-domain B

Under the assumption that volume of sub-domain B is not changes, the integral form (2.7) can be reduced as follows:

$$\dot{\rho}\left(\boldsymbol{X},t\right)=0 \tag{2.8}$$

2.3.3 Balance of linear momentum

The linear momentum of continuum sub-domain B (see Fig. 2.3) is defined in terms of deformation map velocity $\dot{\boldsymbol{\phi}}_t$ as follows:

$$\boldsymbol{I}_B=\int\limits_B \rho\dot{\boldsymbol{\phi}}_t \mathrm{d}V$$

The resultant force $\boldsymbol{F}_B$ acting on the sub-domain B is given by

$$\boldsymbol{F}_B=\int\limits_B \boldsymbol{\gamma}\mathrm{d}V+\int\limits_{\partial B}\boldsymbol{\tau}\mathrm{d}A$$

The balance of linear momentum is postulated by the following relation:

$$\frac{\mathrm{d}}{\mathrm{d}t}\boldsymbol{I}_B=\boldsymbol{F}_B \Rightarrow \frac{\mathrm{d}}{\mathrm{d}t}\int\limits_B \rho\dot{\boldsymbol{\phi}}_t\mathrm{d}V=\int\limits_B \boldsymbol{\gamma}\mathrm{d}V+\int\limits_{\partial B}\boldsymbol{\tau}\mathrm{d}A \tag{2.9}$$

The substitution of the expression for the Cauchy traction force vector (2.5) into (2.9) and the application of the divergence theorem [31, 50, 65] leads to the equation of the body motion:

$$\rho\ddot{\boldsymbol{\phi}}_t=\boldsymbol{\gamma}+\boldsymbol{\nabla}_{\boldsymbol{X}}\cdot\boldsymbol{\sigma}, \tag{2.10}$$

which for quasistatic conditions is simplified to the expression of the *mechanical equilibrium condition*:

$$\boldsymbol{\nabla}_{\boldsymbol{X}}\cdot\boldsymbol{\sigma}+\boldsymbol{\gamma}=\boldsymbol{0} \tag{2.11}$$

2.3.4 Balance of angular momentum

The equilibrium of continuum sub-domain B requires a zero resultant moment, computed with respect to all forces acting on B. The angular momentum L_B of continuum sub-domain B is defined by

$$\boldsymbol{L}_B = \int_B \boldsymbol{\phi}_t \times \rho \dot{\boldsymbol{\phi}}_t \mathrm{d}V$$

The resultant torque $\boldsymbol{T}_B$ action on the continuum sub-domain B is given by following

$$\boldsymbol{T}_B = \int_B \boldsymbol{\phi}_t \times \boldsymbol{\gamma} \mathrm{d}V + \int_{\partial B} \boldsymbol{\phi}_t \times \boldsymbol{\tau} \mathrm{d}A$$

The *balance of angular momentum* is postulated by the following relationship

$$\frac{\mathrm{d}}{\mathrm{d}t}\boldsymbol{L}_B = \boldsymbol{T}_B \Rightarrow \frac{\mathrm{d}}{\mathrm{d}t}\int_B \boldsymbol{\phi}_t \times \rho \dot{\boldsymbol{\phi}}_t \mathrm{d}V = \int_B \boldsymbol{\phi}_t \times \boldsymbol{\gamma} \mathrm{d}V + \int_{\partial B} \boldsymbol{\phi}_t \times \boldsymbol{\tau} \mathrm{d}A \tag{2.12}$$

The substitution of the expression for Cauchy traction force (2.5) into (2.9) and the application of the divergence theorem leads to the following expression, given in the local form:

$$\boldsymbol{\phi}_t \times \rho \ddot{\boldsymbol{\phi}}_t = \boldsymbol{\phi}_t \times \boldsymbol{\gamma} + \nabla_{\boldsymbol{X}} \cdot (\boldsymbol{\phi}_t \times \boldsymbol{\sigma}) \tag{2.13}$$

The above-presented expression (2.13) is the starting point for the derivation of the proof, that the Cauchy stress tensor is a symmetric tensor:

$$\boldsymbol{\sigma} = \boldsymbol{\sigma}^T$$

The above-mentioned feature of the stress tensor was firstly proved by Cauchy. The symmetry of Cauchy stress tensor $\boldsymbol{\sigma}$ allows to reduce the number of independent stress tensor components from nine to six.

2.4 Strain components

The majority of cast irons exhibits low values of strains, which normally do not exceed 1-2% in the steady exploitation mode and 5-10% during the rupture. Within the mentioned operation conditions, the application of Lagrangian or Euler approaches do not give a significant difference and yields $\nabla_{\boldsymbol{x}}\boldsymbol{u} \approx \nabla_{\boldsymbol{X}}\boldsymbol{u} = \nabla\boldsymbol{u}$. Taking into account that $||\boldsymbol{u}|| << 1$ and $||\nabla\boldsymbol{u}|| << 1$, the quadratic term in

(2.3) can be neglected. Thereby, the Green-Lagrangian strain tensor (2.3) takes its linearized form, also called *infinitesimal strain*:

$$\boldsymbol{\varepsilon} = \frac{1}{2}\left[\boldsymbol{\nabla u} + \boldsymbol{\nabla u}^T\right] \tag{2.14}$$

The exploitation of the designs made of cast irons in modern mechanical engineering implies the presence of a complicated set of phenomena in the material, such as elastic deformations, a saturated amount of accumulated inelastic strains of different nature (plasticity, creep, etc.), the deformations induced by the thermal expansion of the material, etc. Corresponding to the different nature of the deformation mechanisms, the strain tensor is represented as follows:

$$\boldsymbol{\varepsilon} = \boldsymbol{\varepsilon}^{\mathrm{el}} + \boldsymbol{\varepsilon}^{\mathrm{p}} + \boldsymbol{\varepsilon}^{\mathrm{th}}, \tag{2.15}$$

where $\boldsymbol{\varepsilon}^{\mathrm{el}}$, $\boldsymbol{\varepsilon}^{\mathrm{p}}$ and $\boldsymbol{\varepsilon}^{\mathrm{th}}$ are elastic, inelastic and thermal parts, respectively.

In general, the thermal strain tensor $\boldsymbol{\varepsilon}^{\mathrm{th}}$ represents the tendency of the matter to change the volume in response to a change of the temperature. With an increase of the temperature, the atoms begin moving faster and usually increase the space between them. Mentioned behavior of the atoms, in general, leads to the increase of the volume. For isotropic materials, the thermal strain tensor $\boldsymbol{\varepsilon}^{\mathrm{th}}$ is defined by the following constitutive equation [43]:

$$\boldsymbol{\varepsilon}^{\mathrm{th}} = \alpha_T \Delta T \boldsymbol{I}, \quad \Delta T = T - T_{\mathrm{ref}},$$

where α_T is the coefficient of thermal expansion, which in the general case is the function of temperature, T_{ref} is the reference temperature.

The elastic strain tensor $\boldsymbol{\varepsilon}^{\mathrm{el}}$ is a second-order symmetric tensor. The elastic strains are the slight distortion of the crystal lattice and, for all materials, are related to stresses. The elastic part of the strain tensor is completely reversible. For a large amount of metallic materials, the relationship between stresses and elastic strains can be sufficiently described by Hooke's law. However, in particular cases the sensitivity to the tensile/compressive loading mode is observed. In order to represent the different material behavior at the different loading regimes by the constitutive model, the elastic strain tensor can be splitted into the positive and negative parts as follows:

$$\boldsymbol{\varepsilon}^{\mathrm{el}} = \boldsymbol{\varepsilon}^{\mathrm{el}}_{+} + \boldsymbol{\varepsilon}^{\mathrm{el}}_{-} \tag{2.16}$$

The contributions of both parts are based on the decomposition, which is well described by Miehe et al. [44]:

$$\boldsymbol{\varepsilon}_{+}^{\mathrm{el}} = \sum_{i=1}^{3} \langle \varepsilon_i^{\mathrm{el}} \rangle_{+} \mathbf{g}_i \otimes \mathbf{g}_i, \quad \boldsymbol{\varepsilon}_{-}^{\mathrm{el}} = \sum_{i=1}^{3} \langle \varepsilon_i^{\mathrm{el}} \rangle_{-} \mathbf{g}_i \otimes \mathbf{g}_i, \tag{2.17}$$

where $\mathbf{g}_i$ are principal directions of the elastic strain tensor $\boldsymbol{\varepsilon}^{\mathrm{el}}$, $\langle\rangle_{+}$ and $\langle\rangle_{-}$ are the following operators:

$$\langle x \rangle_{+} = \frac{x + |x|}{2}, \quad \langle x \rangle_{-} = \frac{x - |x|}{2} \tag{2.18}$$

The inelastic strain tensor $\boldsymbol{\varepsilon}^{\mathrm{p}}$ is a second-order tensor, which, in general, is formulated in a unique manner for each material. The formulation and identification of the material parameters for $\boldsymbol{\varepsilon}^{\mathrm{p}}$ is one of the tasks of the identification problem considered within the framework of current work. The basic principles used for the derivation of the inelastic strain tensor $\boldsymbol{\varepsilon}^{\mathrm{p}}$ are given in Sect. 2.6.

2.5 Elasticity

The formulation of the stress-strain relations within the framework of current research is based on the hyperelasticity principle. The mentioned principle is based on the consideration of the mechanical state of materials through the strain energy density ψ. The following relationship between the energy storage functional ψ, elastic strain tensor $\boldsymbol{\varepsilon}^{\mathrm{el}}$ and Cauchy stress tensor $\boldsymbol{\sigma}$ is postulated for isotropic material as follows:

$$\boldsymbol{\sigma} = \frac{\partial \psi}{\partial \boldsymbol{\varepsilon}^{\mathrm{el}}} \tag{2.19}$$

For the linear elastic material, the energy storage functional ψ is the following:

$$\psi(\boldsymbol{\varepsilon}^{\mathrm{el}}) = \lambda \, \mathrm{tr}^2[\boldsymbol{\varepsilon}^{\mathrm{el}}]/2 + \mu \, \mathrm{tr}[(\boldsymbol{\varepsilon}^{\mathrm{el}})^2], \tag{2.20}$$

where λ and μ are Lamé's parameters. They are related to engineering constants as follows:

$$\lambda = \frac{\nu E}{(1+\nu)(1-2\nu)}, \quad \mu = \frac{E}{2(1+\nu)}, \tag{2.21}$$

where E is Young's modulus, ν is Poisson's ratio and μ is the shear modulus.

In principal, the classic definition fully satisfies the main requirements of the problem definition, except the material behavior, which is observed before

a rupture. In this case, the reduction of stresses is experimentally observed. The reduction taking place during the tensile mode of kinematic loading, applied to a specimen. In order to reproduce the mentioned behavior by the constitutive model, the following form of the energy storage functional ψ can be used [44]:

$$\psi(\boldsymbol{\varepsilon}^{\mathrm{el}},\omega) = \left[\kappa(\omega)+\chi\right]\psi^{+}(\boldsymbol{\varepsilon}^{\mathrm{el}}) + \psi^{-}(\boldsymbol{\varepsilon}^{\mathrm{el}}), \tag{2.22}$$

where function $\kappa(\omega)$ represents the degradation of material caused by the accumulated damage, which normally affects the stiffness only at tensile loads. Parameter χ is chosen to be a small value used for the stabilization of the simulation.

Taking into account compressive/tensile loading modes, the following expressions for ψ^{+} and ψ^{-} are proposed:

$$\psi^{\pm}(\boldsymbol{\varepsilon}^{\mathrm{el}}) = \lambda\langle \mathrm{tr}[\boldsymbol{\varepsilon}^{\mathrm{el}}]\rangle_{\pm}^{2}/2 + \mu\,\mathrm{tr}[(\boldsymbol{\varepsilon}_{\pm}^{\mathrm{el}})^{2}], \tag{2.23}$$

with above-defined by (2.17) brackets $\langle\rangle_{\pm}$ and tensile/compressive parts $\boldsymbol{\varepsilon}_{\pm}^{\mathrm{el}}$ of strain tensor $\boldsymbol{\varepsilon}^{\mathrm{el}}$(2.18), respectively.

With the substitution of the defined profile of the elastic energy functionals ψ^{+} and ψ^{+} into (2.20) and further in (2.19), the constitutive equation for the Cauchy stress tensor $\boldsymbol{\sigma}$ yields:

$$\boldsymbol{\sigma} = \left[\kappa(\omega)+\chi\right]\left[\lambda\langle \mathrm{tr}[\boldsymbol{\varepsilon}^{\mathrm{el}}]\rangle_{+}\boldsymbol{I} + 2\mu\boldsymbol{\varepsilon}_{+}^{\mathrm{el}}\right] + \left[\lambda\langle \mathrm{tr}[\boldsymbol{\varepsilon}^{\mathrm{el}}]\rangle_{-}\boldsymbol{I} + 2\mu\boldsymbol{\varepsilon}_{-}^{\mathrm{el}}\right] \tag{2.24}$$

The obtained stress-strain relation (2.24) is a generalized expression of the well-known Hooke's law, which can be obtained by substitution $\kappa(\omega)+\chi = 1$ in (2.24):

$$\boldsymbol{\sigma} = \lambda\,\mathrm{tr}[\boldsymbol{\varepsilon}^{\mathrm{el}}]\,\boldsymbol{I} + 2\mu\boldsymbol{\varepsilon}^{\mathrm{el}} \tag{2.25}$$

2.6 Rate-dependent material behavior

The formulation of the constitutive model is based mainly on the set of the loading regimes, for which the material response must be described. Taking into account fast loading regimes and holding regimes with stabilized loading conditions in the turbochargers, formulation of the constitutive relations for inelastic strain rates requires to consider fast- and slow-flowing rheological processes: plasticity and creep. In order to describe both of them by the unified constitutive mode, both plasticity and creep are considered from the position of rate-dependent processes.

2.6.1 Steady regime

Steady regime is characterized by holding of the continuous conditions of thermal and mechanical loads. Above-mentioned regime may be observed in the creep process at the constant loads. However, when higher amount of the loads are applied on the representative sample, steady regime of the inelastic strain rate may be observed in the plasticity as well. Thereby, consideration of the material behavior in steady regimes of the loads is important step of the identification of the unified constitutive model for plasticity and creep.

The starting point for the derivation of the inelastic strain rate tensor is the Odqvist flow rule [50, 59, 60]:

$$\dot{\boldsymbol{\varepsilon}}^{\mathrm{p}} = \frac{\partial W}{\partial \boldsymbol{\sigma}}, \tag{2.26}$$

where W is the creep potential, which is scalar-valued function of stress tensor $\boldsymbol{\sigma}$. Under the assumption of isotropic creep behavior, the creep potential W must be an isotropic function of stress tensor $\boldsymbol{\sigma}$. In fact, it means that the creep potential can be formulated with respect to the first invariant of the stress tensor J_1 and quadratic J_2 and cubic J_3 invariants of the stress deviator $\boldsymbol{s}$ [50]:

$$J_1 = \mathrm{tr}\boldsymbol{\sigma}, \quad J_2 = -\frac{1}{2}\boldsymbol{s}\cdot\cdot\boldsymbol{s}, \quad J_3 = \frac{1}{3}(\boldsymbol{s}\cdot\boldsymbol{s})\cdot\cdot\boldsymbol{s}, \tag{2.27}$$

where $\boldsymbol{s} = \boldsymbol{\sigma} - \frac{1}{3}\mathrm{tr}\boldsymbol{\sigma}$ is the deviator of the stress tensor. By substitution of (2.27) in the general flow rule (2.26) the following expression for the inelastic strain rate tensor can be obtained:

$$\dot{\boldsymbol{\varepsilon}}^{\mathrm{p}} = \frac{\partial W}{\partial J_1}\boldsymbol{I} - \frac{\partial W}{\partial J_2}\boldsymbol{s} + \frac{\partial W}{\partial J_3}\left(\boldsymbol{s}^2 - \frac{1}{3}\mathrm{tr}\,\boldsymbol{s}^2\boldsymbol{I}\right) \tag{2.28}$$

Under the assumption that inelastic deformations do not lead to the volume change, the volumetric part of the inelastic strain rate tensor can be neglected:

$$\mathrm{tr}\dot{\boldsymbol{\varepsilon}}^{\mathrm{p}} = \mathrm{tr}\left(\frac{\partial W}{\partial J_1}\boldsymbol{I}\right) = 0, \tag{2.29}$$

that leads to the following expression for the inelastic strain rate tensor:

$$\dot{\boldsymbol{\varepsilon}}^{\mathrm{p}} = -\frac{\partial W}{\partial J_2}\boldsymbol{s} + \frac{\partial W}{\partial J_3}\left(\boldsymbol{s}^2 - \frac{1}{3}\mathrm{tr}\,\boldsymbol{s}^2\boldsymbol{I}\right) \tag{2.30}$$

The presented creep flow rule (2.30) is called tensorial non-linear equation [8, 50, 76]. The part of equation (2.30) including the third invariant of the stress tensor is a non-linear function of the deviatoric stress tensor $\boldsymbol{s}$. The application of the creep flow rule in form (2.30) allows to describe non-classical

second order effects of the material behavior, which take place mainly in composite materials with particle system or in specific loading cases of certain structural elements [9].

The description of engineering materials, such as steels, alloys, cast irons, etc., requires, as a rule, the classical von Mises type potential W based on the second invariant of the stress deviator [84]:

$$\dot{\boldsymbol{\varepsilon}}^{\mathrm{p}} = \frac{3}{2}\frac{\partial W(\sigma_{\mathrm{vM}})}{\partial \sigma_{\mathrm{vM}}}\frac{\boldsymbol{s}}{\sigma_{\mathrm{vM}}}, \qquad \sigma_{\mathrm{vM}} = \sqrt{\frac{3}{2}\boldsymbol{s}\cdot\cdot\boldsymbol{s}} = \sqrt{-3J_2}. \tag{2.31}$$

In other words, the flow rule (2.31) is the generalized constitutive equation for the inelastic strains $\dot{\boldsymbol{\varepsilon}}^{\mathrm{p}}$ derived for the isotropic materials which show inelastic incompressibility. The particular cases of material properties are introduced in the model through the creep potential function W. The dependence on temperature is excluded from the derivation of the flow rule (2.31) for the sake of brevity. However, including the temperature dependence would not affect the general structure of the flow rule.

The introduction of the second invariant $\dot{\varepsilon}^{\mathrm{p}}_{\mathrm{vM}}$ of the inelastic strain rate tensor $\dot{\boldsymbol{\varepsilon}}^{\mathrm{p}}$ leads to the well-known constitutive equation for the steady-state inelastic strain rate, which is well represented among others by Naumenko and Altenbach [50]:

$$\dot{\boldsymbol{\varepsilon}}^{\mathrm{p}} = \frac{3}{2}\frac{\dot{\varepsilon}^{\mathrm{p}}_{\mathrm{vM}}}{\sigma_{\mathrm{vM}}}\boldsymbol{s}, \qquad \dot{\varepsilon}^{\mathrm{p}}_{\mathrm{vM}} = \sqrt{\frac{2}{3}\dot{\boldsymbol{\varepsilon}}^{\mathrm{p}}\cdot\cdot\dot{\boldsymbol{\varepsilon}}^{\mathrm{p}}} = \frac{\partial W}{\partial \sigma_{\mathrm{vM}}} \tag{2.32}$$

The proposed equation is derived in [60] for the secondary steady-state creep stage and can be extended for the primary and tertiary stages of creep by means of introducing additional order parameters into constitutive equations.

2.6.2 Transient regime

Usually, the principles of formulation of the constitutive model for inelastic material behavior is based on the effects, which must be taken into account. The inelastic response of material at long-term constant loading can be sufficiently represented by using the constitutive relation for the ideal viscoplasticity, which is presented above. However, the exploitation of mechanical parts and, in particular, turbine housings also includes the transient regimes with variable loads. Standardized in material science low-cyclic fatigue tests, which are normally performed for constant temperature and saw-type kinematic

loading profiles, and thermo-mechanical tests with more complicated loading profiles, are the simplest cases of the operation conditions taking place in the real construction. Majority of the operational conditions are characterized by the variation of stress, strain and temperature around some average values, and includes the launches and stopping regimes. The application of the single ideal viscoplasticity approach in this case is not sufficient, while the significant part of the inelastic material behavior is characterized as primary creep stage.

In general, the primary creep stage is characterized by the increasing resistivity of material against evolution of inelastic deformations, which are also known as hardening. Hardening is usually associated with the moving of the dislocations, anisotropic inelastic deformations inside the crystals and in the grain boundary layer.

The idea of kinematic hardening within the creep mechanics was originally introduced by Malinin and Khadjinsky [39, 40]. Authors started with the decomposition of the stress tensor $\boldsymbol{\sigma}$ through the active stress tensor $\overline{\boldsymbol{\sigma}}$ and order parameter $\boldsymbol{\alpha}$ known as backstress.

$$\boldsymbol{\sigma} = \overline{\boldsymbol{\sigma}} + \boldsymbol{\alpha} \tag{2.33}$$

It is assumed that only the active stress tensor $\overline{\boldsymbol{\sigma}}$ affects the inelastic strain rate, while the backstress tensor $\boldsymbol{\alpha}$ is introduced as a measure of internal stresses, which are associated with deviation between the loading direction of the polycrystal and preferable slip directions of each crystal [6, 21, 82]. These introduced tensors can be further decomposed into the spherical and deviatoric parts

$$\begin{aligned}
\overline{\boldsymbol{\sigma}} &= \frac{1}{3}\operatorname{tr}\overline{\boldsymbol{\sigma}}\,\boldsymbol{I} + \overline{\boldsymbol{s}}, && \operatorname{tr}\overline{\boldsymbol{s}} = 0, \\
\boldsymbol{\alpha} &= \frac{1}{3}\operatorname{tr}\boldsymbol{\alpha}\,\boldsymbol{I} + \boldsymbol{\beta}, && \operatorname{tr}\boldsymbol{\beta} = 0, \\
\boldsymbol{\sigma} &= \frac{1}{3}\left(\operatorname{tr}\overline{\boldsymbol{\sigma}} + \operatorname{tr}\boldsymbol{\alpha}\right)\boldsymbol{I} + \boldsymbol{s}, && \boldsymbol{s} = \overline{\boldsymbol{s}} + \boldsymbol{\beta}
\end{aligned} \tag{2.34}$$

The backstress deviator serves to reflect kinematic hardening effects such as the Bauschinger effect, creep recovery, etc., and provides a phenomenological measure for internal stress fields generated by the non-uniform inelastic deformation on the microscale. The theoretical background to introduce backstress deviator(s) is based on a mixture composed of two or more constituents with different inelastic material properties [7, 51]. The mixture model approximates the spacial non-uniformity of inelastic deformation and the internal stress redistribution, and characterizes hardening effects. A ro-

bust model is based on two inelastic constituents in such way that one back-stress variable can be introduced [51, 52].

Within the derivation presented above, the creep potential W can be defined in terms of the active stress tensor. Under the assumption, that inelastic deformations do not affect the volume change for classic isotropic creep, we have $W = W(\overline{\boldsymbol{s}})$. Thereby, the expression for the inelastic strain rates in case of ideal viscoplasticity (2.32) proposed in [60] yields the following:

$$\dot{\boldsymbol{\varepsilon}}^{\mathrm{p}} = \frac{3}{2}\frac{\dot{\varepsilon}^{\mathrm{p}}_{\mathrm{vM}}}{\overline{\sigma}_{\mathrm{vM}}}\overline{\boldsymbol{s}}, \tag{2.35}$$

which is able to describe the transient processes observed in the primary creep stage as well as in the secondary steady creep stage. Introduced in (2.35) $\overline{\sigma}_{\mathrm{vM}}$ is the von Mises equivalent active stress:

$$\overline{\sigma}_{\mathrm{vM}} \equiv \sqrt{\frac{3}{2}\overline{\boldsymbol{s}}\cdot\cdot\overline{\boldsymbol{s}}} = \sqrt{\frac{3}{2}(\boldsymbol{s}-\boldsymbol{\beta})\cdot\cdot(\boldsymbol{s}-\boldsymbol{\beta})} \tag{2.36}$$

The different phenomenon takes place during thermo-mechanical loading of mechanical parts. The correlation of the constitutive model in general case depends on the precision of the description of observed phenomenon. For the instance, constitutive models considered in [31, 50] includes isotropic hardening, softening, ageing and damage variables. However, the excessive complexity of the model is undesirable, because it requires higher quality and quantity of experimental data. Taking into account the available set of experimental data and declared loading conditions, the constitutive model includes the single kinematic hardening variable $\boldsymbol{\beta}$.

Within the stated flow rule (2.35) the equivalent von Mises inelastic strain rate is the quantitative representation of the rate of inelastic processes, which takes place in the material. Obviously, the change of the stress or temperature leads to the change of intensity of the creep process. Therefore, the decomposition of the equivalent inelastic strain rates onto constituents, which are representing the influence of temperature and stress, is reasonable [50]:

$$\dot{\varepsilon}^{\mathrm{p}}_{\mathrm{vM}} = R(T)\,f\left(\overline{\sigma}_{\mathrm{vM}}\right) \tag{2.37}$$

The function $R(T)$ including the influence of the temperature into the intensity of flow. The function $f\left(\overline{\sigma}_{\mathrm{vM}}\right)$ is the response function of the effective stress. The temperature response function is normally represented by the Arrhenius type function [26, 50] of absolute temperature:

$$R(T) = \exp\left(-\frac{Q}{R_{\mathrm{a}}T}\right), \tag{2.38}$$

where R_a is the gas constant, Q is the activation energy related to specific material.

2.6.3 Backstress evolution

The evolution equation for the backstress deviator can be derived in order to represent the behavior of the certain material. For instance, in [37, 38] the following evolution equation is postulated:

$$\dot{\boldsymbol{\beta}} = \frac{2}{3} b \dot{\boldsymbol{\varepsilon}}^\mathrm{p} - \frac{g(\beta_\mathrm{vM})}{\beta_\mathrm{vM}} \boldsymbol{\beta}, \quad g(\beta_\mathrm{vM}) = c \exp\left(-\frac{Q}{R_\mathrm{a} T}\right) \beta_\mathrm{vM}^n, \quad \beta_\mathrm{vM} \equiv \sqrt{\frac{3}{2} \boldsymbol{\beta} \cdot\cdot \boldsymbol{\beta}} \tag{2.39}$$

Equation (2.39) is the multiaxial realization of the Bailey-Orowan recovery hypothesis [17, 50, 61]. Here, b, c and n are material constants.

On the other hand, kinematic hardening model proposed in [1] is suitable in cases of ratcheting and includes the opportunity to incorporate several backstresses into the constitutive model:

$$\boldsymbol{\beta} = \sum_{i=1}^{n} \boldsymbol{\beta}_i, \quad \dot{\boldsymbol{\beta}}_i = \xi_i \left[\frac{2}{3} r_i \dot{\boldsymbol{\varepsilon}}^\mathrm{p} - \mu_i \boldsymbol{\beta}_i \dot{\varepsilon}^\mathrm{p}_\mathrm{vM} - H(f_i) \langle \dot{\lambda}_i \rangle \right], \tag{2.40}$$

where n is the number of backstress parts, H and $\langle ... \rangle$ are Heaviside's step function and Macaulay's brackets, correspondingly, ξ_i, r_i and μ_i are material constants. The values $\dot{\lambda}_i$ and f_i are determined as follows:

$$\dot{\lambda}_i = r_i^{-1} \dot{\boldsymbol{\varepsilon}}^\mathrm{p} \cdot\cdot \boldsymbol{\beta}_i - \mu_i \dot{\varepsilon}^\mathrm{p}_\mathrm{vM}, \quad f_i = \frac{3}{2} \boldsymbol{\beta}_i \cdot\cdot \boldsymbol{\beta}_i - r_i^2 \tag{2.41}$$

Within the framework of current research the evolution equation originally proposed by Frederick and Armstrong [19] and derived as well in a different manner by Naumenko et al. [51] is used:

$$\dot{\boldsymbol{\beta}} = \frac{1}{\mu_\mathrm{h}} \frac{\mathrm{d}\mu_\mathrm{h}}{\mathrm{d}T} \dot{T} \boldsymbol{\beta} + \frac{2}{3} \mu_\mathrm{h} \left[\dot{\boldsymbol{\varepsilon}}^\mathrm{p} - \frac{3}{2} \dot{\varepsilon}^\mathrm{p}_\mathrm{vM} \frac{\boldsymbol{\beta}}{\beta_*} \right], \tag{2.42}$$

where μ_h is the *hardening rate* function, which in original papers [19, 51] relates to the shear modulus. In the general case, μ_h is proportional to the shear modulus G. Proposed in [51], definition for μ_h is following:

$$\mu_\mathrm{h} = \frac{3G}{c_\mathrm{h}}, \tag{2.43}$$

where c_h is the material constant.

Elastic material properties especially in case of metals are temperature dependent. Thereby, in general case the hardening rate modulus is the function

of the temperature. For particular cases of temperature-independent shear modulus G, hardening rate modulus μ_{h} becomes the constant, therefore the first part of (2.42) is vanish. Term β_* of (2.42) is the scalar function of the plastic strain path [19], which is also known as *hardening saturation* function. In general case β_* is the function of the stress and temperature. The particular representation of the function differs for various materials and should be determined taking into account the experimental data for the certain material.

2.7 Damaging of material

Current section is focused on the formulation of evolution equations for creep and fatigue damaging mechanisms taking place in turbine housings during the operation. The constitutive model including the creep-fatigue damage interaction.

The aim of continuum damage mechanics is to represent the damaged state of materials. The starting point is the introduction of a damage variable, which affects the behavior of material and further development of the damage. In general, damage in the materials have a different nature. When the micro-crack arises without plastic deformations, such damage is referred to as *brittle damage*. Growing of the spherical and ellipsoidal micro-voids in the material caused by plastic deformation is called *ductile damage* [46]. In case of high temperatures, the diffusional movement of micro-voids and dislocations can leads to the accumulation of the micro-voids on the boundary of grains in polycrystal. Such damage mechanism is referred to as *creep damage*, because on practice it is often observed during the creep [31, 46].

Thereby, the loading conditions have the principal influence on the development of damage in the material. Within the current work we are focused onto the consideration of loading conditions, which are normally take place in creep tests, uniaxial tension tests, low-cycle fatigue tests and thermomechanical fatigue tests. The unified constitutive model is formulated in order to describe the damaging processes taking place in the material at the various thermal and mechanical loads.

Within current research, the unified continuum damage variable $0 \leq \omega < 1$ is introduced. The various loading conditions taking place during the operation of mechanical parts induce the different micro-defects of the material. On the one hand, the variable ω should take into account each of abovementioned damage mechanisms. On the other hand, the introduced damage variable represents general damaged state of the material. Thereby, within

the framework of current work the different damage formation mechanisms are considered.

2.7.1 Creep damage

When crystalline materials are subjected to static stresses and temperature higher than one-third of their melting temperature, the microvoids and microcavities may arise and grow in the grain boundaries [18, 46, 50]. This micromechanical material degradation is known as *creep damage* [46]. Creep damage originate the tertiary creep stage, where the significant increase of inelastic strain rates is observed for constant loading conditions. The shape of the tertiary part of the creep curve, its duration and rupture creep strains depends on the material composition, mechanical load and operation temperature [50].

Nucleation and growth of microvoids and microcavities dominates in the grain boundaries, which are orthogonal to the loading direction. The change of the loading direction leads to the activation of damaging processes in corresponding grain boundaries. Thereby, creep damage in the general loading case is anisotropic and can be characterized by tensor [47]. Above-mentioned loading cases are referred to as *unproportional loading*. On the other hand, in case of the unidirectional loading, known also as *proportional loading*, the scalar damage variable is sufficient in order to describe the internal degradation of the material [31, 46, 47] under the assumption of the coaxiality of the stress and plastic strain tensors [50].

2.7.1.1 Kachanov-Rabotnov model

The phenomenological creep damage equations for scalar valued damage were firstly proposed by Kachanov [25] and Rabotnov [75]. The models are based on the geometrical interpretation of damage in form of discontinuities in the material. An arising of these discontinuities leads to the reduction of the specimen cross-section area.

According to Kachanov-Rabotnov model [25, 50, 75], the cross-section area of virgin material A_0 is reduced by the total area of micro-voids and microcracks A_D. A decreasing of the cross-section area leads to a growth of internal stresses in the specimen, and, consequently, to growth of creep strain rates, which is usually observed on the tertiary stage of creep curves. The proposed introduction of the damaging process in material leads to the following defi-

nitions for the creep damage parameter ω and effective stresses $\tilde{\sigma}$:

$$\omega = \frac{A_{\mathrm{D}}}{A_0}, \quad \tilde{\sigma} = \frac{\sigma}{1-\omega}, \tag{2.44}$$

where ω takes values from 0 for undamaged material state to 1 for completely damaged.

The constitutive relation for the creep strain rates must take into account the current damage value [25]. Substitution of the effective stress (2.44) to constitutive equation (2.37) involves the influence of current damage state on the equivalent inelastic strain rates [25, 50]:

$$\dot{\varepsilon}^{\mathrm{p}}_{\mathrm{vM}} = R(T) f\left(\frac{\overline{\sigma}_{\mathrm{vM}}}{1-\omega}\right) \tag{2.45}$$

2.7.1.2 Kinetic equation

The basic principles of the derivation of a kinetic equation for the description of the creep damage evolution are given, among others, by Lemaitre [30]. The majority of the kinetic equations for evolution of the creep damage are based on the following assumptions:

- Creep damage is irreversible and related to irreversible strain.

$$\dot{\omega}_{\mathrm{c}} = \mathfrak{C}(\omega, T, \boldsymbol{\sigma}, \boldsymbol{\varepsilon}^{\mathrm{p}}, \dot{\boldsymbol{\varepsilon}}^{\mathrm{p}}) \dot{\varepsilon}^{\mathrm{p}}_{\mathrm{vM}} \tag{2.46}$$

  The formulation of a kinetic equation in terms of equivalent von Mises inelastic strain rates $\dot{\varepsilon}^{\mathrm{p}}_{\mathrm{vM}}$ satisfies both assumptions if

$$\mathfrak{C}(\omega, T, \boldsymbol{\sigma}, \boldsymbol{\varepsilon}^{\mathrm{p}}, \dot{\boldsymbol{\varepsilon}}^{\mathrm{p}}) \geq 0 \, \forall \, \omega, T, \boldsymbol{\sigma}, \boldsymbol{\varepsilon}^{\mathrm{p}}, \dot{\boldsymbol{\varepsilon}}^{\mathrm{p}}$$

  The function $\mathfrak{C}$ reflects the state of material.

- Creep damage rates are related to the accumulated damage in material. The contribution of the current damage state in the creep damage rate is performed by means of the accumulated damage response function $r(\omega)$:

$$\dot{\omega}_{\mathrm{c}} = r(\omega) \mathfrak{C}(T, \boldsymbol{\sigma}, \boldsymbol{\varepsilon}^{\mathrm{p}}, \dot{\boldsymbol{\varepsilon}}^{\mathrm{p}}) \dot{\varepsilon}^{\mathrm{p}}_{\mathrm{vM}}, \tag{2.47}$$

  where $r(\omega) > 0$, $r'_{\omega}(\omega) > 0 \, \forall \, \omega \in (0,1]$. The expression for function $r(\omega)$ depends on the profile of the tertiary stage of the creep curve for the certain material.

- The creep damage accumulation rate differs for tensile and compressive loading modes [30, 50, 81]. Under the mentioned constraints the kinetic equation (2.47) yields:

$$\dot{\omega}_{\mathrm{c}} = H_{\mathrm{c}}(\boldsymbol{\sigma})\, Y(\boldsymbol{\varepsilon}^{\mathrm{p}})\, r(\omega)\, \mathfrak{C}(T, \boldsymbol{\sigma}, \boldsymbol{\varepsilon}^{\mathrm{p}}, \dot{\boldsymbol{\varepsilon}}^{\mathrm{p}})\, \dot{\varepsilon}^{\mathrm{p}}_{\mathrm{vM}}, \tag{2.48}$$

  where the functions $H_{\mathrm{c}}(\boldsymbol{\sigma})$ and $Y(\boldsymbol{\varepsilon}^{\mathrm{p}})$ reflect the influence of the tension/compression in terms of the stress and inelastic strain, respectively.

The generalized expression (2.48) covers the majority of kinematic equations available in the literature [26, 30, 46, 50]. The particular cases of functions $r(\omega)$ and $\mathfrak{C}(T, \boldsymbol{\sigma}, \boldsymbol{\varepsilon}^{\mathrm{p}}, \dot{\boldsymbol{\varepsilon}}^{\mathrm{p}})$ are well described, among others, by Naumenko and Altenbach [50].

There are many possible cases for the formulation of the analytic expression for material state function $\mathfrak{C}(T, \boldsymbol{\sigma}, \boldsymbol{\varepsilon}^{\mathrm{p}}, \dot{\boldsymbol{\varepsilon}}^{\mathrm{p}})$ depending on the available experimental data and an acceptable level of complexity. However, the main and most reasonable criterion for large number of models presented in the literature is the minimum of material parameters.

2.7.1.3 Response functions

The profile of the accumulated damage response function $r(\omega)$ in the general case depends on the qualitative and quantitative profile of the tertiary stage of creep strain curves. The templates of $r(\omega)$ are available in [26, 30, 46, 50]. Within the current model is used the expression proposed, among others, in Naumenko and Altenbach [50]:

$$r(\omega) = l\omega^{1-\frac{1}{7}}, \tag{2.49}$$

where l is the temperature-independent material parameter which must be determined. The proposed expression of function (2.49) is useful, because the above-mentioned definition (2.49) allows to obtain the analytic solution for the inelastic strains in the particular cases of the structure of the equivalent inelastic strain rate function $\dot{\varepsilon}^{\mathrm{p}}_{\mathrm{vM}}$ (2.45) and applied loading conditions [50].

According to stated definition of the uniform damage parameter ω, the unique expressions must be used for the accumulated damage response function $r(\omega)$, because the function represents the general state of material independently on the damage nature.

Axiallity functions of stress and inelastic strains are defined in order to restrict the damage accumulation at the compressive loading mode. The expres-

sions presented further are defined in terms of stresses and inelastic strain:

$$\begin{aligned} H_{\mathrm{c}}(\boldsymbol{\sigma}) &= \frac{\sigma_+}{\sigma_{\mathrm{vM}}}, & \sigma_+ &= \frac{\sigma_I + |\sigma_I|}{2}, \\ Y(\boldsymbol{\varepsilon}^{\mathrm{p}}) &= \frac{1}{2}\left[\mathrm{sgn}(\varepsilon_+^{\mathrm{p}}) + 1\right], & \varepsilon_+^{\mathrm{p}} &= \varepsilon_I^{\mathrm{p}} + \varepsilon_{III}^{\mathrm{p}} \end{aligned} \tag{2.50}$$

The functions $H_{\mathrm{c}}(\boldsymbol{\sigma})$ and $Y(\boldsymbol{\varepsilon}^{\mathrm{p}})$ represent the influence of stressed and strained state of material on the creep damage rate. The creep damage rate becomes negligible in cases of compressive stress ($\sigma_+ = 0$) or when the compressive type of the inelastic deformations dominates. The introduced features can be observed in experimental data including both compressive and tensile creep tests [81].

2.7.1.4 State function $\mathfrak{C}$ in the literature

A large number of evolution equations are available in the literature for description of the creep damage growth. They are developed for various materials and differs for the each certain case. For instance, the damage evolution equation proposed by Kachanov [26] is represented in current notation by following:

$$\dot{\omega} = \underbrace{\frac{1}{(1-\omega)^n}}_{r(\omega)} \underbrace{A\overline{\sigma}_{\mathrm{vM}}^n}_{\mathfrak{C}}, \tag{2.51}$$

where n is the temperature-independent material parameter, A is the material parameter, which in general case is the function of temperature. Function $\mathfrak{C}$ here is represented by Norton's law [55]. The presented expression is designed in such a way, that the solution for the time to rupture can be obtained analytically.

The damage evolution equation mentioned in [50, 69] is similar to proposed by Kachanov [26]. However, except to (2.51), this equation utilize the normalized principal stress and inelastic strain rates:

$$\dot{\omega} = H(\boldsymbol{\sigma}) \underbrace{D(T)\left(\frac{\sigma_I}{\sigma_{\mathrm{vM}}}\right)^n \dot{\varepsilon}_{\mathrm{vM}}^{\mathrm{p}}}_{\mathfrak{C}}, \quad D(T) = D_0 e^{-\frac{Q}{R_{\mathrm{a}} T}} \tag{2.52}$$

The above-presented expression includes the dependence not only on stress, but also contains the Arrhenius type temperature function $D(T)$ and the equivalent inelastic strain rates $\dot{\varepsilon}_{\mathrm{vM}}^{\mathrm{p}}$. The evolution equation is included in the constitutive model, which is used for the modeling of the creep phenomena in the different zones of weldment. The influence of accumulated damage

in the current specific case is involved into equation implicitly through dependence of the inelastic strain rates $\dot{\varepsilon}^{\mathrm{p}}_{\mathrm{vM}}$ and stress response $\boldsymbol{\sigma}$ on the damage ω. Function $H(\boldsymbol{\sigma})$ here is Heaviside's function of stress, which is 1 for $\sigma_I > 0$ and 0 otherwise. D_0 here is the temperature independent material parameter. The identification of material parameters is given in [68] and based on experimental data of creep tests for stress range $28-110$ MPa and temperature range $615-690$°C.

The evolution equation proposed in [51] is verified for 12%Cr steel:

$$\dot{\omega} = H(\boldsymbol{\sigma})\, r(\omega) \underbrace{\frac{1}{\varepsilon^{\mathrm{p}}_{*}(\sigma_{\mathrm{vM}})}}_{\mathfrak{C}} \dot{\varepsilon}^{\mathrm{p}}_{\mathrm{vM}}, \quad \varepsilon^{\mathrm{p}}_{*}(\sigma_{\mathrm{vM}}) = \varepsilon_{\mathrm{br}} + \frac{a_\varepsilon}{1+b_\varepsilon e^{-\frac{\sigma_{\mathrm{vM}}}{c_\varepsilon}}}, \tag{2.53}$$

where $\varepsilon^{\mathrm{p}}_{*}(\sigma_{\mathrm{vM}})$ is the response function including information about the creep strain values on the final interval of the tertiary creep stage. The experimental data provided by Straub [81] for X20CrMoV12-1 steel at one value of temperature $T = 600$°C. Taking into account the above-mentioned testing condition, the function $\varepsilon^{\mathrm{p}}_{*}(\sigma_{\mathrm{vM}})$ is only depending on stress (2.53). In general case, the influence of temperature must be taken into account.

2.7.2 Low cycle fatigue damage

When material is subjected to the cyclic loads, the plastic deformation may lead to the formation of the microcavities. Nonmonotonic internal state of material leads to the growth of microcavities to the cracks, which finally leads to fracture of the material. In particular, in metals cyclic loads leads to the transgranular slips, which induce decohesion on the surface and further microcrack initiation [46]. The presented mechanism of the damage formation is referred to as *fatigue damage*. When the material is subjected to high stresses and large amounts of inelastic strains take place, the transgranular slips are accumulated in the large number of grains. It leads to the fracture of the material at respectively low numbers of loading cycles $N_{\mathrm{A}} < 10^4$. The fatigue damage, in this case, is classified as *low cycle fatigue damage*.

The necessity to include into the constitutive model the fatigue damage model is caused as well by the technical, industrial and marketing reasons. The design processes of the mechanical parts includes the *planned obsolescence*, which, in the case of turbine housings, is in the range $10^3 < N_{\mathrm{A}} < 5 \cdot 10^3$ cycles. The marketing reason is the attempt to replace expensive material by the cheap one, in order to reduce the price with the saving of primary technical characteristics of the product at the same time. The industrial reason is the tendency to reduce technological costs of products. Each of above-mentioned

cases requires the reliable estimation of the lifetime of the product, which in turn needs the proper constitutive model for the low-cycle fatigue damage.

The majority of fatigue damage models presented in the literature is based on several assumptions, which in turn are formulated taking into account the behavior of the material observed in the experiments.

- The damage is irreversible [62]. Microcavities and transgranular slips can not vanish once they are arisen.

- Cyclic loads with higher stress magnitudes lead to faster fracture, that the same loading profiles with lower stress magnitudes. Thereby, the accumulation of damage in this case is the growing function of stress [26, 30, 62, 80].

- The starting point of fatigue damage accumulation on the microscale is the arising and growth of the cavities. According to the effective stress concept [12], the damaging depends on the compression/tension loading mode [62, 80].

- While the inelastic strain tensor is the measure of irreversible deformations in the material, transgranular slips arising during the cyclic loading can be characterized by this measure. Thereby, the damage is increasing function of the accumulated inelastic strains [62, 67].

- When the cyclic load with low amplitude is applied, the low stress response and negligible inelastic strain is observed in the experiment. However, even in the mentioned case, the fatigue damage is observed. Therefore, the fatigue damage model must include the complete strain tensor in order to describe the accumulation of damage for low loading amplitudes.

- Fast loads lead to the rupture faster, then the slow one. Therefore, the damage accumulation rate must be proportional to inelastic strain rates [2, 3, 30, 62, 67].

- The temperature affects the damage accumulation rate. The implicit influence of the temperature is included into the constitutive model through the dependence of the inelastic strain rates on the temperature. However, the constitutive models with the explicit dependence of the temperature are available in the literature [2, 3, 30].

2.7.2.1 Kinetic equation

The fatigue damage evolution equation within the framework of continuum damage approach can only be formulated in terms of variable, which describe the state of material in a current moment of time. Taking into account abovementioned principles of the formulation, which are widespread in the literature in the particular or complete manner [2, 3, 26, 30, 62, 67, 80], the following fatigue damage evolution equation is introduced:

$$\dot{\omega}_{\mathrm{f}} = H_{\mathrm{f}}(\boldsymbol{\sigma})\, r(\omega) \mathfrak{F}\left(T, \boldsymbol{\sigma}, \boldsymbol{\varepsilon}, \boldsymbol{\varepsilon}^{\mathrm{p}}\right) \dot{\varepsilon}^{\mathrm{p}}_{\mathrm{vM}}, \tag{2.54}$$

where $r(\omega)$ is the response function which characterizes the influence of accumulated damage on the current damage rate (see Sect. 2.7.1.3), $H_{\mathrm{f}}(\boldsymbol{\sigma})$ reflects the influence of the compression/tension loading regimes (see Sect. 2.7.1.3) and $\mathfrak{F}$ is the scalar-valued isotropic function of the material state. The equation is formulated with respect to equivalent von Mises plastic strain rates $\dot{\varepsilon}^{\mathrm{p}}_{\mathrm{vM}}$ in order to represent the influence of inelastic deformation on the damaging of the material.

The profile of function $\mathfrak{F}$ depends on the particular behavior of specific material. To determine an expression for this function is the main task of the fatigue damage identification problem, which is shown in details in Chapt. 3.

2.7.2.2 State function $\mathfrak{F}$ in the literature

A large number of evolution equations for continuous fatigue damage are developed for various materials. For instance, Lemaitre and Desmorat [32] proposed the fatigue damage evolution equation in the following form:

$$\dot{\omega} = \underbrace{\frac{\overline{Y}}{S}}_{r(\omega)\mathfrak{F}} \dot{\varepsilon}^{\mathrm{p}}_{\mathrm{vM}} H(\varepsilon^{\mathrm{p}}_{\mathrm{vM}} - \varepsilon^{\mathrm{p}}_{0}), \tag{2.55}$$

where $\overline{Y}$ is the thermodynamically conditioned driving force of the damage accumulation rate, S is the temperature depended material parameter and $H(x)$ is Heaviside's function. $\varepsilon^{\mathrm{p}}_{0}$ denotes the threshold value of strains, which are necessary for the development of the fatigue damage. The function $\overline{Y}$ is stated as analogue of the strain energy density and formulated as follows:

$$\overline{Y} = \frac{\sigma^2_{\mathrm{vM}} R_\nu}{2E(1-\omega)^2}, \quad R_\nu = \frac{2}{3}(1+\nu) + 3(1-2\nu)\left(\frac{\sigma_{\mathrm{H}}}{\sigma_{\mathrm{vM}}}\right)^2,$$

where R_ν is the triaxiality factor, $\sigma_{\mathrm{H}} = \frac{1}{3}\,\mathrm{tr}\boldsymbol{\sigma}$ is the hydrostatic stress.

The fatigue damage evolution law developed by Kachanov [26] is based on the assumption that increment of fatigue damage $\mathrm{d}\omega$ is proportional to the stress increment $\mathrm{d}\sigma$:

$$\mathrm{d}\omega = \underbrace{\frac{1}{(1-\omega)^k}}_{r(\omega)} \underbrace{\left[\frac{\langle \sigma_{\mathrm{vM}} - \sigma_0 \rangle}{(\sigma_{\mathrm{u}} - \sigma_0)}\right]^k \frac{\langle \mathrm{d}\sigma_{\mathrm{eq}} \rangle}{\sigma_{\mathrm{u}} - \sigma_0}}_{\mathfrak{F}} \tag{2.56}$$

Here σ_{u} is the ultimate strength, k is the material constant. In contrast to [32] the damage model of Kachanov [26] utilizes the threshold of stress σ_0. σ_{eq} is defined by following relation:

$$\sigma_{\mathrm{eq}} = \sigma_{\mathrm{T}} \left[2(1+\nu) + 3(1-2\nu)\left(\frac{\sigma_{\mathrm{H}}}{\sigma_{\mathrm{T}}}\right)^2\right]^{1/2},$$

where $\sigma_{\mathrm{T}} = \frac{1}{2}(\sigma_I - \sigma_{III})$ is Tresca stress.

The model proposed by Paas [62] is developed accounting the microcracks formation process, which is prior to macrocrack initiation:

$$\dot{\omega} = H(\varepsilon^{\mathrm{p}}_{\mathrm{vM}} - \varepsilon^{\mathrm{p}}_0) \underbrace{\alpha\omega^{\beta}}_{r(\omega)} \underbrace{\varepsilon^{\mathrm{p}}_{\mathrm{vM}}{}^{\gamma}}_{\mathfrak{F}} \dot{\varepsilon}^{\mathrm{p}}_{\mathrm{vM}} \tag{2.57}$$

Here α, β and γ are material parameters, $\varepsilon^{\mathrm{p}}_0$ is the inelastic strain threshold. Moreover, parameter β may depend on the loading.

The model developed by Peerlings et al. [67] is used for the modeling of high cyclic fatigue. This model is similar to one proposed by [62], except for the part reflecting the influence of accumulated fatigue damage:

$$\dot{\omega} = \underbrace{A\exp(B\omega)}_{r(\omega)} \underbrace{\varepsilon^{\mathrm{p}}_{\mathrm{vM}}{}^{C}}_{\mathfrak{F}} \dot{\varepsilon}^{\mathrm{p}}_{\mathrm{vM}} \tag{2.58}$$

Here A, B and C are material parameters.

The fatigue damage evolution equation introduced by Sommitsch et al. [80] allows to describe cases of disproportionately high damaging compared to the low stresses:

$$\dot{\omega} = \underbrace{\left(\frac{\sigma_{\mathrm{vM}}}{S_0}\right)^m \left(\frac{\dot{\varepsilon}^{\mathrm{p}}_{\mathrm{vM}}}{\dot{p}_0}\right)^n \dot{p}_0}_{\mathfrak{F}\dot{\varepsilon}^{\mathrm{p}}_{\mathrm{vM}}}, \tag{2.59}$$

where $\dot{p}_0$ is the normalization constant. The parameters S_0 and m regularize the influence of the stress on the lifetime. The parameter n describes the time-dependence of the lifetime: rate-independent behavior $n > 0$ and $n = 0$ means that lifetime behavior is fully time-dependent.

The overview of available fatigue damage evolution equations leads to the conclusion, that, in general, the function of material state $\mathfrak{F}$ is depending on temperature, stresses, total and inelastic strains. The choice of expression for $\mathfrak{F}$ is more a personal decision of the scientist or mechanical engineer, which may only depend on the available experimental data and the knowledge of the designer. However, the minimum of the material parameters is the recommended property not only for the evolution equation of the fatigue damage, but for the complete constitutive model of the material.

2.7.3 Creep-fatigue damage interaction

The operation conditions taking place in applications normally include cyclic loads, where the fatigue damage growth is assumed, and steady regimes with a constant level of the load, where creep damage processes are usually observed. Taking into account the above-mentioned statement, the creep-fatigue damage interaction mechanisms must be considered.

2.7.3.1 Accumulation of damages of different nature

The creep and fatigue damages defined in Sect. 2.7.1 and Sect. 2.7.2 are considered from the position that only one creep or fatigue damage process takes place at the unique moment of time. Thereby, the evolution equations for the creep and fatigue damage are written in the independent manner:

- The creep damage characterizing the accumulation of intercrystalline defects:
$$\dot{\omega}_{\mathrm{c}} = H_{\mathrm{c}}(\boldsymbol{\sigma})\, Y(\boldsymbol{\varepsilon}^{\mathrm{p}})\, r(\omega_{\mathrm{c}})\, \mathfrak{C}(T, \boldsymbol{\sigma}, \boldsymbol{\varepsilon}^{\mathrm{p}}, \dot{\boldsymbol{\varepsilon}}^{\mathrm{p}})\, \dot{\varepsilon}^{\mathrm{p}}_{\mathrm{vM}}$$
- The fatigue damage characterizing transcrystallyne processes initiating on the surface:
$$\dot{\omega}_{\mathrm{f}} = H_{\mathrm{f}}(\boldsymbol{\sigma})\, r(\omega_{\mathrm{f}})\, \mathfrak{F}\left(T, \boldsymbol{\sigma}, \boldsymbol{\varepsilon}, \boldsymbol{\varepsilon}^{\mathrm{p}}\right) \dot{\varepsilon}^{\mathrm{p}}_{\mathrm{vM}} \tag{2.60}$$

Obviously, under the real operation conditions material is affected by both kinds of the defects in the same time. Therefore, the contribution of the macroscopic effects must be taken into account in each evolution equation:

$$\begin{aligned}
\dot{\omega}_{\mathrm{c}} &= H_{\mathrm{c}}(\boldsymbol{\sigma})\, Y(\boldsymbol{\varepsilon}^{\mathrm{p}})\, r(\omega_{\mathrm{c}} + \omega_{\mathrm{f}})\, \mathfrak{C}(T, \boldsymbol{\sigma}, \boldsymbol{\varepsilon}^{\mathrm{p}}, \dot{\boldsymbol{\varepsilon}}^{\mathrm{p}})\, \dot{\varepsilon}^{\mathrm{p}}_{\mathrm{vM}}, \\
\dot{\omega}_{\mathrm{f}} &= H_{\mathrm{f}}(\boldsymbol{\sigma})\, r(\omega_{\mathrm{c}} + \omega_{\mathrm{f}})\, \mathfrak{F}\left(T, \boldsymbol{\sigma}, \boldsymbol{\varepsilon}, \boldsymbol{\varepsilon}^{\mathrm{p}}\right) \dot{\varepsilon}^{\mathrm{p}}_{\mathrm{vM}}
\end{aligned}$$

The experimental determination of the creep and fatigue damage contribution in the generalized damaged state of the material on practice is not a realistic task. Therefore, and in order to simplify the problem, the single damage

variable ω can be introduced. The evolution of ω must be dependent on both creep and fatigue damage processes, according to the loading conditions. The influence of the creep and fatigue damage on the general damaged state of the material is referred to as *creep-fatigue damage interaction.*

The simplest case of the accounting of creep-fatigue damage interactions can be described by the following expression:

$$\dot{\omega} = \dot{\omega}_{\mathrm{c}} + \dot{\omega}_{\mathrm{f}}, \tag{2.61}$$

however, there are several more complicated and more convenient variants for the description of the creep-fatigue damage interaction in the literature [31, 46].

2.7.3.2 Law of linear accumulation and interaction

This rule was originally introduced by Palmgren [63] and further developed by Miner [45]. Formulated in terms of the current notation, the linear accumulation rule is defined by the following expression:

$$\mathrm{d}\omega = \frac{\mathrm{d}t}{t_{\mathrm{c}}(T,\boldsymbol{\sigma})} + \frac{\mathrm{d}t}{t_{\mathrm{f}}(T,\boldsymbol{\sigma},\boldsymbol{\varepsilon},\boldsymbol{\varepsilon}^{\mathrm{p}},\dot{\boldsymbol{\varepsilon}}^{\mathrm{p}})}, \tag{2.62}$$

where $t_{\mathrm{c}}(T,\boldsymbol{\sigma})$ is the time to rupture in creep under constant load $\boldsymbol{\sigma}$ and temperature T, $t_{\mathrm{f}}(T,\boldsymbol{\sigma},\boldsymbol{\varepsilon},\boldsymbol{\varepsilon}^{\mathrm{p}},\dot{\boldsymbol{\varepsilon}}^{\mathrm{p}})$ is the time to rupture under pure periodic loading with generalized loading conditions:

$$\begin{aligned}
&\boldsymbol{\sigma} = \boldsymbol{\sigma}(t),\\
&\boldsymbol{\varepsilon} = \boldsymbol{\varepsilon}(t),\\
&\boldsymbol{\varepsilon}^{\mathrm{p}} = \boldsymbol{\varepsilon}^{\mathrm{p}}(t),\\
&T = T(t)
\end{aligned}$$

The represented summation rule is the simplest approach in order to take into account the creep-fatigue damage interaction. Satisfactory in some cases, this method is ineffective for many materials [31].

2.7.3.3 Law of nonlinear accumulation and interaction

The nonlinear summation rule is based on the assumption on the additivity of creep and fatigue damage. In particular, during the formulation of the generalized law for the creep and fatigue damages and their interaction the following physical effects must be taken into account:

- The presence of creep damage accelerates the nucleation and growth of transgranular microcracks

- Fatigue damage increases the creep damage accumulation rate, because transgranular effects induces internal stress concentrators affecting the creep damage rates.

Within the current notation, the simplest case of the nonlinear accumulation rule is given by (2.61). The generalized expression, which may represent the main principles of nonlinear damage summation law, is the following:

$$\dot{\omega} = F(\dot{\omega}_{\mathrm{c}}, \dot{\omega}_{\mathrm{f}}), \tag{2.63}$$

where $\dot{\omega}_{\mathrm{f}}$ is corresponding to the accumulation of fatigue damage, $\dot{\omega}_{\mathrm{c}}$ is the damage accumulation, which is induced by creep processes and takes place during the creep test. Obviously, the presented expression is represented by certain mixture rule.

Presented approach (2.63) is used in current research for accounting of the creep-fatigue damage interaction. Application of continuous fatigue damage model allows to stay in single time scale, however it affects the computational costs needed for current approach. On the other hand, the continuous fatigue damage model allows to estimate the lifetime of the material for cases of complicated loading profiles, which are not available for the testing equipment.

The particular expression for the above-mentioned mixture rule F can be derived only taking into account properties of the specific material. However, the formulation of the expression is the task of engineer and, therefore, depends on the knowledges of the developer. In additional, the usability of the constitutive model is also depends on its complexity, therefore simple models with less number of the material parameters are preferable.

2.8 Complete set of governing equations

The complete set of basic equations includes the relationship of strains, stresses, backstress deviator and damage variables. Derived in terms of implicitly defined functions, the system of governing equations includes the following relations:

- Kinematic equation

$$\boldsymbol{\varepsilon} = \frac{1}{2}\left[\nabla \boldsymbol{u} + \nabla \boldsymbol{u}^{\mathrm{T}}\right]$$

- Equilibrium equation

$$\boldsymbol{\nabla}\cdot\boldsymbol{\sigma}+\boldsymbol{\gamma}=\boldsymbol{0}$$

- Constitutive equations

$$\boldsymbol{\varepsilon}=\boldsymbol{\varepsilon}^{\mathrm{el}}+\boldsymbol{\varepsilon}^{\mathrm{p}}+\boldsymbol{\varepsilon}^{\mathrm{th}}$$

$$\boldsymbol{\sigma}=\left[\kappa(\omega)+\chi\right]\left[\lambda\langle\mathrm{tr}[\boldsymbol{\varepsilon}^{\mathrm{el}}]\rangle_{+}\boldsymbol{I}+2\mu\boldsymbol{\varepsilon}_{+}^{\mathrm{el}}\right]+\left[\lambda\langle\mathrm{tr}[\boldsymbol{\varepsilon}^{\mathrm{el}}]\rangle_{-}\boldsymbol{I}+2\mu\boldsymbol{\varepsilon}_{-}^{\mathrm{el}}\right]$$

$$\dot{\boldsymbol{\varepsilon}}^{\mathrm{p}}=\frac{3}{2}\frac{\dot{\varepsilon}^{\mathrm{p}}_{\mathrm{vM}}}{\overline{\sigma}_{\mathrm{vM}}}\overline{\boldsymbol{s}},\quad \dot{\varepsilon}^{\mathrm{p}}_{\mathrm{vM}}=R(T)f\left(\frac{\overline{\sigma}_{\mathrm{vM}}}{1-\omega}\right),\quad \overline{\boldsymbol{s}}=\boldsymbol{s}-\boldsymbol{\beta}$$

$$\overline{\sigma}_{\mathrm{vM}}=\sqrt{\frac{3}{2}\overline{\boldsymbol{s}}\cdot\cdot\overline{\boldsymbol{s}}}$$

- Evolution equations

$$\dot{\boldsymbol{\beta}}=\frac{1}{\mu_{\mathrm{h}}}\frac{\mathrm{d}\mu_{\mathrm{h}}}{\mathrm{d}T}\dot{T}\boldsymbol{\beta}+\frac{2}{3}\mu_{\mathrm{h}}\left[\dot{\boldsymbol{\varepsilon}}^{\mathrm{p}}-\frac{3}{2}\dot{\varepsilon}^{\mathrm{p}}_{\mathrm{vM}}\frac{\boldsymbol{\beta}}{\beta_{*}(T,\boldsymbol{\sigma})}\right]$$

$$\dot{\omega}=F(\dot{\omega}_{\mathrm{c}},\dot{\omega}_{\mathrm{f}})$$

$$\dot{\omega}_{\mathrm{c}}=H_{\mathrm{c}}(\boldsymbol{\sigma})\,Y(\boldsymbol{\varepsilon}^{\mathrm{p}})\,r(\omega)\mathfrak{C}(T,\boldsymbol{\sigma},\boldsymbol{\varepsilon}^{\mathrm{p}},\dot{\boldsymbol{\varepsilon}}^{\mathrm{p}})\dot{\varepsilon}^{\mathrm{p}}_{\mathrm{vM}}$$

$$\dot{\omega}_{\mathrm{f}}=H_{\mathrm{f}}(\boldsymbol{\sigma})\,r(\omega)\mathfrak{F}\left(T,\boldsymbol{\sigma},\boldsymbol{\varepsilon},\boldsymbol{\varepsilon}^{\mathrm{p}}\right)\dot{\varepsilon}^{\mathrm{p}}_{\mathrm{vM}}$$

Functions $\kappa(\omega)$, $R(T)$, $f\left(\overline{\sigma}_{\mathrm{vM}}\right)$, μ_{h}, β_{*}, F, $r(\omega)$, $\mathfrak{C}(T,\boldsymbol{\sigma},\boldsymbol{\varepsilon}^{\mathrm{p}},\dot{\boldsymbol{\varepsilon}}^{\mathrm{p}})$, $\mathfrak{F}(T,\boldsymbol{\sigma},\boldsymbol{\varepsilon},\boldsymbol{\varepsilon}^{\mathrm{p}})$ are given in implicit form within the current chapter. Identification of the structure and parameters for them are given in Chapt. 3.

2.9 Summary

The aim of current chapter was to discuss the constitutive model and basic modeling principles which are used for the formulation of mathematical expressions for phenomena, which in particular are observed in cast irons. Chapter is focused on the constitutive model for inelastic material behavior, creep and fatigue damaging processes and their interaction. The elasticity is described by means of the linear elastic material model, taking into account only the dependence of the stiffness on the temperature and damage. The model is formulated under assumption of small strains, that is sufficient for strains upto $5-6\%$.

The following principles were used for the formulation of the constitutive model:

- the constitutive model must completely encompass major phenomenon taking place in the material
- the structure of the constitutive model is designed in order to unify the model for several materials of that class
- the aspiration to minimize the number of the model parameters is one of the principles which is used within the formulation of the model.

In particular, the described constitutive model is focused on material behavior, which is observed in cast irons GJV and D5-S with the vermicular and spherical graphite inclusions [29, 48, 49] . The model is formulated in general form. The customization of the implicit functions mentioned in Sect. 2.8 allows the use current constitutive model in both particular cases.

CHAPTER

3 Identification basics

The current chapter is focused on the discussion of existing methods for the solution of identification problem. The identification scheme is mainly focused on the application for the materials, which exhibit elastic and inelastic properties including creep and fatigue damage. The chapter presents available basic approaches for a solution of the identification problems, describing the step-by-step identification strategy structured by applied methods and flexibility to the experimental data.

3.1 Identification problem

The majority of constitutive models are usually formulated by means of a phenomenological approach, which gives good results within the qualitative analysis of the material's behavior. Nevertheless, the formulated framework of the constitutive model requires a detailed definition of functions, which describes the particular processes in the material, and the determination of their parameters.

A mathematical formulation of the constitutive model is termed the *structure identification* [36]. In general, the structure identification problem is represented by the following expression:

$$\boldsymbol{c} = \arg\left[\xi(\boldsymbol{c}, \boldsymbol{d}) = 0\right],$$

where $\boldsymbol{c}$ is the target constitutive model, $\boldsymbol{d}$ is the vector of experimental data and ξ is the Gauß function, representing deviation between the experimental data $\boldsymbol{d}$ and estimation by constitutive model $\boldsymbol{c}$. Within the framework of current work, the structure of the constitutive model $\boldsymbol{c}$ is formulated by means of

a phenomenological modeling approach (see Chapt. 2), taking into account the behavior of the material observed in given experimental data.

A phenomenological formulation of the framework of a constitutive model reduces the structure identification problem to *a parameters identification* problem. Taking into account the reduction of the size of the identification problem, the parameters identification problem is represented by the following expression:

$$\boldsymbol{p} = \arg\left[\xi(\boldsymbol{c}(\boldsymbol{p}), \boldsymbol{d}) = 0\right],$$

where $\boldsymbol{p}$ are model parameters. Within the framework of the shown problem structure, the determination of material parameters is the *inverse problem* [36]. However, the discrete nature of experimental data $\boldsymbol{d}$ and concomitant measurement error leads to the scatter of solutions $\boldsymbol{p}_i$.

When the error function ξ becomes undesirably high, the majority of constitutive models in practice are extending, which normally leads to an increase of the number of material parameters. However, the error of experimental data and their discrete structure in particular cases leads to the situation, that a further extension of the model does not make sense. Moreover, an excessive increasing of the model complexity may lead to *overparametrization* problems. Thereby, the minimalistic approach in the formulation of the constitutive model $\boldsymbol{c}$ is preferable, because it reduces the size of the parameters identification problem and avoids possible overparameterization problems.

By the application identification approaches, specific experimental data and time-consumption, the identification problem can be contingently separated on two different parts: primary and secondary identification stage. The identification of the structure of the constitutive model and preliminary estimation of the material parameters of this model is the main task of the primary identification. The step is restricted by the identification approaches and includes only the experimental data which explicitly represents the phenomenological processes taking place in the material. In except to the previous one, the secondary identification step is mainly related to an additional calibration of the constitutive model according to entire set of the available experimental data.

3.1.1 Trial approach

The trial approach is based on the solution of the direct problem (SDP) represented in Fig. 3.1. The current approach allows the determination the individual vector of material parameters simultaneously. The method includes the iteration process with the following steps:

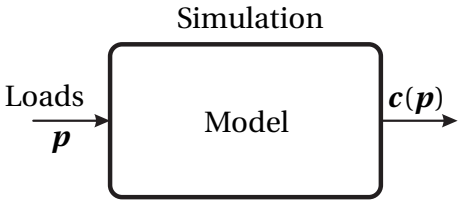

Figure 3.1: Direct problem scheme

- estimate guess values of $\boldsymbol{p}$,
- solve direct problem for given $\boldsymbol{p}$,
- if error function $\xi(\boldsymbol{c}(\boldsymbol{p}), \boldsymbol{d})$ does not satisfy the accuracy requirements, then change $\boldsymbol{p}$ and iterate again.

The trial approach is useful for solving the inverse problem for a wide range of constitutive models, and simply realizable by programming tools. However, applications of the trial approach for the identification of constitutive models with a large number of parameters are time-consuming and can lead to inaccurate solutions. Moreover, an overparametrization of the constitutive model in this particular case leads to the situation, when the several variants of $\boldsymbol{p}_i$ satisfies the requirements of the problem.

3.1.2 Hand fitting approach

The hand fitting approach is useful when material parameters are related to processes explicitly observed in the experimental curves. In the particular cases, the application of the hand fitting [36] method is also available for processed experimental curves. For instance, hand fitting is easily used for the determination of Young's modulus E, yields strength R_{p02}, tensile strength σ_{u}, fracture strength σ_{f} and others explicitly observed representative measures. A more complicated example of the hand fitting approach is given by Lemaitre and Chaboche [31] in the determination of Norton's law parameters, which can be identified in a trivial way by the plot of $\dot{\varepsilon}^{\mathrm{p}}$ versus σ in double logarithmic scale. The mentioned above approach do not requires complicated computations and can give instant results in the structure and parameters identification problem.

When the part of the constitutive model related to explicitly observed concomitant processes is identified, the experimental data in the particular cases

can be decomposed into the constituents representing more implicit components of the material behavior like backstress or damage. Therefore, the application of the hand-fitting identification approach, in some cases, allows us to determine a complete set of material parameters. However, the accuracy of such an identification decreases within each processing of the experimental data. Mainly it is related to the magnification of the existing error of the experimental data by the error of the estimation of the constitutive model.

Hand fitting approach is useful for a rapid estimation of material parameters. It requires experimental data representing mechanical phenomena in explicit form. However, in some cases, the implicit phenomena (e.g. hardening, softening, etc.) can be identified by means of hand fitting approach. Within the current work, the above-mentioned approach is used for the determination of a guess vector of material parameters.

3.1.3 Optimization

Optimization is the problem of the search for the best solution among all feasible solutions. Within the framework of the identification problem, the optimization is more corresponding to the deterministic minimization problem intended for the solution of the inverse parameters problem. The essential idea of optimization in the identification problem is mathematically represented by the following expression:

$$\boldsymbol{p} = \arg\min_{\boldsymbol{p}\in\mathbb{P}} \left[\xi(\boldsymbol{c}(\boldsymbol{p}), \boldsymbol{d})\right], \tag{3.1}$$

where $\mathbb{P}$ is the space of material parameters $\boldsymbol{p}$.

The optimization method may be grouped by the restrictions according to the target function. Thus, the zero-order method requires only existence of the target function $\xi(\boldsymbol{c}(\boldsymbol{p}), \boldsymbol{d})$, while first-order methods use in addition the gradient $\nabla_{\boldsymbol{p}}\xi(\boldsymbol{c}(\boldsymbol{p}), \boldsymbol{d})$, and, therefore, requires differentiability of the target function $\xi(\boldsymbol{c}(\boldsymbol{p}), \boldsymbol{d})$. Examples of zero-order deterministic optimization methods available for target functions of a vector argument are Simplex algorithm [53, 86] and Powell's conjugate directional method [70, 71, 74]. Above mentioned approaches are useful by means of their unpretentiousness to the target function. In except to zero-order methods, the gradient-based optimization methods together with existence of the target function and differentiability requires also continuity of the target function and their derivative in the space of material parameters $\mathbb{P}$. In principal, high requirements to the target function is compensated by the efficiency of the approach. However, when the mentioned condition may be not satisfied, the application of zero-

order methods is preferable. Examples of gradient-based methods are Gauss-Newton method [87], Broyden-Fletcher-Goldfarb-Shanno (BFGS) method of unconstrained optimization [14, 87], modified L-BFGS-B algorithm for optimization with constraints [11, 89], among others.

3.1.4 Neural networks

Neural networks were first introduced in a research paper by McCulloch and Pitts [42]. The paper was focused on the modeling of biological processes in the brain, therefore the approach was named *neural networks*. General information on neural networks is given by Haykin [22]. The particular application of neural networks in the solution of the inverse problem is described by Yoshimura et al. [88] and Huber [23].

The concept of neural networks is based on the simulation of the relationship between the *neuron cell*. Neurons are arranged in layers. Each cell has synaptic weights $\boldsymbol{w}$ defining the behavior of the cell. The determination of synaptic weights is referred to as *training process*.

Neural networks are useful in a wide range of direct and inverse problems, including the parameters identification problem. The trained neural network gives the instant result of the parameters identification problem. However, there are disadvantages of the identification based on the neural networks: neural networks require a large volume of input data for the training process, the training data must be representative and may not be contradictory. Moreover, the excessive training of the network can lead to the *overtraining* problems. In order to avoid the overtraining problems, the training data must be diversified.

The training of neural networks requires the formulated structure of the constitutive model $\boldsymbol{c}(\boldsymbol{p})$. Mainly training may be mathematically represented by the following expression:

$$\xi(\boldsymbol{w}) = \sum_{i=1}^{N} ||\boldsymbol{p}_i - \boldsymbol{y}_{\text{out}}(\boldsymbol{c}(\boldsymbol{p}_i), \boldsymbol{w})|| + \gamma||\boldsymbol{w}||, \tag{3.2}$$

where $\xi(\boldsymbol{w})$ is the target error function using for the training of the neural network, the response of the constitutive model $\boldsymbol{c}(\boldsymbol{p}_i)$ is used as input of the network, $\boldsymbol{y}_{\text{out}}$ is the signal on the output of the network, γ is the regularization parameter, $\boldsymbol{p}_i$ is the arbitrary chosen set of the material parameters, $i = 1, 2, ..., N$, $||.||$ is the norm operator, which can differs for different constitutive models.

Thereby, the feature of the training process restrict the application of the neural networks on the solution of the parameters identification problem.

3.1.5 Remarks

The above-mentioned identification approaches can be used for the solution of the structure and parameters identification problem. Each of the approaches have the different requirements to the amount and quality of experimental data, restrictions to the solving problems, and limitations induced by the requirements to Gauß function ξ. Obviously, the application of a composition of the above-mentioned identification methods increases the efficiency of the identification, makes the solution more flexible and invulnerable to the artefacts and error of experimental data.

Within the current work, the combined identification approach is used, including the primary and the secondary identification steps. The primary identification step is mainly focused on the determination of the structure of the material-dependent functions, used in the constitutive model, and estimation of the material parameters for the model. For above-mentioned step only trial and hand-fitting approaches are used. The secondary identification step is optimization-based and may take into account complete set of the available experimental data.

3.2 Experimental data

The current section is focused on the representation of the available experimental data. The data are provided according to the research project subjected to the modeling of the inelastic material behavior of the GJV cast iron including the creep-fatigue damage. The experimental values are secured by the confidence agreement, and, therefore, within the current work are presented in the normalized form with respect to normalizing factors σ_n, ε_n, $\varepsilon^\mathrm{p}_\mathrm{n}$, $\dot{\varepsilon}^\mathrm{p}_\mathrm{n}$, N^* and melting temperature of the material T_m.

3.2.1 Young's modulus

Majority of steels and cast irons exhibit a significant influence of temperature on the elastic properties. In general, an increase of the operation temperature leads to the reducing of the material stiffness. GJV cast iron is not an exception: the stiffness for $0.573\,T_\mathrm{m}$ is almost two times lower than for $0.253\,T_\mathrm{m}$. Therefore, in order to determine the temperature dependence of Young's modulus a series of experiments at different temperatures is required. The available experimental data of Young's modulus for GJV cast iron are shown in Fig. 3.2.

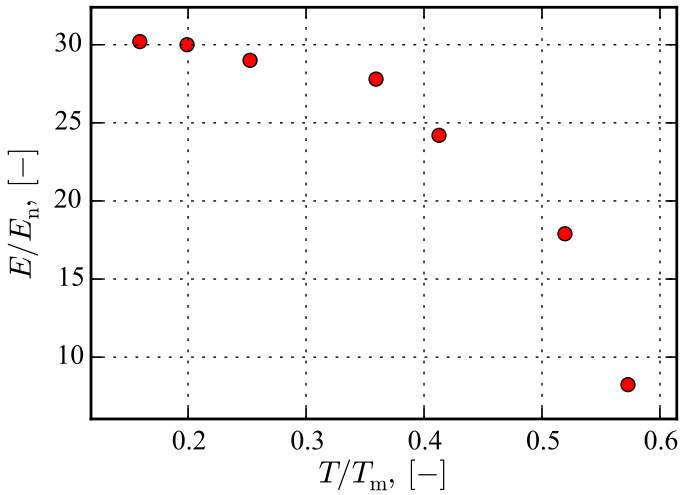

Figure 3.2: Young's modulus at different temperatures

3.2.2 Creep tests

The experimental data of creep tests are given for temperatures of $0.359\,T_{\mathrm{m}}$, $0.466\,T_{\mathrm{m}}$, $0.519\,T_{\mathrm{m}}$ and $0.573\,T_{\mathrm{m}}$ and different levels of applied loads. The resultant experimental data are provided in the form of inelastic strains with respect to time. The current step of the identification require the operation with measured by the experimental data inelastic strain rates. Thereby, the application of the experimental data from creep tests in the identification procedures requires the processing of proven experimental data, the evaluation of inelastic strain rates, and the removing of undesired noises, which arise after the differentiation of the experimental inelastic strains. In order to reduce noises in the experimental data, the approximation of the smoothed inelastic strain is performed according to available experimental data, which for the particular loads T =0.519T_{m}, σ =0.37σ_{n} shown in Fig. 3.3a. The smoothing algorithm is based on the approximation of the experimental data by the polynomial functions of different order and further averaging. Thereby artificial fluctuations of the calculated inelastic strain rates can be avoided.

For instance, the average approximation of the creep curve presented in Fig. 3.3b is based on the fittings with orders of polynomials from three to ten. In principal, the application of the orders of polynomials upto half of the length of vector of experimental data $\boldsymbol{d}$ is acceptable, because the averaging technique reduces the fluctuations normally taking place in the polynomial fittings of high order.

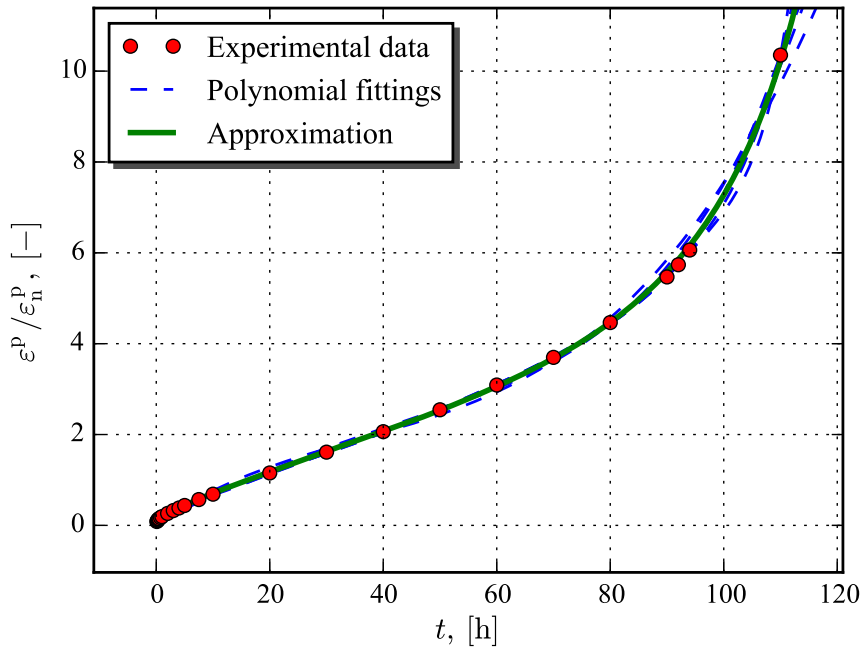

(a)

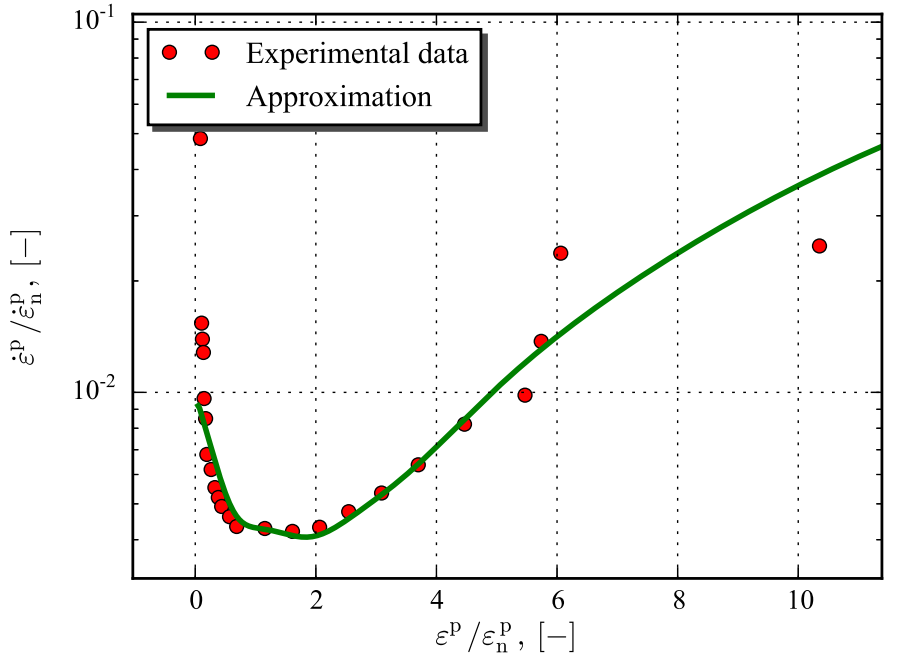

(b)

Figure 3.3: Processing of experimental data: **(a)** smoothing of experimental creep strains, **(b)** computing creep strain rates by the differentiation of experimental data and obtained smoothed values

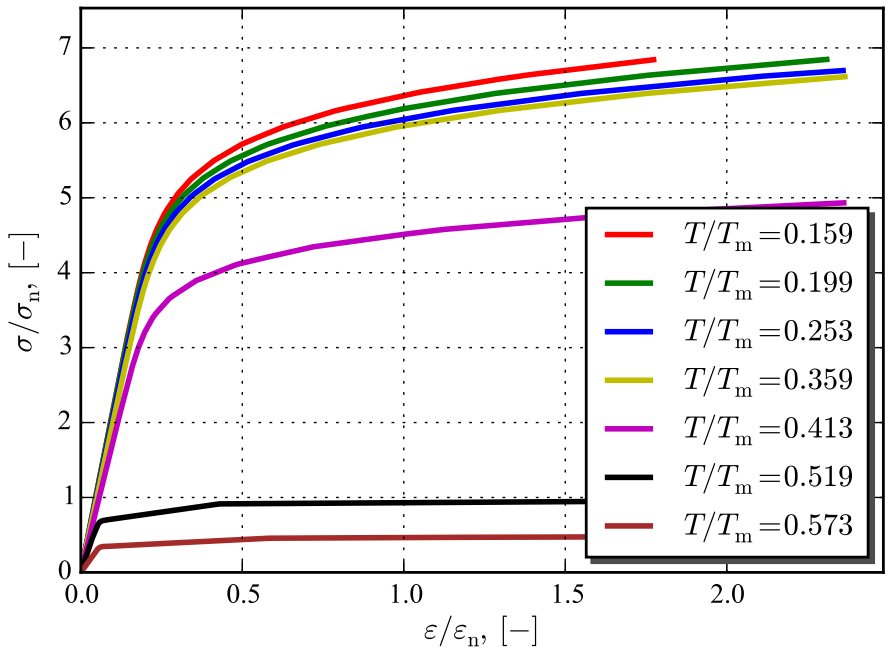

Figure 3.4: Tensile tests at different temperatures

3.2.3 Tensile tests

Tensile tests of GJV material are given for temperatures $0.159T_m$, $0.199T_m$, $0.253T_m$, $0.359T_m$, $0.413T_m$, $0.519T_m$ and $0.573T_m$. These tests are strain controlled. The loading rates within current tensile tests are the same, $\dot{\varepsilon} = 3.6\,\mathrm{h}^{-1}$. The results of tensile tests are given in Fig. 3.4.

The presented experimental data includes the elastic and inelastic material behavior at the different temperatures and can be utilized in the identification of the corresponding constitutive model.

3.2.4 Cyclic loading at constant temperature

Cyclic loading at the specific temperatures is normally applied in low-cycle fatigue (LCF) tests. There are two principal kinds of information, which one can obtain from such experiments: a stress response for a given profile of the load and the number of cycles to rupture N_A. The first one is used for the identification of a part of the constitutive model required to describe the inelastic material behavior. On the other hand, the number of cycles to rupture can be used for the identification of the creep-fatigue damage model.

Within the frame of current work the experimental data from low-cycle fatigue tests performed for the specific temperatures $0.253T_m$, $0.359T_m$,

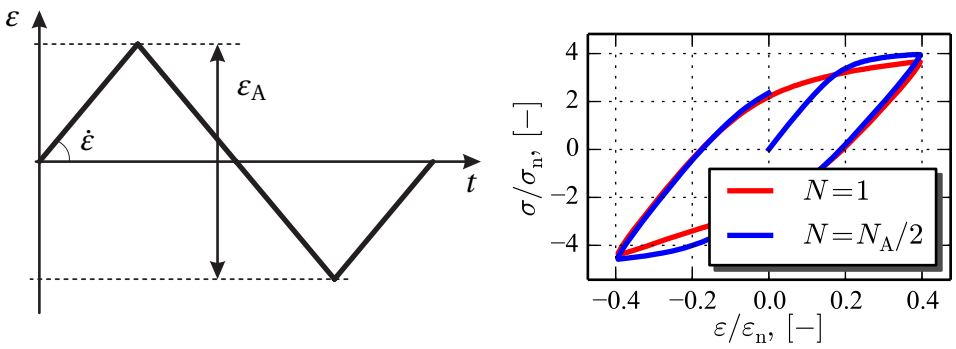

(a) **(b)**

Figure 3.5: LCF tests: **(a)** saw-type strain loading profile, **(b)** stress-strain hysteresis loops

$0.413T_m$, $0.519T_m$, $0.573T_m$ and saw-type loading profiles of strains with different magnitudes were used. The magnitudes of strain are given in the different variations from the smallest $\varepsilon_A = 7.96 \cdot 10^{-2}\varepsilon_n$ to highest $\varepsilon_A = 1.581\varepsilon_n$. The identification of the constitutive model for the inelastic material behavior with the frame of single temperature can be performed by means of the experimental data from the LCF test with highest strain amplitude. Mainly it is related to fact, that inelastic material behavior is represented in such curves in the most complete way. Moreover, the representative cycles of the stress for initial ($N = 1$) and steady ($N = N_A/2$) regimes can be used within the identification of the constitutive model.

The available experimental data are given for the same strain rate $\dot{\varepsilon} = 3.6\,\mathrm{h}^{-1}$ and have a symmetric saw-type loading profile schematically shown in Fig. 3.5a. The stress response for represented the strain loading profiles are given for the initial $N = 1$ and steady $N = N_A/2$ loading cycles. The hysteresis of the stress response is represented for the specific case of loading conditions ($T = 0.413T_m$, $\varepsilon_A = 0.79\varepsilon_n$) in Fig. 3.5b.

The experimentally measured lifetime of the material at the different loading conditions is given in terms of the number of cycles to rupture in Fig. 3.6. The experimental results are given for the above-mentioned set of temperatures and different amplitudes of applied strain.

It must be mentioned, that damage in LCF test may be induced only by cyclic inelastic deformations and normally leads to the failure at $N_A \in [10^3, 5 \cdot 10^3]$ accounting to different loading conditions. Thereby, only the experimental data corresponding to the above-mentioned conditions can be used for the identification with the frame of current research. However, experimental data

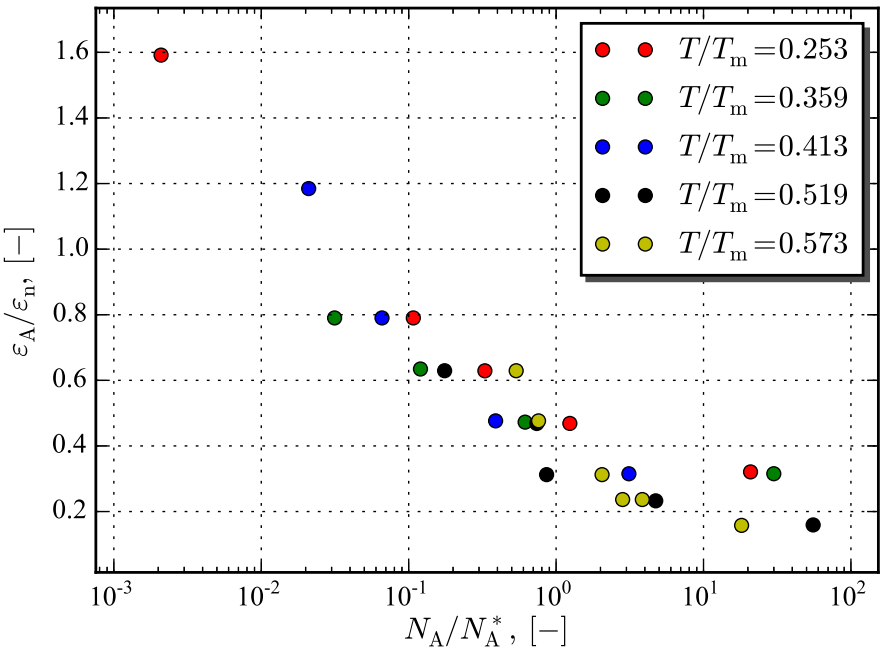

Figure 3.6: Number of cycles to rupture of GJV cast iron at the different loading conditions

lying out of mentioned range are also utilized in the secondary identification with significantly reduced weighting factors.

3.2.5 Cyclic thermo-mechanical loading

Experimental data from the thermo-mechanical fatigue tests (TMF) are also available for the GJV cast iron. The results of above-mentioned tests can be used for the identification of the constitutive model for the inelastic material behavior and creep-fatigue damage model. Similar to LCF tests, the experimental results for initial and steady loading cycles can be used in the identification of inelastic material properties. Available experimental numbers of cycles to rupture can be used for the identification of the constitutive model for GJV cast iron. The complicated loading profile of strain and temperature can be used to perform the verification of the identified constitutive model for inelastic material behavior and creep-fatigue damage.

TMF tests are performed by the application of cyclic strain and temperature. Within the framework of provided experimental data, the strain profiles differ by the shape of the loading profile and by the magnitude (see Fig. 3.7b). The temperature profiles are similar (see Fig. 3.7a). The shown temperature

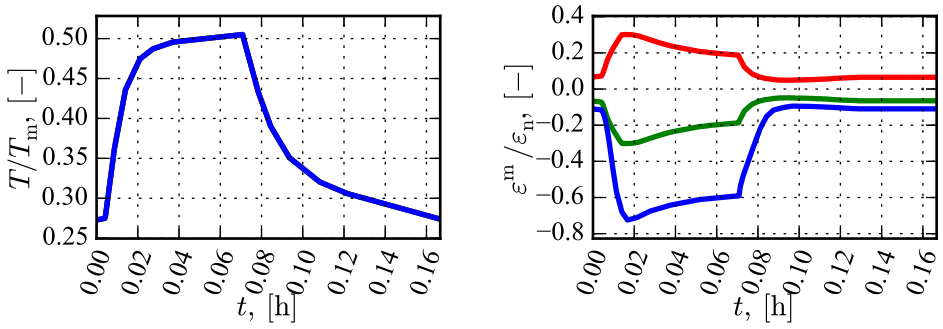

(a) **(b)**

Figure 3.7: Loading profiles of TMF tests (– Probe 1, – Probe 2, – Probe 3): **(a)** temperate, **(b)** mechanical strain (3.3)

and strain profiles are particular cases of loading profiles utilized within the different TMF tests. It must be noted that variable ε^{m} represented in Fig. 3.7b is the mechanical part of strain (3.3). The stress responses on the mentioned above loads are shown in Fig. 3.8.

$$\varepsilon^{\mathrm{m}} = \varepsilon - \varepsilon^{\mathrm{th}} \tag{3.3}$$

The lifetime of the material sample measured at the TMF test can be also used for the identification and verification of the constitutive model for the creep-fatigue damage. It must be noted, that except the LCF tests, the accumulation of damage in current case can not be described in terms of the amplitudes of strains and stresses, because the profile of the applied loads in this case plays significant role and, unfortunately, can not be completely represented by means of amplitudes. The absence of reliable discrete models is one of the reasons for the development of the continuous damage model.

In addition, the degradation of the stiffness of the material can be estimated by means of the TMF tests. The bounding values of the stress response is shown in Fig. 3.9 for the particular TMF test. The reduction of stresses is typically observed at the last cycles of the test and corresponds to the last stage of the damaging, when the macrocrack growth in the material. The significant reduction stress at the last cycles of the TMF test is assumed to be the result of above-mentioned damaging process.

Also it must be noted, that the reduction of stresses is typically observed at cycles $N > 0.9N_{\mathrm{A}}$ and can be easily neglected, because the scatter of the experimental estimation of the lifetime can reach higher values. Moreover, the error of estimation provided by the constitutive model for creep-fatigue

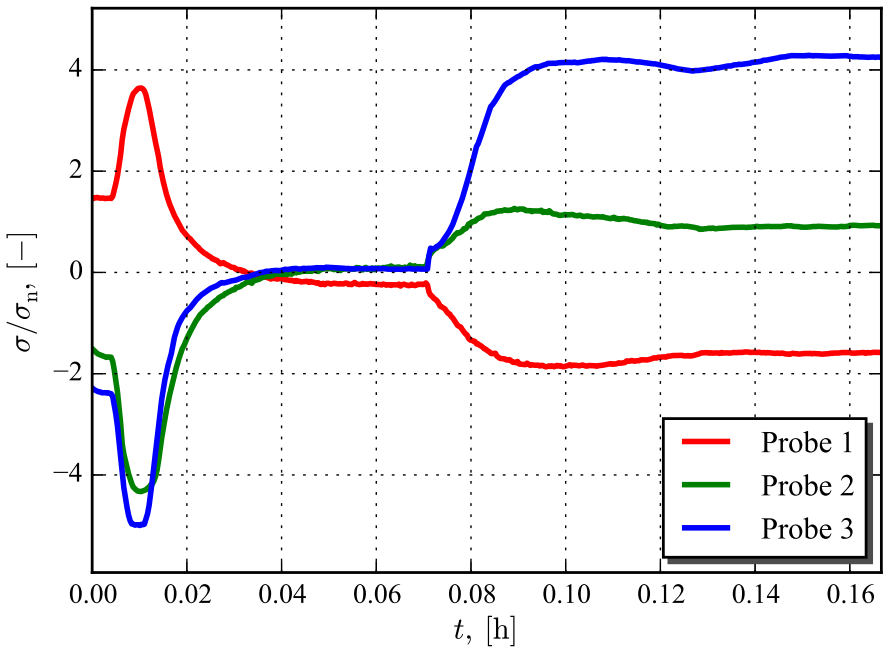

(a)

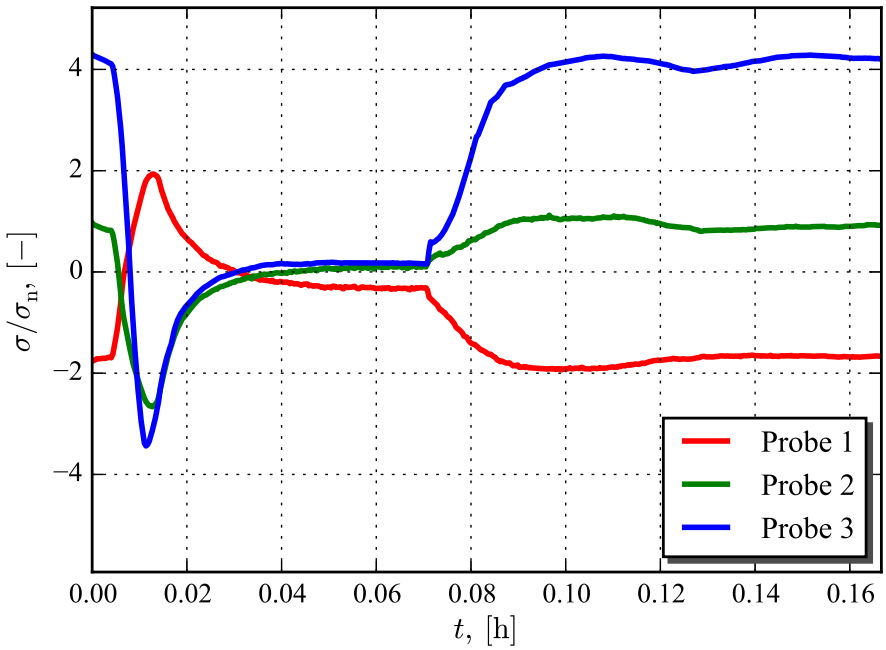

(b)

Figure 3.8: Experimental data from TMF tests: **(a)** stress response at $N = 1$, **(b)** stress response at $N = N_A/2$

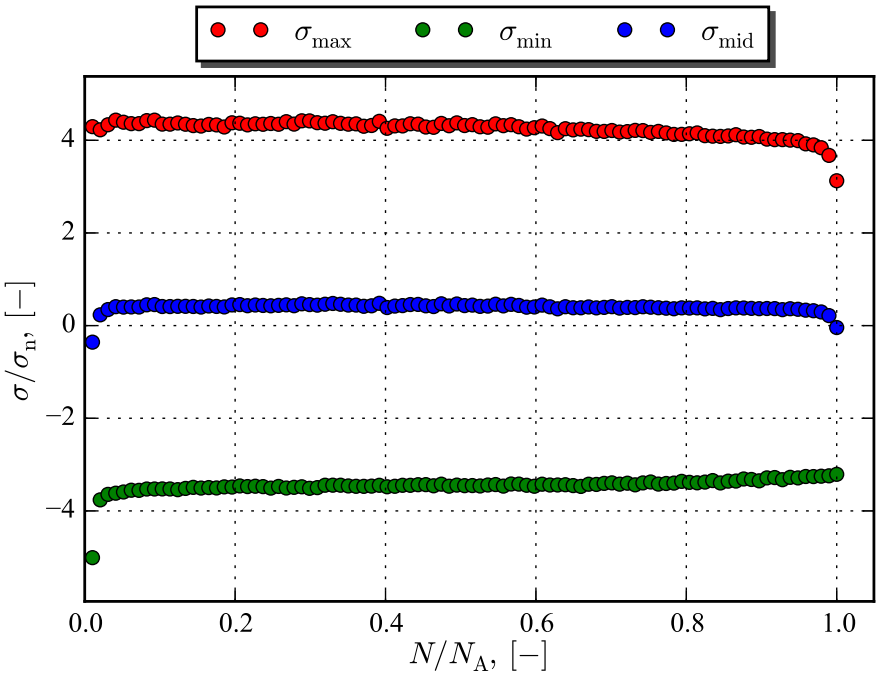

Figure 3.9: The stress bounds during the TMF tests

damage can have in the best case factor two. Thereby, the reduction of the stiffness of the material within the frame of current research is considered only for the sake of complicity.

3.3 Identification strategy

The current section presents the general strategy of the identification. Obviously, the proper identification must include the determination of the structure of the constitutive model based on the phenomenological approach and the determination of the material parameters including the consideration of the generalized model response in the different kinds of the experiments. Thus, in this work, the constitutive model is developed in order to represent the behavior of the material at creep regime, strain controlled tensile loads, isothermal cyclic loads with saw-type strain loading profile, cyclic loads with complicated strain and temperature loading profiles, etc. Therefore, the formulation of the constitutive model and determination of material parameters must take into account the entire set of the experimental data mentioned above.

3.3.1 Primary identification step

The starting point of the solution of the identification problem is the determination of the structure of the constitutive model. Particularly, the structure identification problem can be resolved by means of the phenomenological modeling of the process observed in the general response of the material on the applied loads. This part of the solution of the structure identification problem (see Chapt. 2) is general and valid for wide class of materials representing the similar behavior. However, the material-dependent functions introduced in the constitutive model must be identified with respect to each specific material.

Mainly, the primary identification is performed using the trial and hand-fitting identification approaches. Simple plotting of the experimental data in the different scales may give the sufficient volume of information for the formulation of the structure of the relations able to describe the considered data. However, the mentioned above method requires the specific type of the experimental data, where identifying processes are reflected in explicit form. For instance, the temperature relation of Young's modulus may be identified by means of hand-fitting approach because it is not affected by other implicit phenomenological processes. However, the damage is exception of this statement, because it exhibits the significant influence on the elastic material properties at the terminal stage of the cyclic tests preceding to the failure.

The identification of the constitutive model for the inelastic material behavior in general case can be performed independently to the elastic properties. However, the application of tensile tests in this part of identification requires the information about the elastic material properties that makes obligatory the preliminary identification of the elastic properties. Obviously, the influence of the damage on the elastic material properties can be neglected at this stage of the identification. It should be noted, that constitutive model identified upto current stage is able to represent the inelastic material behavior on the primary and secondary creep stages of the creep tests and completely describe the response of the material in stresses and inelastic strains during the cyclic loading.

In order to predict the material behavior at the tertiary creep stage the identification of the creep damage model is required. It can be performed only in the case, when the constitutive model of the elastic and inelastic material properties is completely identified. Thereby, the identification of elastic and inelastic material properties must precede the identification of the creep damage.

The structure of the fatigue damage model and preliminary estimation of

the material parameters can be identified with use of the idealized stress hysteresis, which can be obtained under the assumption about the ideal plasticity of the material. In principle, the identification of the fatigue damage model can be performed independently from the elastic and inelastic material properties because it mainly based on the experimental data. Thus, the primary identification of the fatigue damage model can be performed independently from the rest part of the constitutive model.

According to the structure of the current constitutive model, the mentioned above three stages of the identification belongs to the primary identification step. The identification of advanced phenomenon taking place in the material during the complex thermo-mechanical loads (i.e. hardening rate, creep-fatigue damage interaction) can not be performed by means of only hand-fitting and trial identification approaches and requires more sophisticated scheme of the identification.

3.3.2 Secondary identification step

When the primary identification step is completed, the secondary identification step based on the optimization technique can be performed. The advantage of the optimization-based identification is the good flexibility and unpretentiousness to the experimental data. In the secondary identification step entire set of the available experimental data can be used, including tests with complex loads. Within the frame of the current work, such tests are represented by LCF and TMF.

The application of the optimization approach requires the definition of the error function. The different types of experimental data require detailed consideration of the specific error functions for the each case. Moreover, the output error must be normalized in order to unify the influence of the comparing data of different type, i.e. stress, inelastic strain, number of cycles to rupture, etc.

In order to take into account the different influence of the experimental data onto the general result, the weight factors are considered. Within the current research the choice of the weights including the following aspects:

- The trustability of the experimental data must be taken into consideration. The presence in experimental data the artificial noises, interruptions, non-realistic abrupt jumps, etc., requires corresponding regulation of the weight factor. The significant decreasing or even elimination of the weight allows us to include into the identification the experimental data with even low trustability and quality.

- The formulation of the constitutive model must account the main operation conditions of material. The focusing of the constitutive model onto the strict operation conditions can be regulated by means of the decrease of the weights for the experimental data, which are not correspond to the mentioned range of the loading conditions. For instance, if a constitutive model is needed for the simulation of the material behavior subjected to constant load, than experimental data from creep tests must include the major contribution into the error function. If the constitutive model is developed for the description of the cyclic material behavior, then weights corresponding to the cyclic tests must be significantly higher than rest.

The important point of the secondary step of the identification is the choice of the optimization method. Within the particularity of the current problem, the zero-order optimization approaches, i.e. Simplex method [53, 86] or Powell's method [70, 71, 74], are preferable. Mainly they are related to the quality of the experimental data: the application of high-performance gradient-base optimization methods requires the existence and smoothness of the error function for each next iteration of the algorithm, which is not satisfied due to the quality of experimental data. However, the application of Powell's method becomes very time-consuming with a number of material parameters more than 20. In this case the application of Simplex approach is recommended.

3.4 Summary

Within the current chapter general strategy of the solution of the identification problem is discussed, main approaches for solution of a structure and parameters identification problem are described, step-by-step approach for the solution of the identification problem for the specific material is presented. The identification is recommended to split onto the primary and secondary steps, which differs by the definition of the solving problem, methodology and requirements to the experimental data.

Given for the particular material, the presented strategy of the identification is valid for constitutive models describing the inelastic material behavior including creep-fatigue damage in the wide class of cast irons. The identification of the inelastic material properties and material damage model is recommended to divide onto the primary step, which is focused on the structure identification and determination of the preliminary vector of material param-

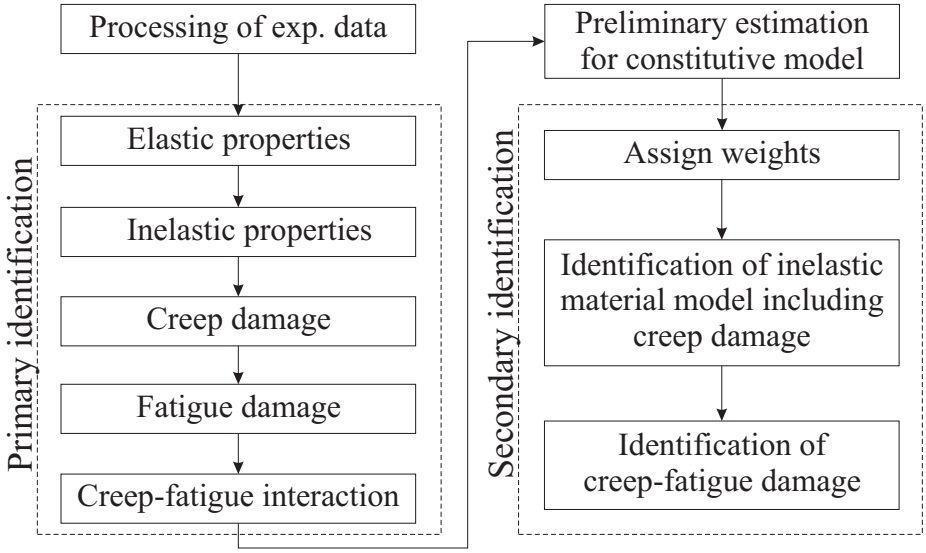

Figure 3.10: General structure of the identification scheme

eters, and the secondary step based on the numerical optimization-based approach and focused on the solution of the parameters identification problem.

Identification of the complete constitutive model is preferable to perform through the decomposing the constitutive model into the independent or one-side dependent constituents classified by the phenomenological types (i.e. elastic and inelastic properties, creep and creep-fatigue damage, etc.). The consecutive identification of the conditionally independent parts of the constitutive model allows us to decompose the problem into the independent units with the particular "parent-child" dependence. However, the mentioned identification structure leads to certain difficulties related to the chain of the modifications induced by the change of "parent" unit. The mentioned difficulties are mainly belong to the primary identification step, whereas the secondary identification is not vulnerable to the modification of constitutive model. Resultant identification scheme described within the framework of the current chapter is shown in Fig. 3.10.

CHAPTER

4 Primary identification

In this chapter, the primary stage of the identification problem is discussed. Mainly, the primary step is based on the trial and hand fitting identification approaches and needed for the determination of the material dependent functions $g(\omega)$, $R(T)$, $f\left(\overline{\sigma}_{\mathrm{vM}}\right)$, μ_{h}, β_*, F, $r(\omega)$, $\mathfrak{C}(T,\boldsymbol{\sigma},\boldsymbol{\varepsilon}^{\mathrm{p}},\dot{\boldsymbol{\varepsilon}}^{\mathrm{p}})$, $\mathfrak{F}(T,\boldsymbol{\sigma},\boldsymbol{\varepsilon},\boldsymbol{\varepsilon}^{\mathrm{p}})$ and the estimation of guessing values for the material parameters.

The behavior of the material, subjected to complex operation conditions, includes different phenomena, such as elasticity, inelastic behavior, creep-fatigue damage, etc. The majority of the above-mentioned processes are independent or one-side dependent. Therefore, the identification problem for the complete constitutive model, in particular, can be decomposed on the identification problems of less dimension for the independent (or one-side dependent) material properties. The reduction of the problem size allows us to utilize the different identification approaches for different nature of processes observed in the material at the operation conditions. Moreover, the application of identified material parameters allows us to process the available experimental data in order to clarify phenomena taking place in material.

4.1 Reduction of constitutive model

The identification procedures require the simplification of the constitutive model for the uniaxial case. The stress tensor at the uniaxial loading of the material sample is following:

$$\boldsymbol{\sigma} = \sigma \boldsymbol{e}_1 \otimes \boldsymbol{e}_1, \Rightarrow \sigma = \boldsymbol{\sigma} \cdot\cdot \boldsymbol{e}_1 \otimes \boldsymbol{e}_1, \tag{4.1}$$

where the unit vector $\boldsymbol{e}_1$ designate the loading direction.

The substitution of (4.1) into Hooke's law (2.24), neglecting influence of the damage of the elastic properties and further simplifications lead to the well known expression for the stress $\sigma = E\varepsilon^{\mathrm{el}}$. The uni-axiallity conditions (4.1), the co-axiallity assumption for the backstress and stress tensors and the uniaxial representation of the backstress $\boldsymbol{\alpha} = \beta \boldsymbol{e}_1 \otimes \boldsymbol{e}_1$ lead to reduction of the relations for the stress (2.24), inelastic strain rate (2.35), backstress evolution rate (2.42), creep and fatigue damage rates (2.48, 2.54) to the following set of equations:

$$\sigma = E\varepsilon^{\mathrm{el}}, \tag{4.2a}$$

$$\dot{\varepsilon}^{\mathrm{p}} = R(T) f(\overline{\sigma}) \operatorname{sgn}\overline{\sigma}, \quad \overline{\sigma} = \sigma - \beta, \tag{4.2b}$$

$$\dot{\beta} = \frac{1}{\mu_{\mathrm{h}}} \frac{\mathrm{d}\mu_{\mathrm{h}}}{\mathrm{d}T} \dot{T}\beta + \mu_{\mathrm{h}} \left[|\dot{\varepsilon}^{\mathrm{p}}| - \dot{\varepsilon}^{\mathrm{p}} \frac{\beta}{\beta_*} \right], \tag{4.2c}$$

$$\dot{\omega}_{\mathrm{c}} = H(\sigma) H(\varepsilon^{\mathrm{p}}) r(\omega) \mathfrak{C}(T, \sigma, \varepsilon^{\mathrm{p}}, \dot{\varepsilon}^{\mathrm{p}}) |\dot{\varepsilon}^{\mathrm{p}}|, \tag{4.2d}$$

$$\dot{\omega}_{\mathrm{f}} = H(\sigma) r(\omega) \mathfrak{F}\left(T, \sigma, \varepsilon, \varepsilon^{\mathrm{p}}\right) |\dot{\varepsilon}^{\mathrm{p}}|, \tag{4.2e}$$

$$\dot{\omega} = F(\dot{\omega}_{\mathrm{f}}, \dot{\omega}_{\mathrm{c}}). \tag{4.2f}$$

where H is Heaviside's function, sgn is the sign function. The damage influence on the stiffness is excluded from the basic equations used in the majority of identification procedures.

The derived system of the constitutive equations is valid for the description of the material behavior under the cyclic loads, e.g. low-cycle fatigue tests, thermo-mechanical fatigue tests. The reduction of general constitutive model to the uniaxial loading case allows us to reduce the number of solving constitutive equations from 20 to 5. Further reduction is possible for the loading conditions observed in the creep tests. The reduction can be reached by means of the resolving of the differential equation for the backstress (4.2c) taking into account constant stress and temperature during the test. In addition, the fatigue damage function can be neglected according to definition of the fatigue damage, and evolution equation for the creep damage resolved and included into the expression for inelastic strain rates according to [25, 75]. Thereby, the system of the constitutive equations can be reduced to single differential equation for the inelastic strain rates as follows:

$$\dot{\varepsilon}^{\mathrm{p}} = R(T) f \left[\frac{\sigma - \beta_* \left(1 - \exp\left(-\frac{\mu_{\mathrm{h}} \varepsilon^{\mathrm{p}}}{\beta_*}\right)\right)}{1 - (\mathfrak{C}\varepsilon^{\mathrm{p}})^l} \right] \tag{4.3}$$

The reduction of the dimensionality of basic equations is strongly recommended for the application of trial identifications as well as for the identification based on the optimization approaches. Decomposition of complete identification problem into independent sub-problems allows us to reduce computational cost significantly and to utilize principally different approaches.

4.2 Elastic material properties

The temperature dependence of the material stiffness parameters affects the inelastic material behavior and damage processes. However, it may be identified independently based on the concomitant processes. The profile of $E(T)$ can generally be represented by the n^{th} order polynomial (4.4).

$$E(T) = \sum_{i=0}^{n} E_i T^i \tag{4.4}$$

The parameter of the polynomial can be determined by means of the linear least-square approach [36]. The important aspect of the identification is the order of the polynomial: the application of polynomial high order terms improves the correlation of the resulting function for each single data point, however leads to undesirable fluctuations of the function which are magnifying during the evaluation of the derivative. Therefore, the reduction of the number of parameters in above-mentioned problem is one of the purposes of the identification.

The accepted identification result corresponding to the optimal ratio between the correlation with experimental data and the number of material parameters, is shown in Fig. 4.1 and represented by the following expression:

$$E(T) = E_{\text{a}} + E_{\text{b}} T^3, \tag{4.5}$$

where E_{a} and E_{b} are the material parameters.

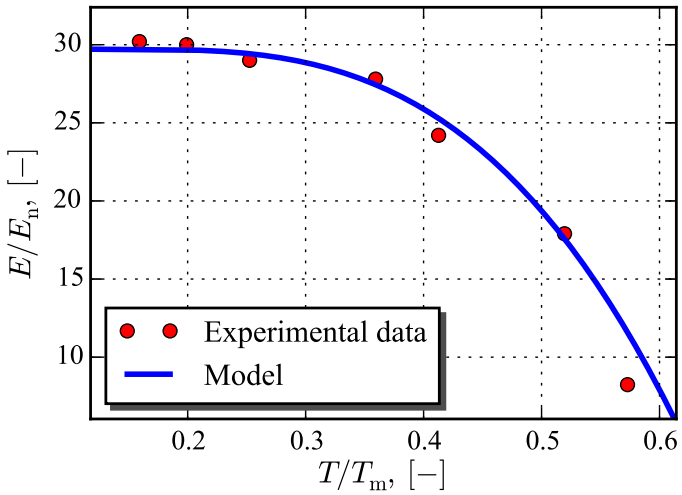

Figure 4.1: Identified temperature dependence of Young's modulus

4.3 Inelastic material behavior

The identification of inelastic material behavior is divided into several sub-problems. Performing a decompositions allows us to reduce computational costs and to apply different identification approaches within each sub-problem. Moreover, the decomposition into sub-problems simplifies the understanding of the physical background of each component of process.

The following experimental data may be used within the primary identification of the inelastic material properties: creep tests, tensile tests, LCF and TMF tests. The accuracy of the experimental data must be considered and in the particular case inaccurate experimental data can be excluded from the problem. However, the influence of inaccurate experimental data can be accounted by means of the weights system, which may be chosen according to the quality of experimental data.

4.3.1 Inelastic strain rates

The standard operation conditions of a typical turbine housing require to identify the inelastic strain rates from different tests. The design is subjected to steady loads the major part of lifetime, which proceeds in the secondary creep regime characterized by minimal inelastic strain rates. However, the presence of transient loading regimes requires a detailed consideration of primary creep stage, which, in general, is characterized by higher values of inelastic strain rates.

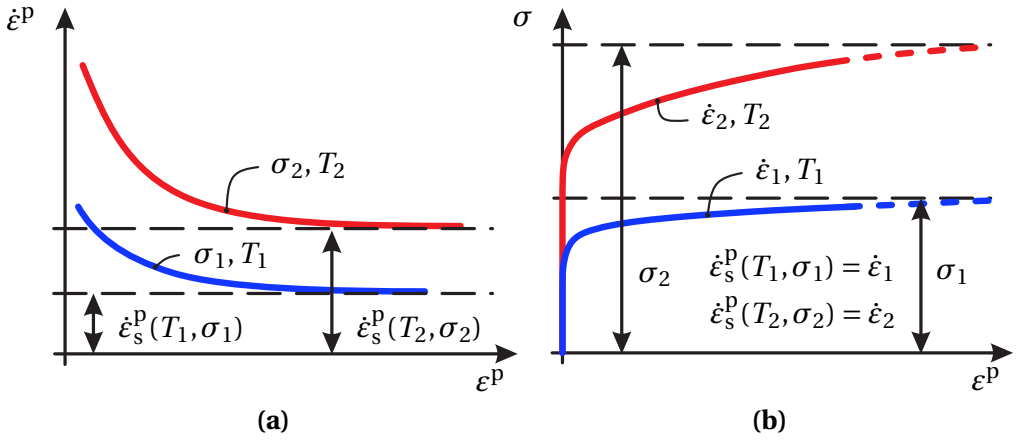

Figure 4.2: Collecting of input data for identification of inelastic steady strain rates: **(a)** measurement of inelastic steady strain rate by creep tests, **(b)** measurement of saturated stress by tensile tests

Within the framework of the current section, the problem of the identification of inelastic strain rates is considered. The majority of approaches useful for the identification of inelastic strain rates are based on the experimental data of creep tests at constant loading. Within the current research, the enchanted identification approach is used. In contrast to widely used identification methods accounting only the inelastic strain rate in the steady regimes of creep, the inelastic behavior of the material at initial moment of load is considered. The identification of creep models is normally starting with computing inelastic strains rates from creep curves. The experimental data from tensile tests can be used as well.

The application of tensile tests in the identification requires a detailed consideration of the stress-strain curves. Taking into account the constant temperature during the test, the slope of the stress-inelastic strain curve is defined by the following expression:

$$\frac{\mathrm{d}\sigma}{\mathrm{d}\varepsilon^{\mathrm{p}}} = \frac{\dot{\sigma}}{\dot{\varepsilon}^{\mathrm{p}}} = E\left(\frac{\dot{\varepsilon}}{\dot{\varepsilon}^{\mathrm{p}}} - 1\right), \Rightarrow \dot{\varepsilon}^{\mathrm{p}} = \frac{\dot{\varepsilon}}{1 + E^{-1}\frac{\mathrm{d}\sigma}{\mathrm{d}\varepsilon^{\mathrm{p}}}} \tag{4.6}$$

where $\dot{\varepsilon}$ is the constant value applied in test. Values of $\frac{\mathrm{d}\sigma}{\mathrm{d}\varepsilon^{\mathrm{p}}}$ can be measured by means of the experimental curve. When the elongation is started, but no inelastic deformations are reached, the slope value $\frac{\mathrm{d}\sigma}{\mathrm{d}\varepsilon^{\mathrm{p}}}$ tends into infinity and inelastic strain rate $\dot{\varepsilon}^{\mathrm{p}}$ is nearly to zero. On the other hand, when the large elongation is reached and the response stress is saturated, the slope $\frac{\mathrm{d}\sigma}{\mathrm{d}\varepsilon^{\mathrm{p}}}$ becomes almost zero and inelastic strain rates $\dot{\varepsilon}^{\mathrm{p}}$ tends to the rate of the applied strain $\dot{\varepsilon}$.

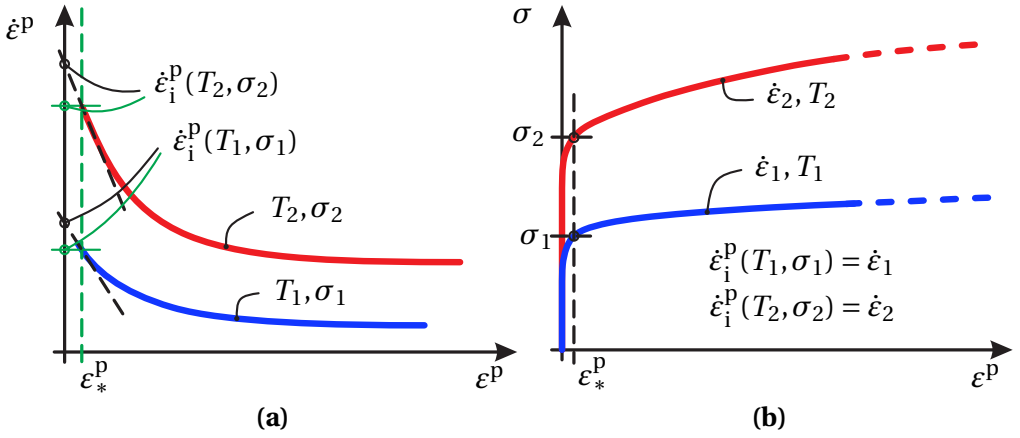

Figure 4.3: Collecting of input data for identification of inelastic initial strain rates: **(a)** measurement of initial inelastic strain rates by experimental data from creep tests, **(b)** measurement of initial inelastic strain rates by experimental data from tensile tests

Steady inelastic strain rate $\dot{\varepsilon}^{\mathrm{p}}_{\mathrm{s}}$ corresponds to the saturated strain rate, which can be easily determined from creep curves (see Fig. 4.2) or from tensile curves (see Fig. 4.2b). In particular, inelastic steady strain rates in the case of creep tests corresponds to the secondary stage of the creep curve, where minimum creep strain rates are observed. Thereby, in the case of creep tests the inelastic steady strain rates $\dot{\varepsilon}^{\mathrm{p}}_{\mathrm{s}}$ corresponds to minimum inelastic strain rates $\dot{\varepsilon}^{\mathrm{p}}_{\mathrm{min}}$. In the case of tensile tests, inelastic steady strain rate corresponds to the stage of the stress-strain curve, in which stress exhibits a saturation to some asymptotic value. Inelastic steady strain rates for the mentioned stage of a tensile test tend to the rates of applied loads: $\dot{\varepsilon}^{\mathrm{p}}_{\mathrm{s}} \to \dot{\varepsilon}$.

The initial inelastic strain rate $\dot{\varepsilon}^{\mathrm{p}}_{\mathrm{i}}$ corresponds to the inelastic strain rate at the beginning of the creep process. Two approaches are available for the estimation of initial strain rate $\dot{\varepsilon}^{\mathrm{p}}_{\mathrm{i}}$ from creep curves: extrapolation and direct measurement. Within the direct measurement the inelastic strains are measured at the point of a creep curve, in which some preassigned amount of plastic deformations is reached. Thereby, results obtained in this case are slightly underestimated. The alternative approach is based on the extrapolation of initial strain rates. The extrapolative approach gives the values of inelastic strain rates directly at the initial moment of time. However, the above-mentioned method have a significantly reduced accuracy, which reduction is mainly related to the great scatter of experimental data at the initial loading moment and limited accuracy of an experimental set-up.

The measured inelastic initial and steady strain rates are collected in the

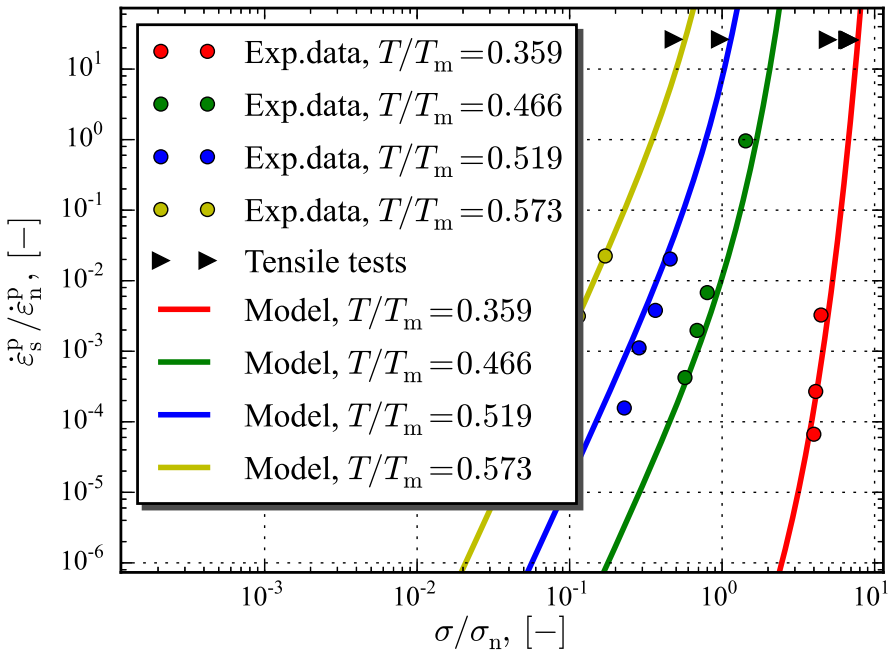

Figure 4.4: Primary identification of steady inelastic strain rates

representative sets of data, which used further for the identification of the material model. Inelastic steady strain rates with respect to different temperatures and stresses are shown in Fig. 4.4. The represented data are related to slow loading regimes with $\dot{\varepsilon}^p << 0.1\,h^{-1}$ corresponding to creep processes and fast loading regimes with $\dot{\varepsilon}^p \geq 0.1\,h^{-1}$, which correspond to the behavior of the cast irons in low-cycle fatigue and tensile tests.

Obviously, an increase of the operating temperature leads to the growth of steady strain rates. The influence of the temperature on the inelastic strain rates in the current constitutive model is represented by the temperature response functions $R_i(T)$ and $R_s(T)$. Taking into account the particular properties of GJV cast iron considered within the current work, the influence of the temperature differs for $0.199\,T_m$-$0.359\,T_m$ and $0.359\,T_m$-$0.573\,T_m$. Thereby, the constitutive model require the special mechanisms in order to represent low and high temperature regimes, which switching approximately between $0.359\,T_m$ and $0.413\,T_m$. Therefore, the application of the standard Arrhenius-type expression (2.38) for the temperature response function is not sufficient.

It should be noted, that some experimental data are excluded form the primary identification by the accuracy reasons. Majority of excluded data are belongs to the creep and tensile tests at temperature $0.359\,T_m$ and overloaded creep tests.

The relationship between inelastic strain rates and stress represents the duality as well. Within the frame of single temperature conditions, the dependence of the steady and initial inelastic strain rates on the stress variation can be characterized as follows:

- The power-law relationship of inelastic strain rates with stresses is observed for low stresses. The accumulation of the inelastic deformations at low loads with low rate characterizes creep processes.

- The exponential influence of the stresses on the inelastic strain rates is observed for high loads. Such combination represents well the behavior of the material in tensile, LCF and TMF tests.

Prandtl [73] and Garofalo [20], among others, proposed the stress response functions, which are able to represent the above-mentioned behavior:

Prandtl [73]: $$f(\sigma) = \sinh\left(\frac{\sigma}{B}\right)$$

Garofalo [20]: $$f(\sigma) = \left[\sinh\left(\frac{\sigma}{B}\right)\right]^n$$

Both functions characterize the inelastic strain rate dependence, however, the stress response function proposed by Garofalo [20] includes as well the function of Prandtl [73] as the specific case at $n = 1$. Thereby, the identification is based on the model proposed by Garofalo [20], due to a higher flexibility of the stress response function.

The inelastic strain rate functions $\dot{\varepsilon}^{\mathrm{p}}_{\mathrm{s}}(T,\sigma)$ and $\dot{\varepsilon}^{\mathrm{p}}_{\mathrm{i}}(T,\sigma)$ are identified taking into account the general sketch of the constitutive model (2.37) represented in Sect. 2.6. The resultant expressions for initial and steady inelastic strain rates are represented as follows:

$$\dot{\varepsilon}^{\mathrm{p}}_{\mathrm{s}}(T,\sigma) = R_{\mathrm{s}}(T) f_{\mathrm{s}}(\sigma), \quad \dot{\varepsilon}^{\mathrm{p}}_{\mathrm{i}}(T,\sigma) = R_{\mathrm{i}}(T) f_{\mathrm{i}}(\sigma), \tag{4.7}$$

where $R_{\mathrm{s}}(T)$ and $R_{\mathrm{i}}(T)$ are Arrhenius type temperature response functions with two regimes, $f_{\mathrm{s}}(\sigma)$ and $f_{\mathrm{i}}(\sigma)$ are Garofalo stress response functions:

$$\begin{aligned}
&f_{\mathrm{s}}(\sigma) = A_{\mathrm{s}}\left[\sinh\left(\frac{\sigma}{B_{\mathrm{s}}}\right)\right]^{n_{\mathrm{s}}}, \quad f_{\mathrm{i}}(\sigma) = A_{\mathrm{i}}\left[\sinh\left(\frac{\sigma}{B_{\mathrm{i}}}\right)\right]^{n_{\mathrm{i}}},\\
&R_{\mathrm{s}}(T) = \exp\left(-\frac{\alpha^{\mathrm{H}}_{\mathrm{s}}}{T}\right)\left(1+\exp\left(-(\alpha^{\mathrm{H}}_{\mathrm{s}}-\alpha^{\mathrm{L}}_{\mathrm{s}})(\frac{1}{T^{\mathrm{s}}_{*}}-\frac{1}{T})\right)\right),\\
&R_{\mathrm{i}}(T) = \exp\left(-\frac{\alpha^{\mathrm{H}}_{\mathrm{i}}}{T}\right)\left(1+\exp\left(-(\alpha^{\mathrm{H}}_{\mathrm{i}}-\alpha^{\mathrm{L}}_{\mathrm{i}})(\frac{1}{T^{\mathrm{i}}_{*}}-\frac{1}{T})\right)\right).
\end{aligned} \tag{4.8}$$

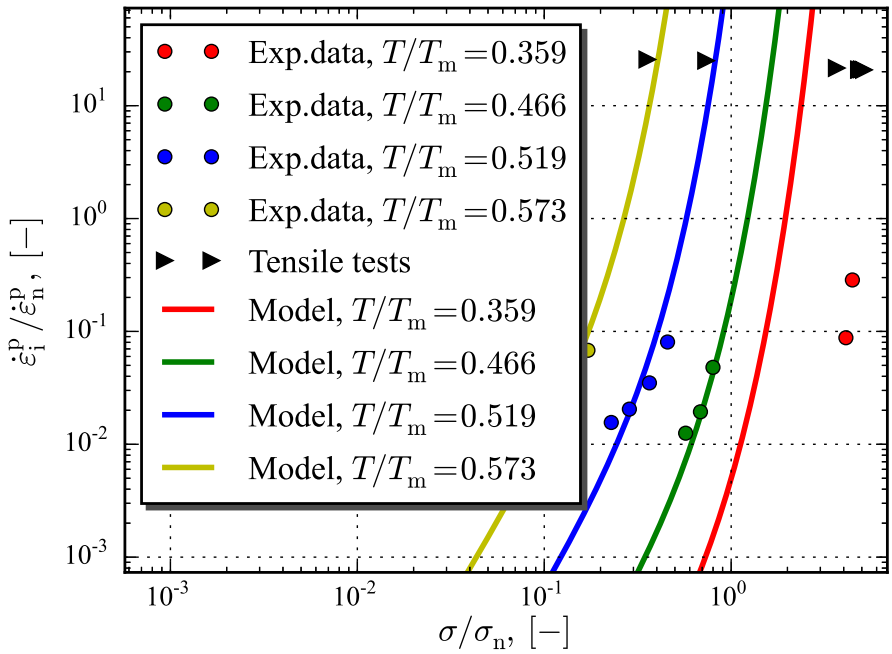

Figure 4.5: Primary identification of initial inelastic strain rates

Here α_s^H, α_i^H, α_s^L, α_i^L, T_*^s, T_*^i, A_s, A_i, B_s, B_i, n_s and n_i are the identified material parameters. The obtained relations for the initial and steady inelastic strain rates are shown in Fig. 4.5 and Fig. 4.4. The solid lines in both figures represent the determined inelastic strain rate functions. Obviously, the application of experimental points measured in tensile tests completes the creep data at the high strain rates. Thereby, the identification of the unified constitutive model for low and high inelastic strain rates can be performed. The experimental points at temperature $0.359\,T_m$ are excluded from the identification of the initial inelastic strain rates by the reason of low accuracy induced by the extrapolation.

It should be mentioned, that the major purpose of the primary identification is the determination of the structure of the constitutive relation and estimation of material parameters. Taking into account the statement above, the quality of identification of the initial and steady inelastic strain functions is sufficient for further development of the model. However, the application of the identified constitutive model for the simulation of the GJV cast iron behavior is possible only in restricted cases corresponding to the loading conditions in creep tests.

There are some particular features in the evolution of inelastic strain rates in creep tests. Obviously, the inelastic strain rate at the initial point of the

creep curve is close to the identified initial inelastic strain rate. Taking into account the uni-axiallity of creep tests and the absence of the backstress in the initial state, the following relationship is valid:

$$\dot{\varepsilon}^{\mathrm{p}}_{\mathrm{vM}}(T,\overline{\sigma}) = \dot{\varepsilon}^{\mathrm{p}}_{\mathrm{i}}(T,\sigma) \tag{4.9}$$

The primary stage of the creep curve can be characterized by the sufficiently fast decrease of the inelastic strain rate till some minimal value is reached. This strain rate corresponds to the secondary stage of the creep curve and coincides with the identified steady inelastic strain rate. Thus, the inelastic strain rate for the secondary creep stage can be represented as follows:

$$\dot{\varepsilon}^{\mathrm{p}}_{\mathrm{vM}}(T,\overline{\sigma}) = \dot{\varepsilon}^{\mathrm{p}}_{\mathrm{s}}(T,\sigma) \tag{4.10}$$

Thereby, initial and steady inelastic strain rates are the particular cases of the inelastic strain rate function $\dot{\varepsilon}^{\mathrm{p}}_{\mathrm{vM}}(T,\overline{\boldsymbol{\sigma}})$:

$$\dot{\varepsilon}^{\mathrm{p}}_{\mathrm{vM}}(T,\overline{\sigma}) = \dot{\varepsilon}^{\mathrm{p}}_{\mathrm{i}}(T,\sigma-\beta) \tag{4.11}$$

4.3.2 Hardening saturation

The backstress evolution equation requires the explicit definition of the hardening saturation function $\beta_*(T,\boldsymbol{\sigma})$. There are two approaches in order to identify this function. The most simple is based on the evaluation of the experimental data by means of expression for inelastic strain rates (4.11) resolved with respect to the backstress β:

$$\beta = \sigma - f_{\mathrm{i}}^{-1}\left(\frac{\dot{\varepsilon}^{\mathrm{p}}_{\mathrm{vM}}}{R_{\mathrm{i}}(T)}\right) \tag{4.12}$$

The substitution of experimental values of the inelastic strain rates into expression (4.12) allows us to obtain the experiment-based data representing the backstress β in the explicit form (see Fig. 4.6a). This approach is independent from the shape of the functions, which used for initial and steady inelastic strain rates, and allows instantly determine the shape of the hardening saturation β_* and hardening rate μ_{h} functions according the particular experimental data. The evaluated examples of the hardening saturation and hardening rate functions for the particular loads (creep tests at T =0.519T_{m}, σ =0.29σ_{n}) are shown in Fig. 4.6.

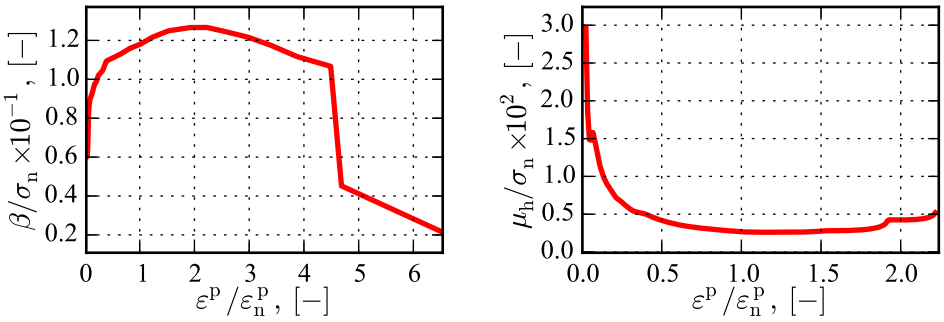

(a) **(b)**

Figure 4.6: Estimation of backstress and hardening rates: **(a)** extracted backstress values, **(b)** extracted hardening rate values

The backstress contribution in the creep process evaluated through (4.12) is shown in Fig. 4.6a. Because the backstress is defined as increasing function of the inelastic strain, obviously, the description of the evaluated curve at $\varepsilon^p > 1.976\varepsilon_n^p$ requires the consideration of additional phenomena such as softening, high geometrical nonlinearity, volume change induced by the inelastic deformation, damage, etc. In particular, in the current work, the creep damage is considered in order to represent the increase of the inelastic strain rates during tertiary stage of creep curves. Within the sake of simplicity, the constitutive equations describing the softening phenomena are not included into the material model. The constitutive model is focused on the description of the material behavior at specific operation conditions, which contain mainly the primary stage and initial part of the secondary creep stage. Therefore, the contribution of the softening phenomena in the material behavior is neglected.

The hardening rate function represents the rate of the redistribution of the internal stresses in the polycrystalline material. In practice, the rate of the transformation of the creep curve from the initial point into the primary stage, and then into the secondary, is the basic meaning of hardening rate μ_h. The evaluation of the experimental data according to expression (4.12) and known values of the hardening saturation β_* allows us to extract the experiment-based estimation for the hardening rate μ_h(see Fig. 4.6b). The mentioned extracting procedures are described in details in Sect. 4.3.3. As it mentioned before, the processing of the experimental data with assumed deterministic expressions induce an additional error. Thus, the mentioned above approach is valid only for the preliminary estimation of the hardening rate function, and

requires the secondary identification step.

The approach (4.12) allows us to determine the value of function β_* for specific loads. The application of above-mentioned expression in the case, when the constitutive model must be identified for the wide range of temperatures and applied stress, can lead to the excessive efforts and error induced by the structure of identification itself. Thereby, the first approach is not recommended in cases, when the designed model is required for the limited range of the loading conditions.

The second approach is based on the initial and steady inelastic strain rate functions. Identified analytic expressions for initial and steady inelastic strain rates allow us to derive the hardening saturation function in the purely analytical way. Considering (4.10) and (4.11), the following relationship can be obtained:

$$\dot{\varepsilon}^{\mathrm{p}}_{\mathrm{s}}(T,\sigma) = \dot{\varepsilon}^{\mathrm{p}}_{\mathrm{i}}(T,\sigma-\beta_*) \Rightarrow R_{\mathrm{s}}(T)\, f_{\mathrm{s}}(\sigma) = R_{\mathrm{i}}(T)\, f_{\mathrm{i}}(\sigma-\beta_*) \tag{4.13}$$

where, functions $R_{\mathrm{s}}(T)$, $f_{\mathrm{s}}(\sigma)$, $R_{\mathrm{i}}(T)$ and $f_{\mathrm{i}}(\sigma)$ are known (Sect. 4.3.1). Thereby, expression (4.13) may be resolved with respect to hardening saturation function β_* as follows:

$$\beta_*(T,\sigma) = \sigma - f_{\mathrm{i}}^{-1}\left[\frac{R_{\mathrm{s}}(T)}{R_{\mathrm{i}}(T)} f_{\mathrm{s}}(\sigma)\right] \tag{4.14}$$

The above expression is valid for any particular case of the functions $R_{\mathrm{i}}(T)$, $R_{\mathrm{s}}(T)$, $f_{\mathrm{i}}(\sigma)$, and $f_{\mathrm{s}}(\sigma)$ within the framework of the current structure of the constitutive model. The presented sequence of the identification allows us to determine the hardening saturation function with respect to temperature ans stress in the analytical form. However, in contrast to the simple approach presented in the beginning of section, only hardening saturation function can be identified by that way. Thereby, the identification of the hardening rate μ_{h} must be performed in addition.

Within the current research, the identification of the hardening saturation β_* is performed according to the second approach. Taking into account the identified expressions and material parameters for the initial and steady inelastic strain rates, the explicit form of β_* for the uniaxial case can be represented as follows:

$$\beta_*(T,\sigma) = \sigma - B_{\mathrm{i}}\,\mathrm{arcsinh}\left[\left(\frac{A_{\mathrm{s}}R_{\mathrm{s}}(T)}{A_{\mathrm{i}}R_{\mathrm{i}}(T)}\right)^{1/n_{\mathrm{i}}} \sinh\left(\frac{\sigma}{B_{\mathrm{s}}}\right)^{n_{\mathrm{s}}/n_{\mathrm{i}}}\right] \tag{4.15}$$

The identified expression for the hardening saturation function presented above is mainly based on the measured initial and steady inelastic strain rates

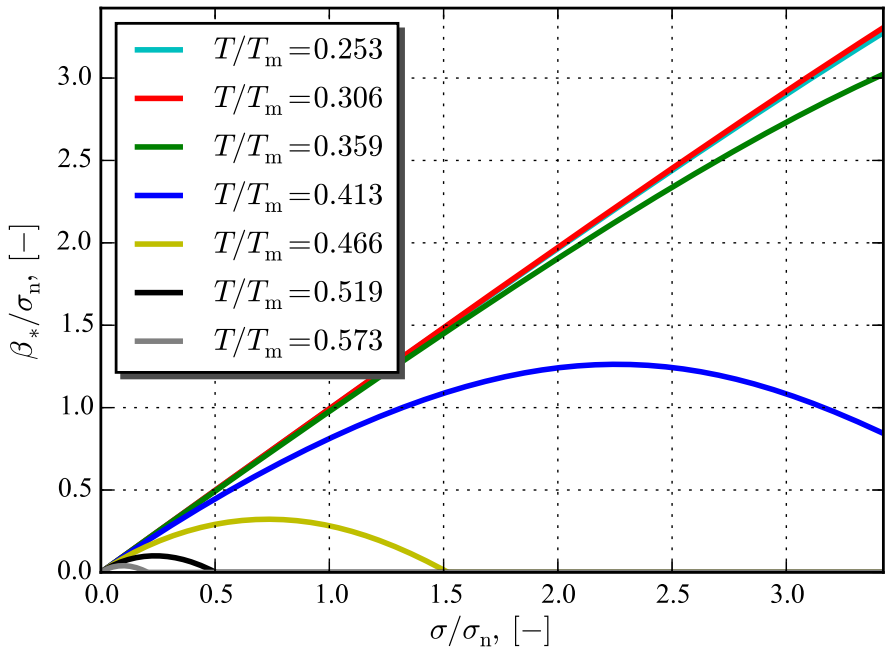

Figure 4.7: Hardening saturation function (primary identification)

and does not require additional material parameters. The hardening saturation function can be extended for three-dimensional cases by means of application of equivalent von Mises stress: The results of the primary identification of the hardening saturation function evaluated according GJV cast iron are shown in Fig. 4.7.

There are several requirements to the hardening saturation functions based on the features of the phenomenological model used within the current work:

$$\begin{aligned} &\sigma_1 > \sigma_2, T_1 = T_2 \Rightarrow \beta_*(T_1,\sigma_1) \geq \beta_*(T_2,\sigma_2), \\ &\sigma_1 = \sigma_2, T_1 > T_2 \Rightarrow \beta_*(T_1,\sigma_1) \leq \beta_*(T_2,\sigma_2). \end{aligned} \tag{4.16}$$

The obtained hardening saturation function β_* is based on the initial and steady inelastic strain rates determined independently according only to the available experimental data. Thereby, the requirements (4.16) in general can be not satisfied, that is observed in Fig. 4.7 for the temperature $0.253\,T_\mathrm{m}$ and $0.306\,T_\mathrm{m}$. Within the current particular case, the successful application of the backstress saturation function in the current form can be performed only in the range of the operation conditions corresponding to the available experimental data from creep tests. The application of the model outside of mentioned above range of the operation conditions requires to provide the secondary step of the identification.

4.3.3 Hardening rate

The backstress evolution equation (4.2c) in particular case of creep regime can be resolved analytically:

$$\beta = \beta_* \left[1 - \exp\left(-\frac{\mu_\mathrm{h} \varepsilon^\mathrm{p}}{\beta_*} \right) \right] \tag{4.17}$$

Taking into account identified function β_* (4.15), hardening rate can be determined as follows:

$$\mu_\mathrm{h} = -\frac{\beta_*}{\varepsilon^\mathrm{p}} \ln\left(\frac{\beta_* - \beta}{\beta_*} \right), \tag{4.18}$$

where β is the evaluated according to (4.12). The experimental data from creep tests can be processed according to expression (4.18) by the use of the identified hardening saturation function $\beta_*(T,\sigma)$. The estimated according to (4.18) hardening rates for the particular case of the experimental data (creep tests at T =0.519T_m, σ =0.29σ_n) are shown in Fig. 4.8a. The estimated value of the hardening rate function μ_h here is obtained taking into account the low accuracy of the experimental data at the initial moment of the creep tests. Therefore, the presented estimation of μ_h is correlated mainly for the experimental data, which correspond to inelastic strains $\dot{\varepsilon}^\mathrm{p}$ >0.396$\varepsilon^\mathrm{p}_\mathrm{n}$. The measured for the particular experimental data value of μ_h and β_* allows us to estimate the backstress evolution for the corresponding loading conditions (see Fig. 4.8b). The numerical values of the hardening rate function μ_h obtained for different thermal conditions allows us to determine shape of μ_h with respect to the temperature (see Fig. 4.8c).

It should be mentioned, that estimation of the hardening rate by means of the approach presented above must take into account the experimental data corresponding to the primary stage of creep curves, because the change of the backstress takes place directly at this stage of creep curve.

Taking into account the relationship between the hardening rate μ_h and elastic material properties (2.43) mentioned by Naumenko and Altenbach [50], the general profile of the function $\mu_\mathrm{h}(T)$ is defined in the similar way to the temperature dependence of Young's modulus (4.5) (see Fig. 4.8c) and represented by the following expression:

$$\mu_\mathrm{h}(T) = \mu_\mathrm{a} + \mu_\mathrm{b} T^3, \tag{4.19}$$

where μ_a and μ_b are resulting material parameters.

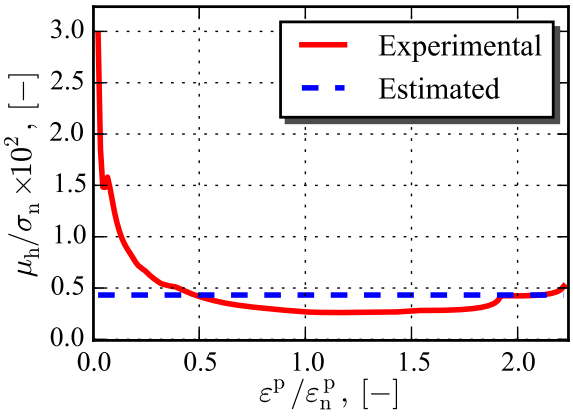

(a)

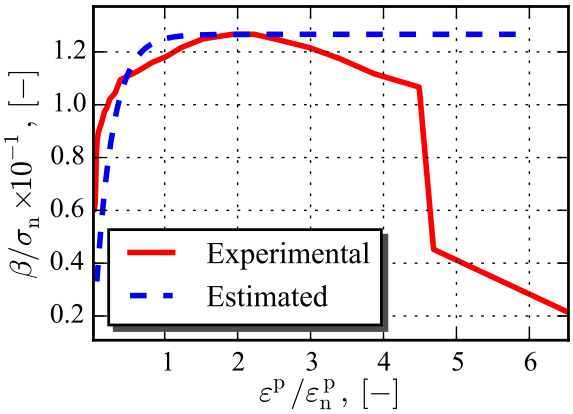

(b)

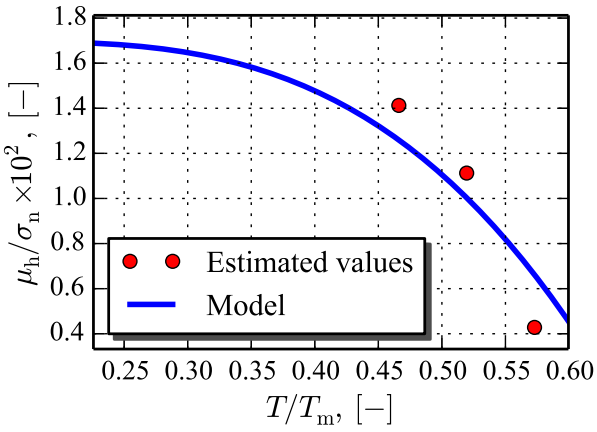

(c)

Figure 4.8: Identification of the hardening rate modulus μ_h: **(a)** evaluated hardening rates according to experimental data and estimated value, **(b)** extracted from experimental data backstress evolution and rough estimation by the constitutive model, **(c)** primary estimation of the hardening rate function μ_h vs temperature

4.4 Creep damage

The identification of the constitutive equations for the creep damage can be provided only after identification of the elastic and inelastic material properties. Mainly, the source of the experimental data used by this identification is the tertiary stage of creep curves (Sect. 3.2.2).

The creep regime of loads allows us to perform the identification based on the single differential equation for inelastic strain rate (4.3). It should be noted, that at the current stage of identification model for elastic and inelastic material behavior is formulated, and further task includes the determination of the state function $\mathfrak{C}$ and parameter l of accumulated damage response function $r(\omega)$. The following expressions represent the state of material at rupture moment:

$$\omega = \mathfrak{C}\varepsilon^{\mathrm{p}} = 1 \Rightarrow \mathfrak{C} = \frac{1}{\varepsilon^{\mathrm{p}}_{*}}, \tag{4.20}$$

where $\varepsilon^{\mathrm{p}}_{*}$ is the inelastic strain at the rupture moment. The substitution of (4.20) into (4.2d) leads to the creep damage evolution equation (2.53) mentioned in Sect. 2.7.1.4. The proposed definition for the creep damage state function $\mathfrak{C}$ is preferable for the use, because the ruptures strains concept gives the clear representation of the mechanisms lying behind this function. However, in order to apply creep damage equation for general case of loads, the stress and temperature dependence of the state function $\mathfrak{C}$ must be determined.

The identification of the function $\mathfrak{C}$ requires the experimental values of the inelastic rupture strains at different temperatures and stresses. The abovementioned data may be generated from creep curves. The obtained set of experimental values is shown in Fig. 4.9.

Obviously, the temperature and the stress have significant influence on the inelastic rupture strains. The increase of the temperature leads to ductility of the material, and, therefore, to the increase of the inelastic strains at the rupture moment. The level of the mechanical loads affects the inelastic strain rates as well, and, finally, also leads to change of the rupture strains $\varepsilon^{\mathrm{p}}_{*}$. Therefore, the rupture strain function $\varepsilon^{\mathrm{p}}_{*}$ must include the temperature and stress response functions.

Obviously, the mechanism with which the temperature affects the rupture strain is similar with the influence of the temperature on inelastic strain rates. Therefore, the temperature response function may be represented by the Arrhenius-type function. On the other hand, the stress response function must be chosen according to the particular properties of the identified material. Within the current work, the stress response function proposed in [50] is

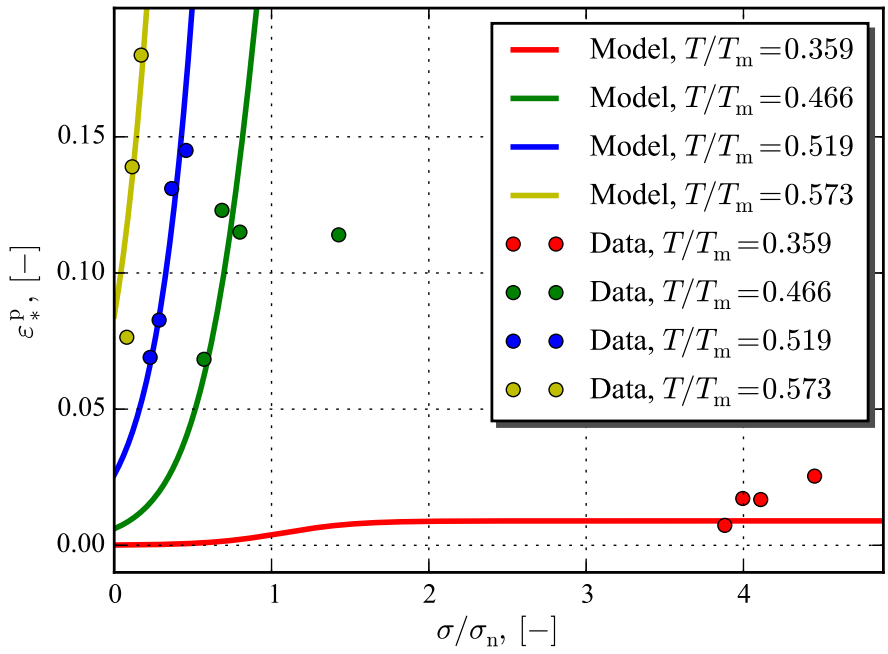

Figure 4.9: Inelastic rupture strains function (4.20)

chosen. Thus, the following structure of the inelastic rupture strain function is used:

$$\varepsilon^{\mathrm{p}}_*(T,\boldsymbol{\sigma}) = \underbrace{\epsilon_{\mathrm{br}} D(T)}_{\varepsilon_{\mathrm{br}}(T)} + \frac{D(T)\, a_\varepsilon}{1 + b_\varepsilon e^{-\frac{\sigma_{\mathrm{vM}}}{c_\varepsilon}}}, \quad D(T) = \exp\left(-\frac{\alpha_{\mathrm{D}}}{T}\right), \tag{4.21}$$

where $\varepsilon_{\mathrm{br}}(T)$ is the strain of brittle rupture of the material, $D(T)$ is the Arrhenius-type function of temperature, ϵ_{br}, a_ε, b_ε, c_ε and α_{D} are the material parameters. The identified state function $\mathfrak{C}$ is shown in Fig. 4.9. Equation 4.21 can be extended to the three-dimensional case as follows:

$$\dot{\omega}_{\mathrm{c}} = H(\boldsymbol{\sigma})\, Y(\boldsymbol{\varepsilon}^{\mathrm{p}})\, r(\omega) \frac{|\dot{\varepsilon}^{\mathrm{p}}_{\mathrm{vM}}|}{\varepsilon^{\mathrm{p}}_*(T,\boldsymbol{\sigma})}. \tag{4.22}$$

The parameter l of accumulated damage response function $r(\omega)$ is also must be estimated. Mainly, the variation by this parameter allows to regulate the intensity of tertiary stage of creep curves simulated by means of the provided constitutive model. Schematically this influence is shown in Fig. 4.10.

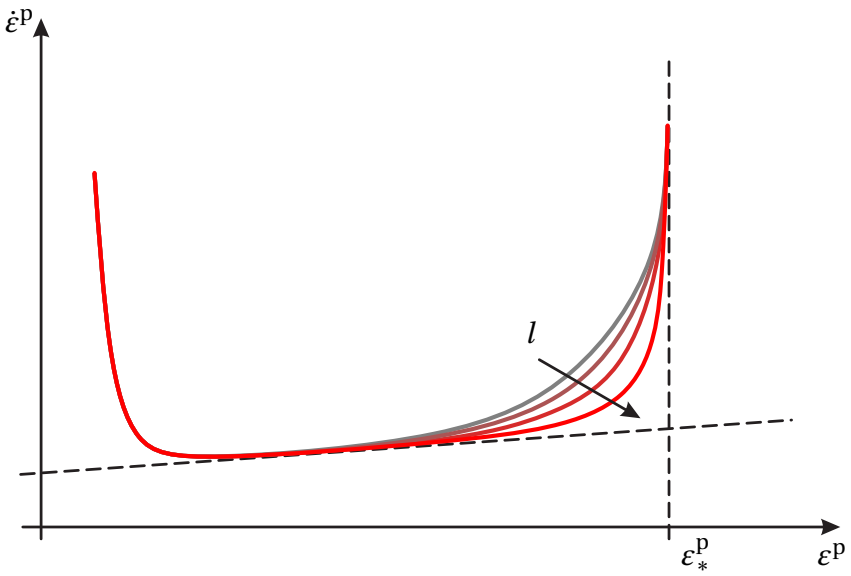

Figure 4.10: Influence of parameter l on response of creep damage model

4.5 Fatigue damage

The primary identification of the fatigue damage model can be performed only based on the formulated and identified constitutive model for the inelastic material behavior. The identification is based on the results of the low-cycle fatigue tests (see Fig. 3.6). On the initial identification step the constitutive model of the fatigue damage is considered in terms of integral characteristics: the amplitudes of strains ε_{A}, the amplitudes of stresses σ_{A} and the number of loading cycles N. The above-mentioned form of the constitutive model is convenient for the identification, because it requires the integration over the cycles N except the continuous damage models requiring the integration over time t that is much faster. However, the approach includes the significant error involved by the required idealization of the LCF response cycle in stress, therefore it can be used only for the preliminary identification step.

In order to switch to time-scale measured in the cycles the several simplification must be used:

- The material is assumed to be perfectly plastic
- Only positive part of the stress is accounting

The idealized representative cycle and experimental one for the particular case of T =0.519T_{m} and ε_{A} =0.632ε_{n} are shown in Fig. 4.11.

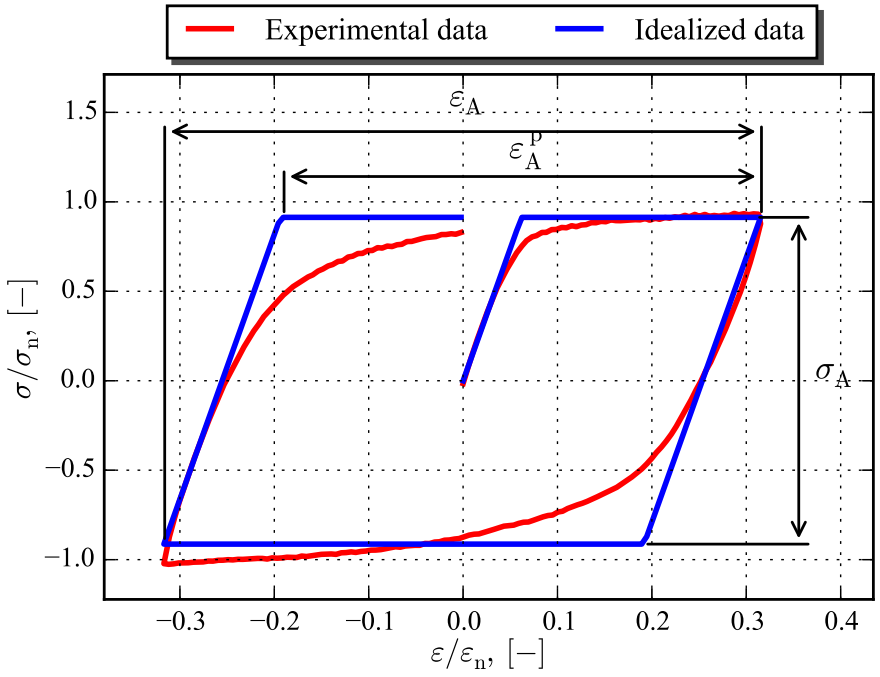

Figure 4.11: The idealized hysteresis of stress

Within the specific case of GJV case iron, the state function $\mathfrak{F}$ is assumed to be the power-law function of the strain energy density. For the uniaxial loading case the following expression for $\mathfrak{F}$ is assumed:

$$\mathfrak{F} = S\left(\sigma\varepsilon^{\mathrm{m}}\right)^{n}, \tag{4.23}$$

where S and n are the material parameters, which must be determined, ε^{m} is the mechanical strain including the elastic and plastic strain components. The above-mentioned function is based on the assumption that the fatigue damage accumulation rates are proportional to the dissipated strain energy $\int_{\mathrm{cycle}} \sigma\dot{\varepsilon}^{\mathrm{p}}\mathrm{d}t$. However, the proposed state function includes the mechanical strain ε^{m} in order to take into account the particular cases of high-cycle fatigue observed in the experiments.

The proposed above state function $\mathfrak{F}$ leads to the following expression for the fatigue damage accumulation rates:

$$\dot{\omega} = H(\sigma)r(\omega)S(\sigma\varepsilon^{\mathrm{m}})^{n}|\dot{\varepsilon}^{\mathrm{p}}| \tag{4.24}$$

The fatigue damage evolution equation (4.24) is given for the uniaxial loading case and requires some modification for the use in the general three-dimensional case. Assuming isotropy of the damage, the equation (2.54) can

be rewritten as follows:

$$\dot{\omega} = H(\boldsymbol{\sigma})\, r(\omega) S (\sigma_{\mathrm{vM}} \varepsilon_{\mathrm{eq}})^n |\dot{\varepsilon}^{\mathrm{p}}_{\mathrm{vM}}|, \tag{4.25}$$

where $\varepsilon_{\mathrm{eq}}$ is the equivalent total strain sensitive to the tension/compression modes of the loading:

$$\varepsilon_{\mathrm{eq}} = \frac{\sigma_{\mathrm{vM}} S_{\boldsymbol{\sigma}}}{E} + \varepsilon^{\mathrm{p}}_{\mathrm{vM}} S_{\boldsymbol{\varepsilon}^{\mathrm{p}}} \tag{4.26}$$

The functions $S_{\boldsymbol{\sigma}}$ and $S_{\boldsymbol{\varepsilon}^{\mathrm{p}}}$, which involves the influence of the tension/compression modes, are derived based on the stress and strain tensors as follows:

$$\begin{aligned} S_{\boldsymbol{\sigma}} &= \mathrm{sgn}\,(\sigma_I - \delta), \quad \delta << 1 \\ S_{\boldsymbol{\varepsilon}^{\mathrm{p}}} &= \mathrm{sgn}\left(\frac{\varepsilon^{\mathrm{p}}_I + \varepsilon^{\mathrm{p}}_{III}}{2}\right). \end{aligned} \tag{4.27}$$

In order to switch to the cycles-based time-scale, equation (4.24) must be integrated for the single cycle of loads under the perfect plasticity assumption (see Fig. 4.11). Therefore, the cycle-based fatigue damage accumulation law can be represented as follows:

$$\frac{\Delta\omega}{\Delta N} = \frac{r(\omega) S}{n+1} \left(\frac{\sigma_{\mathrm{A}}}{2}\right)^n \left[\left(\frac{\varepsilon_{\mathrm{A}}}{2}\right)^{n+1} - \left(\frac{\sigma_{\mathrm{A}}}{2E}\right)^{n+1} - \left(\frac{\sigma_{\mathrm{A}}}{E} - \frac{\varepsilon_{\mathrm{A}}}{2}\right)^{n+1} \right] \tag{4.28}$$

The following analytic relation between the damage ω and number of cycle N can be further obtained:

$$\omega = (CN)^l,\, C = \frac{S}{n+1} \left(\frac{\sigma_{\mathrm{A}}}{2}\right)^n \left[\left(\frac{\varepsilon_{\mathrm{A}}}{2}\right)^{n+1} - \left(\frac{\sigma_{\mathrm{A}}}{2E}\right)^{n+1} - \left(\frac{\sigma_{\mathrm{A}}}{E} - \frac{\varepsilon_{\mathrm{A}}}{2}\right)^{n+1} \right], \tag{4.29}$$

where C is the part of (4.28) constant for each loading cycle. The fatigue rupture is reached when $\omega = \omega_*$. From this condition the expression for the number of cycles to rupture N_{A} can be obtained:

$$N_{\mathrm{A}} = C^{-1} \omega_*^{1/l} \tag{4.30}$$

The value of ω_* corresponding to the failure of material on practice is about $0.95 - 0.99$.

The primary identification of the material parameters of the fatigue damage accumulation law (4.24) can be performed by means of the experimental data (see Fig. 3.6) and reduced fatigue damage evolution equation (4.28). The estimation of the material parameters n and S of the cycle-based fatigue damage accumulation rates is performed using the trivial and hand-fitting identification approaches and shown in Fig. 4.12.

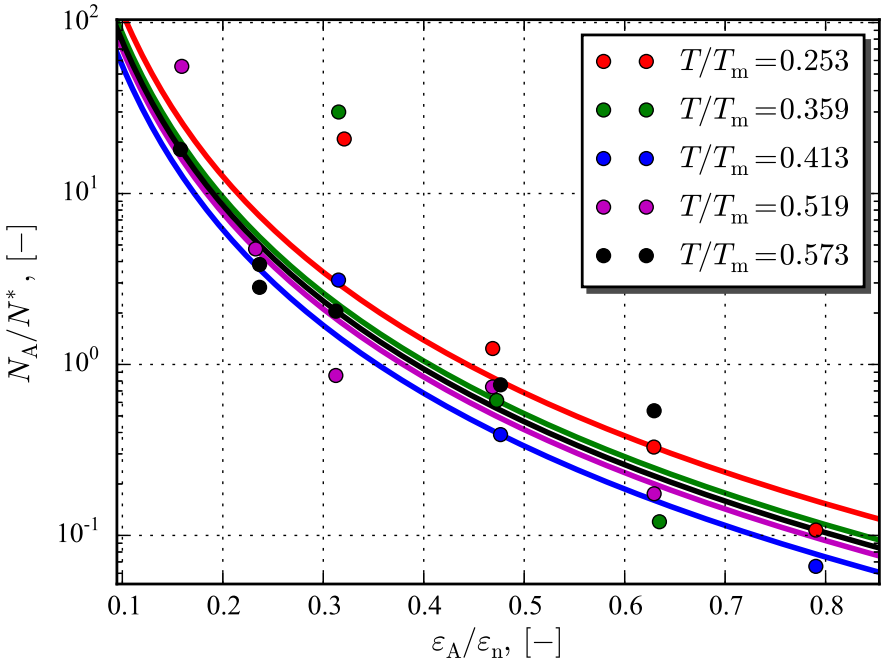

(a)

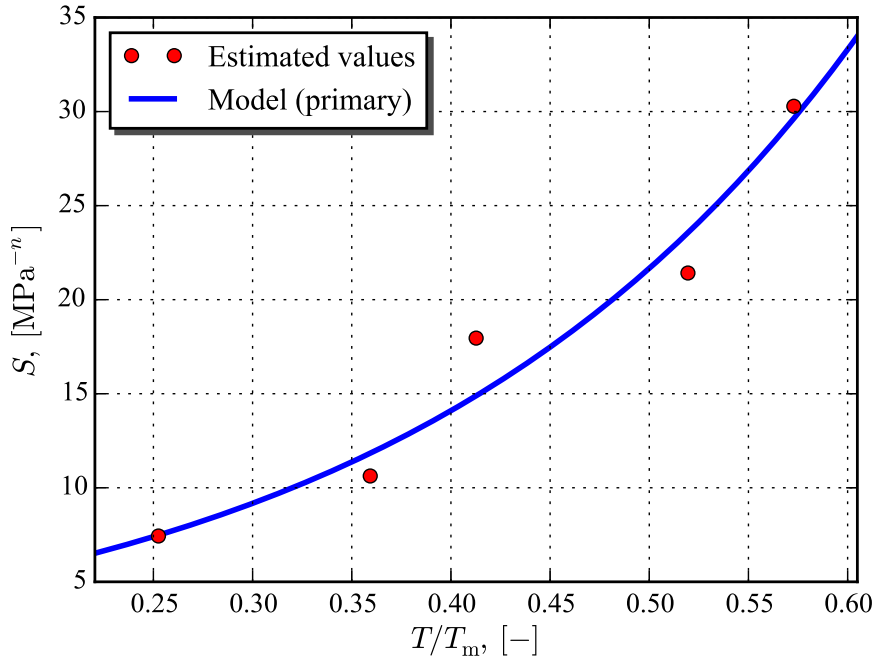

(b)

Figure 4.12: Primary estimation of fatigue damage model: **(a)** prediction for the number of cycles to rupture, **(b)** temperature response function S (4.31)

The results shown in Fig. 4.12 are obtained independently for each temperature based on the available experimental data. The parameter n is assumed to be temperature independent, therefore the same parameter value is used for each temperature. However, the material parameter S represents the influence of the temperature on the fatigue damage accumulation rate, therefore it is determined independently for each temperature. The obtained values of S for different temperatures are shown in Fig. 4.12b. The shown temperature dependence can be approximated by the exponential function with the sufficient accuracy and minimun number of parameters:

$$S(T) = s_{\mathrm{a}} \exp(s_{\mathrm{b}} T), \tag{4.31}$$

where s_{a} and s_{b} are the material parameters.

Nevertheless, the application of material parameters obtained within the current section leads to excessive error, which is included into the consideration through the assumed restrictions concerning the perfect plasticity (see Fig. 4.11). Therefore, the identification of the continuum fatigue damage model can not be performed only by means of the primary identification step described above and requires the direct integration of the constitutive equations within the global time-scale. The current section is focused only on the determination of the structure of the state function $\mathfrak{F}$ and guess of the material parameters for the further optimization-based identification step.

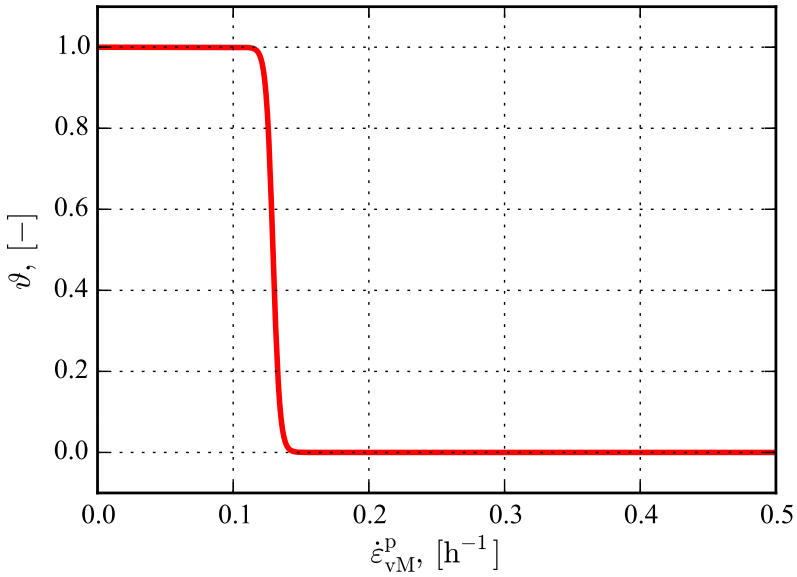

Figure 4.13: Damage fraction function

4.6 Derivation of the cycle based fatigue evolution law

The primary identification of the fatigue damage requires the simplification of the evolution law (4.25) to the cycle based evolution law. In order to switch form the integration by the general time to the integration by the number of cycle, the following transformation must be considered:

$$\dot{\omega} = \frac{\partial \omega}{\partial N}\frac{dN}{\mathrm{d}t}, \Rightarrow \frac{\partial \omega}{\partial N} = \int\limits_{t_0}^{t_0+t_\mathrm{c}} \dot{\omega}\mathrm{d}t, \tag{4.32}$$

where t_c is the period of the single loading cycle. The analytic integration (4.32) may be performed only in situation, when changes of stress and inelastic strain are the explicit functions of time. Therefore, in order to obtain such solution, idealized hysteresis shown in Fig. 4.14 is considered.

The stress hysteresis presented in Fig. 4.14 is based on the assumption about the ideal plastic behavior of the material after the reaching some yield stress level σ_y. Now let us consider the stages of the loading cycles presented above:

$t \in [t_0, t_1]$: $\dot{\varepsilon}^\mathrm{p} = 0, \dot{\omega} = 0$
$t \in [t_1, t_2]$: $\sigma = \sigma_\mathrm{y}, \dot{\varepsilon}^\mathrm{p} = \dot{\varepsilon}, \dot{\omega} > 0$
$t \in [t_2, t_4]$: $\dot{\varepsilon}^\mathrm{p} = 0, \dot{\omega} = 0$
$t \in [t_3, t_6]$: $H(\sigma) = 0, \dot{\omega} = 0$
$t \in [t_5, t_7]$: $\dot{\varepsilon}^\mathrm{p} = 0, \dot{\omega} = 0$
$t \in [t_7, t_8]$: $\sigma = \sigma_\mathrm{y}, \dot{\varepsilon}^\mathrm{p} = \dot{\varepsilon}, \dot{\omega} > 0$

Thereby, the integration of the fatigue damage evolution equation for complete loading cycle can be reduced as follows:

$$\Delta\omega = \int\limits_{t_0}^{t_0+t_\mathrm{c}} \dot{\omega}\mathrm{d}t\Delta N = \left(\int\limits_{t_1}^{t_2} \dot{\omega}\mathrm{d}t + \int\limits_{t_7}^{t_8} \dot{\omega}\mathrm{d}t\right)\Delta N \tag{4.33}$$

Despite of fatigue damage, the change of stress and inelastic strain must be considered on the complete integration interval. However, the integration of the corresponding constitutive equations can be performed analytically for idealized cycle shown in Fig. 4.14. Thereby, the stress and inelastic strain are known functions of time, and fatigue damage increment for one cycle can be obtained analytically and the assumption that the change of damage ω within the framework of single loading cycle is negligible value.

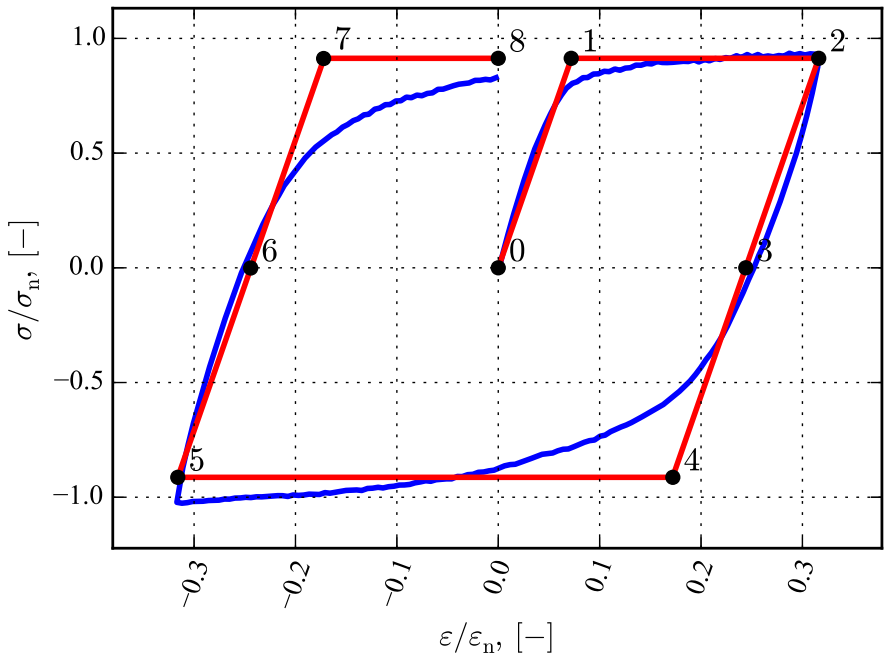

(a)

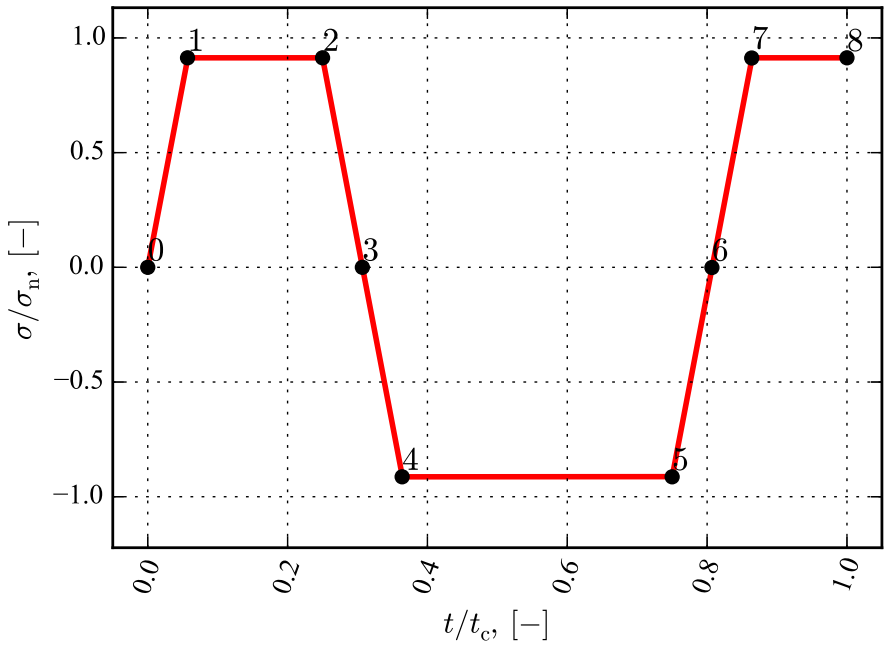

(b)

Figure 4.14: Idealization of LCF test: **(a)** stress hysteresis, **(b)** stress response vs time

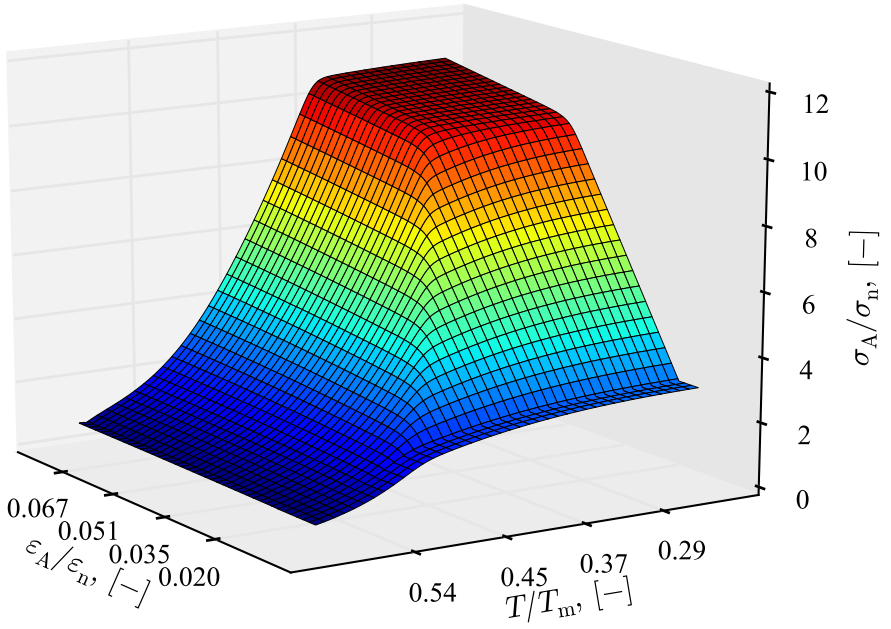

Figure 4.15: Function of stress amplitudes

$$t \in [t_1, t_2]: \quad I_1 = \int_{t_1}^{t_2} r(\omega) S (\sigma\varepsilon)^n \dot{\varepsilon}^p \mathrm{d}t = \left| \begin{array}{lll} \sigma = \sigma_A/2, & \varepsilon = \dot{\varepsilon} t & \dot{\varepsilon}^p = \dot{\varepsilon} \\ t_1 = \dfrac{\sigma_A}{2E\dot{\varepsilon}}, & t_2 = \dfrac{\varepsilon_A}{2\dot{\varepsilon}} & \end{array} \right| =$$

$$= r(\omega) S \left(\frac{\sigma_A}{2}\right)^n \frac{\dot{\varepsilon}^n}{n+1} t^{n+1} \Big|_{t_1}^{t_2} = \frac{r(\omega) S}{n+1} \left(\frac{\sigma_A}{2}\right)^n \left(\left(\frac{\varepsilon_A}{2}\right)^{n+1} - \left(\frac{\sigma_A}{2E}\right)^{n+1} \right) \tag{4.34}$$

$$t \in [t_7, t_8]: \quad I_2 = \int_{t_7}^{t_8} r(\omega) S (\sigma\varepsilon)^n \dot{\varepsilon}^p \mathrm{d}t = \left| \begin{array}{l} \sigma = \sigma_A/2, \quad \varepsilon = -2\varepsilon_A + \dot{\varepsilon} t, \quad \dot{\varepsilon}^p = \dot{\varepsilon} \\ t_7 = \dfrac{1}{\dot{\varepsilon}} \left(\dfrac{3}{2}\varepsilon_A + \dfrac{\sigma_A}{E} \right), t_8 = \dfrac{2\varepsilon_A}{\dot{\varepsilon}} \end{array} \right| =$$

$$= r(\omega) S \left(\frac{\sigma_A}{2}\right)^n \frac{\dot{\varepsilon}^n}{n+1} \left(t - \frac{2\varepsilon_A}{\dot{\varepsilon}} \right)^{n+1} \Big|_{t_7}^{t_8} = -\frac{r(\omega) S}{n+1} \left(\frac{\sigma_A}{2}\right)^n \left(\frac{\sigma_A}{E} - \frac{\varepsilon_A}{2} \right)^{n+1} \tag{4.35}$$

Thereby, the increment of fatigue damage can be computed as follows:

$$\frac{\Delta\omega}{\Delta N} = \frac{r(\omega) S}{n+1} \left(\frac{\sigma_A}{2}\right)^n \left[\left(\frac{\varepsilon_A}{2}\right)^{n+1} - \left(\frac{\sigma_A}{2E}\right)^{n+1} - \left(\frac{\sigma_A}{E} - \frac{\varepsilon_A}{2}\right)^{n+1} \right] \tag{4.36}$$

It must be noted, that σ_A for specific material is the function of amplitudes ε_A and temperature T, and can be computed according to the identified constitutive model for the inelastic material behavior. Obviously, the increment

of the fatigue damage (4.35) can not be a negative, therefore the values of n can not be even. The function of stress amplitude is evaluated according to the current constitutive model and presented in Fig. 4.15. Within the current work, the function of the stress amplitudes is computed numerically through the simulation of the material behavior under cyclic loads at different strain amplitudes and temperatures. It must be noted, that determination of this function requires the formulated constitutive model for the inelastic material behavior.

4.7 Creep-fatigue damage interaction

The important aspect of the creep-fatigue damage is the structure mixture function F (2.63). The profile of this function depends on the several conditions including the quality of the available set of the experimental data. The principal difference between creep tests, where only creep damage accumulation is observed, and low-cycle fatigue damage are rates of the inelastic strain. Within the framework of current research, the inelastic strain rate observed in the creep tests reach the highest values $\dot{\varepsilon}^{\mathrm{p}} \approx 0.01\,\mathrm{h}^{-1}$, while the low-cycle fatigue tests and tensile tests are performed at the assigned strain rates $\dot{\varepsilon} = 3.6\,\mathrm{h}^{-1}$. Therefore, in particular cases, the creep damage during the cyclic loading of high rates can be neglected. However, the consideration of the complete creep-fatigue damage model is necessary especially in cases of the mechanical loads observed in the thermo-mechanical fatigue tests.

Within the frame of current work the following profile of the creep-fatigue interaction function F is assumed:

$$\begin{aligned} F(\dot{\omega}_{\mathrm{c}}, \dot{\omega}_{\mathrm{f}}) &= \vartheta \dot{\omega}_{\mathrm{c}} + (1-\vartheta)\dot{\omega}_{\mathrm{f}}, \\ \vartheta(\dot{\boldsymbol{\varepsilon}}^{\mathrm{p}}) &= \frac{1}{2}\left[1 - \tanh\left(\vartheta_{\mathrm{a}}(\dot{\varepsilon}^{\mathrm{p}}_{\mathrm{vM}} - \vartheta_{\mathrm{b}})\right)\right], \end{aligned} \tag{4.37}$$

where ϑ is the function formulated taking into account available experimental data. The parameters of above-mentioned function are not included in the optimization-based secondary identification step. The material parameters $\vartheta_{\mathrm{a}} = 200\,\mathrm{h}$ and $\vartheta_{\mathrm{b}} = 0.1293\,\mathrm{h}^{-1}$ are chosen in order to satisfy the requirements to the constitutive model: the intergranular damage corresponds to the slow loading regimes, transgranular damage corresponds to the cyclic loads with high rates of strains. The function ϑ identified within the current work is shown in Fig. 4.13. In addition, the above-mentioned formulation of the creep-fatigue damage interaction function (4.37) allows us to apply the defined creep damage evolution equation (4.22) and to take into account the

fatigue damage evolution equation (2.54), which is predefined in the primary identification step (Sect. 4.5).

4.8 Identification results

Within the framework of the primary identification the structure of the constitutive model is determined and the preliminary estimation of the material parameters is performed. Taking into account the determined functions and material parameters, the constitutive model describing the inelastic behavior of the GJV cast including the creep-fatigue damage is:

(2.15) $\boldsymbol{\varepsilon} = \boldsymbol{\varepsilon}^{\mathrm{el}} + \boldsymbol{\varepsilon}^{\mathrm{p}} + \boldsymbol{\varepsilon}^{\mathrm{th}},$

(2.24) $\boldsymbol{\sigma} = \left[\kappa(\omega) + \chi\right]\left[\lambda\langle \mathrm{tr}[\boldsymbol{\varepsilon}^{\mathrm{el}}]\rangle_{+}\boldsymbol{I} + 2\mu\boldsymbol{\varepsilon}^{\mathrm{el}}_{+}\right] + \left[\lambda\langle \mathrm{tr}[\boldsymbol{\varepsilon}^{\mathrm{el}}]\rangle_{-}\boldsymbol{I} + 2\mu\boldsymbol{\varepsilon}^{\mathrm{el}}_{-}\right],$

(2.21) $\lambda = \dfrac{\nu E}{(1+\nu)(1-2\nu)}, \quad \mu = \dfrac{E}{2(1+\nu)}, \quad E(T) = E_{\mathrm{a}} + E_{\mathrm{b}}T^3,$

(2.45) $\dot{\boldsymbol{\varepsilon}}^{\mathrm{p}} = \dfrac{3}{2}\dfrac{\dot{\varepsilon}^{\mathrm{p}}_{\mathrm{vM}}}{\overline{\sigma}_{\mathrm{vM}}}\overline{\boldsymbol{s}}, \quad \dot{\varepsilon}^{\mathrm{p}}_{\mathrm{vM}} = R(T) f\left(\dfrac{\overline{\sigma}_{\mathrm{vM}}}{1-\omega}\right), \quad \overline{\boldsymbol{s}} = \boldsymbol{s} - \boldsymbol{\beta},$

(2.36) $\overline{\sigma}_{\mathrm{vM}} = \sqrt{\dfrac{3}{2}(\boldsymbol{s}-\boldsymbol{\beta})\cdot\cdot(\boldsymbol{s}-\boldsymbol{\beta})},$

(4.8) $R_{\mathrm{s}}(T) = \exp\left(-\dfrac{\alpha^{\mathrm{H}}_{\mathrm{s}}}{T}\right)\left[1 + \exp\left(-\left(\alpha^{\mathrm{H}}_{\mathrm{s}} - \alpha^{\mathrm{L}}_{\mathrm{s}}\right)\left(\dfrac{1}{T^{\mathrm{s}}_{*}} - \dfrac{1}{T}\right)\right)\right],$

(4.8) $R_{\mathrm{i}}(T) = \exp\left(-\dfrac{\alpha^{\mathrm{H}}_{\mathrm{i}}}{T}\right)\left[1 + \exp\left(-\left(\alpha^{\mathrm{H}}_{\mathrm{i}} - \alpha^{\mathrm{L}}_{\mathrm{i}}\right)\left(\dfrac{1}{T^{\mathrm{i}}_{*}} - \dfrac{1}{T}\right)\right)\right],$

(4.8) $f_{\mathrm{s}}(\sigma) = A_{\mathrm{s}}\left[\sinh\left(\dfrac{\sigma}{B_{\mathrm{s}}}\right)\right]^{n_{\mathrm{s}}}, \quad f_{\mathrm{i}}(\sigma) = A_{\mathrm{i}}\left[\sinh\left(\dfrac{\sigma}{B_{\mathrm{i}}}\right)\right]^{n_{\mathrm{i}}},$

(2.42) $\dot{\boldsymbol{\beta}} = \dfrac{1}{\mu_{\mathrm{h}}}\dfrac{\mathrm{d}\mu_{\mathrm{h}}}{\mathrm{d}T}\dot{T}\boldsymbol{\beta} + \dfrac{2}{3}\mu_{\mathrm{h}}\left[\dot{\boldsymbol{\varepsilon}}^{\mathrm{p}} - \dfrac{3}{2}\dot{\varepsilon}^{\mathrm{p}}_{\mathrm{vM}}\dfrac{\boldsymbol{\beta}}{\beta_{*}}\right],$

(4.15) $\beta_{*}(T,\boldsymbol{\sigma}) = \sigma - B_{\mathrm{i}}\,\mathrm{arcsinh}\left[\left(\dfrac{A_{\mathrm{s}}R_{\mathrm{s}}(T)}{A_{\mathrm{i}}R_{\mathrm{i}}(T)}\right)^{1/n_{\mathrm{i}}}\left[\sinh\left(\dfrac{\sigma}{B_{\mathrm{s}}}\right)\right]^{n_{\mathrm{s}}/n_{\mathrm{i}}}\right],$

(4.18) $\mu_{\mathrm{h}}(T) = \mu_{\mathrm{a}} + \mu_{\mathrm{b}}T^3,$

(4.37) $\dot{\omega} = \vartheta\dot{\omega}_{\mathrm{c}} + (1-\vartheta)\dot{\omega}_{\mathrm{f}}, \quad \vartheta = \dfrac{1}{2}\left(1 - \tanh\left(\vartheta_{\mathrm{a}}(\dot{\varepsilon}^{\mathrm{p}}_{\mathrm{vM}} - \vartheta_{\mathrm{b}})\right)\right),$

(4.22) $\dot{\omega}_{\mathrm{c}} = H_{\mathrm{c}}(\boldsymbol{\sigma})\,Y(\boldsymbol{\varepsilon}^{\mathrm{p}})\,r(\omega)\mathfrak{C}(T,\boldsymbol{\sigma})\dot{\varepsilon}^{\mathrm{p}}_{\mathrm{vM}},$

(2.50) $H_{\mathrm{c}}(\boldsymbol{\sigma}) = \dfrac{\sigma_I + |\sigma_I|}{2}, \quad Y(\boldsymbol{\varepsilon}^{\mathrm{p}}) = \dfrac{1}{2}\left(\mathrm{sgn}(\varepsilon^{\mathrm{p}}{}_I + \varepsilon^{\mathrm{p}}{}_{III}) + 1\right),$

(2.49),(4.20) $r(\omega) = l\omega^{1-\frac{1}{l}}, \quad \mathfrak{C}(T,\boldsymbol{\sigma}) = \varepsilon^{\mathrm{p}}_{*}(T,\boldsymbol{\sigma})^{-1},$

(4.21) $$\varepsilon^{\mathrm{p}}_{*}(T,\boldsymbol{\sigma}) = \epsilon_{\mathrm{br}} D(T) + \frac{D(T)\, a_{\varepsilon}}{1 + b_{\varepsilon} e^{-\frac{\sigma_{\mathrm{vM}}}{c_{\varepsilon}}}}, \quad D(T) = \exp\left(-\frac{\alpha_{\mathrm{D}}}{T}\right),$$

(2.54) $$\dot{\omega}_{\mathrm{f}} = H_{\mathrm{f}}(\boldsymbol{\sigma})\, r(\omega) \mathfrak{F}\left(T,\boldsymbol{\sigma},\boldsymbol{\varepsilon},\boldsymbol{\varepsilon}^{\mathrm{p}}\right) \dot{\varepsilon}^{\mathrm{p}}_{\mathrm{vM}},$$

(2.60),(4.23) $$H_{\mathrm{f}}(\boldsymbol{\sigma}) = H_{\mathrm{c}}(\boldsymbol{\sigma}), \quad \mathfrak{F}\left(T,\boldsymbol{\sigma},\boldsymbol{\varepsilon},\boldsymbol{\varepsilon}^{\mathrm{p}}\right) = S(T) (\sigma_{\mathrm{vM}} \varepsilon_{\mathrm{eq}})^{n} \dot{\varepsilon}^{\mathrm{p}}_{\mathrm{vM}},$$

(4.31) $$S(T) = s_{\mathrm{a}} \exp(s_{\mathrm{b}} T)$$

4.9 Summary

The primary identification step is focused on the formulation of the structure of the material-dependent functions and determination of the material parameters for them. Mainly, the primary step is based in the trial and hand-fitting identification approaches. Within the framework of current research, the primary identification step allows us to determine complete constitutive model describing the material behavior under the creep loads including the creep and fatigue damage model, and particularly the inelastic behavior of the material during the isothermal cyclic tests (LCFs). The obtained parameters can be used as final result as well as for the secondary identification step as guess values. It must be stated, that the accuracy of the primary identification is low and can be sufficient only for the cases, when the constitutive model is utilized for simulation of the material behavior under the similar conditions, which were used in the identification. The resulting constitutive model can give the inaccurate results in the simulations of the material behavior under TMF loads, which is not used in the primary identification. Therefore, the secondary identification step is required.

CHAPTER

5 Secondary identification

The current chapter is mainly focused on the application of the numerical integration and optimization methods for the solution of the parameters identification problem. Within the framework of current part of the work, all available types of the experimental data including the creep tests, tensile tests, LCF and TMF tests are used. The secondary identification step is focused on the identification of the complete constitutive model (elasticity, inelasticity, creep-fatigue damage, etc.). The identification of the creep-fatigue damage model requires defined constitutive model for the inelastic behavior, therefore its identification is the initial step of the secondary identification problem. Taking into account the different nature of the inelastic deformations and damaging process, the secondary identification of the corresponding parts of the constitutive mode is performed separately.

5.1 Strategy of identification

The secondary identification is based on the minimization of the error function described in Sect. 5.2. Within the framework of current work, the minimization algorithm proposed by Powell [71] is used. The above-mentioned approach representing the unconstrained zero-order conjugate directional minimization algorithm, which can be used for the unrestricted minimization of the target function. The opportunities to extend the unrestricted optimization to the optimization with restriction are discussed in the Sect. 5.4.

One feature of the current identification problem includes the application the different types of experimental data. The error values in the each specific

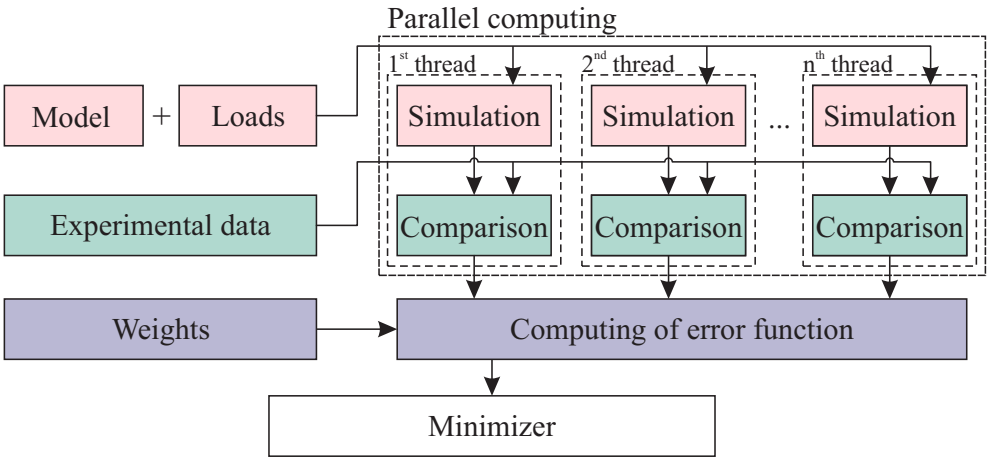

Figure 5.1: Scheme of single iteration of the secondary identification step

case can be computed independently within the frame of the same set of material parameters. Thereby, the large number of the different numerical computations can be performed in the various computational threads. Therefore, the computation scheme presented in Fig. 5.1 is utilized.

The optimization is used in the secondary identification problem within two cases, when the constitutive model for the inelastic material properties and creep-fatigue damage were determined. In the both cases the principal computational scheme shown in Fig. 5.1 is used.

The information about the quality of the experimental data, level of the confidence to specific tests may be also included

5.2 Computing of the error

The current section is focused on the formulations for the target error functions. Within the framework of identification problem several different types of experimental data can be used. For instance, in case of creep tests the results are inelastic strain, in case of cyclic tests the stress values and number of cycles to rupture, etc. The aim of the current section is to formulate the error functions, which allows us to represent the deviation of the simulated and experimental data taking into account the different nature and dimension.

The result of the creep test are inelastic deformations accumulated in the sample. In the primary creep stage they reach the values upto 1%. Moreover, the operation under the inelastic regime requires the comparison of data, which in some cases can have different orders. In such cases, the logarithmic length-scale is preferable.

In addition, different values of the inelastic strains and strain rates at different loading conditions may lead to the situation, when the error values depend on the loading conditions, that is artificial and non-realistic. Therefore, the normalization of the experimental data must be applied. Taking into account the above-mentioned features, the Gauß function ξ within the each single experiment can be calculated as follows:

$$\xi^i = \left| \frac{\ln(e^i) - \ln(s^i)}{\ln(e^i)} \right| = \left| 1 - \log_{e^i} s^i \right|, \; i \in \mathfrak{E}_1, \tag{5.1}$$

where e^i is the representative measure of i^{th} experiment of the sub-set $\mathfrak{E}_1$ of the experimental data $\mathfrak{E}$, which requires the logarithmic scale (inelastic strains or strain rates), s is the value of corresponding measure estimated by the constitutive model. However, the application logarithmic error definition in the case of negative operating values is not possible, therefore in this case the other definitions for the error must be considered.

The comparison of estimated and experimental stress responses is sufficient to perform in the linear length-scale. However, by the objective reasons, the normalization of the error is still required:

$$\xi^i = \left| \frac{e^i - s^i}{e^i} \right|, \; i \in \mathfrak{E}_2, \tag{5.2}$$

where $\mathfrak{E}_2$ is the sub-set of the experimental data, where the resulting values of the experiments and simulations at the different loading conditions have approximately the same order. The above-mentioned condition is useful for the stress comparison in the tensile, LCF and TMF tests.

In particular, in the case of cyclic tests the normalization of the error function (5.2) can lead to artefacts related to the zero division problem. The application of the logarithmic scale is this case is also not possible, because positive values of argument are required for logarithmic scale. Therefore, the maximum stress amplitude, measured within the each single experiments, can be used for the normalization of the deviation:

$$\xi^i = \left| \frac{e^i - s^i}{\Delta e^i} \right|, \; \Delta e_i = \max(e^i) - \min(e^i), \; i \in \mathfrak{E}_2, \tag{5.3}$$

where Δe^i is the maximal fluctuation amplitude of the representative measure.

The natural noise, presenting normally in the experimental data for each kind of tests, can not be identified by using the deterministic constitutive

model. Therefore, the additional mechanism is considered in order to exclude the influence of experimental error on the identification quality. Obviously, the quality of the identification of the constitutive model is sufficient, when the deviation of the the model prediction and experimental data is minimal. However, the determination of the constitutive model with the accuracy higher then the accuracy of the experimental data is not necessary. Therefore, the following expression is proposed in order to include the above-mentioned features:

$$\widetilde{\xi}^i = \xi^i_{\mathrm{e}} \left(\frac{\xi^i}{\xi^i_{\mathrm{e}}} \right)^{\widetilde{k}}, \; i \in \mathfrak{E}, \tag{5.4}$$

where $\widetilde{\xi}^i$ is updated value of Gauß function including the information about deviation ξ^i_{e} of experimental data, $\widetilde{k}$ is the coefficient, $\widetilde{k} > 1$. The increasing of $\widetilde{k}$ coefficient reduces the influence of the error ξ^i, if it is less then the error of the experiment ξ^i_{e}. The proposed scheme can be used for any kinds of the error functions mentioned above.

The error functions computed for the simulated LCF test at T =0.413T_{m} and ε_{A} =0.79ε_{n} are shown in Fig. 5.2. Obviously, the linear (5.2) and logarithmic (5.1) error definitions are not useful for shown kind of tests, while the normalized linear error function (5.3) and advanced error definition (5.4), taking into account the accuracy of the experimental data, are more appropriate.

Different errors computed taking into account the specific experiments contributes and summarized into the resultant error, which representing the summary deviation of the constitutive model and experimental data. However, the weight factors must be taken into account during the computation of the resulting error:

$$\xi = \sum_{i \in \mathfrak{E}} w^i \widetilde{\xi}^i_{\mathrm{e}} \tag{5.5}$$

where w_i is the weight ratio of each single experiment. The choice of the weights depends on different factors, including the field of application of the constitutive model, the confidence of the experimental data, etc.

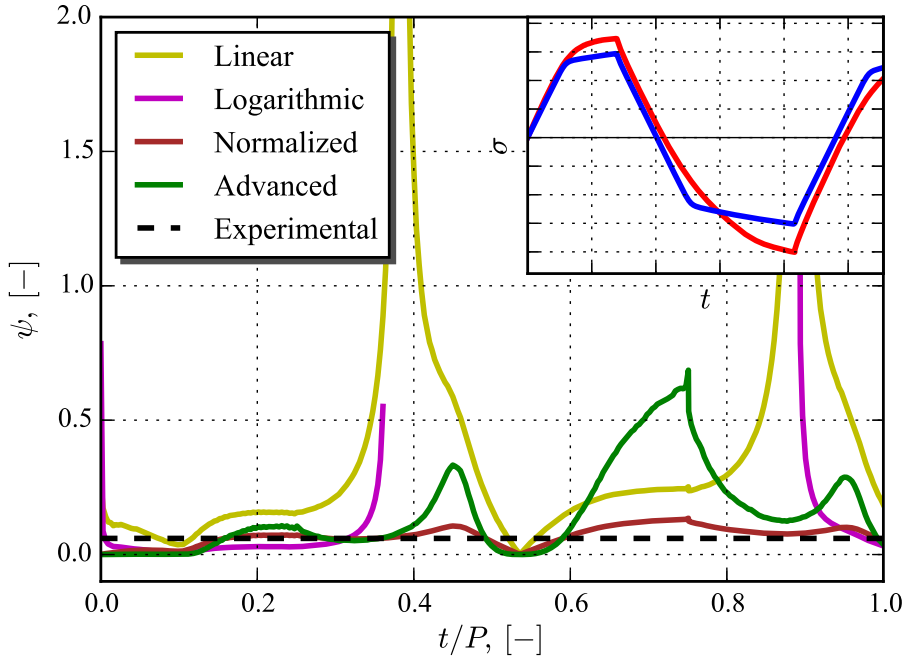

Figure 5.2: Different types of error function in the simulation of LCF test

5.3 Choice of weights

The application of the weighting parameters in the secondary identification allows us to manage the influence of the different factors affecting the efficiency of the constitutive model. In general, the weights can be chosen with respect to the factual features of the target material and also can include some desired aspects, which may be required for the application of the constitutive model. Mainly, the factual requirements are related to the amount, accuracy and quality of the experimental data. However, the conditions of exploitation of entire design, in which identified material is planned for application, can be accounted during the choice of weights. Within the frame of current section the several useful cases of the weights functions are considered.

On practice, the material model is normally develop for the fixed operation conditions, which are mainly take place in the mechanical parts. The information about the mentioned operation conditions can be used in the identification in order to reduce the influence of experimental data, which are not included in the requirements to the model. For instance, weights may be chosen according to temperatures, stresses, strains or plastic strains, which are observed in the mechanical parts of the design. In this case the shape of the weight functions can be represented by the arbitrary functions with the fol-

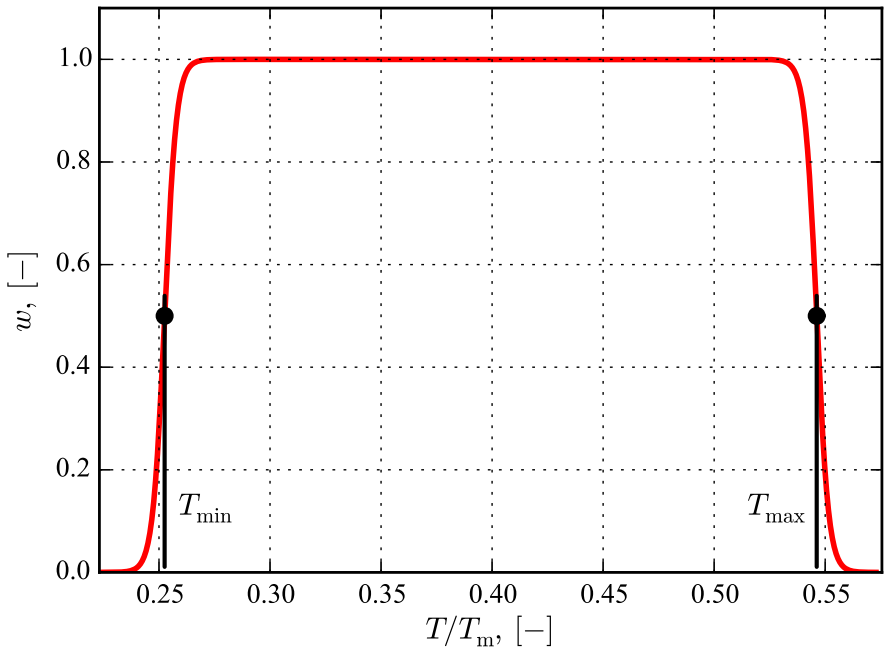

Figure 5.3: Weight function of temperature

lowing requirements:

$$w(x) = w_{\max} \forall x \in [x_{\min}, x_{\max}],$$
$$w(x) = w_{\min} \forall x \notin [x_{\min}, x_{\max}]$$

where x is the assigned representative measure using for the calibration of the constitutive model. Within the frame of current work only restrictions by the range of temperature is used, however approach is not limited only by it. The utilized shape of the weight function that regulates the influence of the temperature conditions on the resultant vector of the material parameters is shown in Fig. 5.3.

The proposed shape of the weight function is not restricted to be the same for each controlling characteristic and can be chosen in the arbitrary way in order to satisfy the particular requirements to the constitutive model. The weights can be applied in order to manage the influence of the experimental data and to calibrate the target constitutive model for narrow range of the loading profiles. Application of weights in this case can reduce the universality of the constitutive model, however increase the accuracy of description for particular case of the mechanical loads.

Taking into account the different weight factors representing the varied number of the requirements to the constitutive model, the general weight for

certain test can be formulated as follows:

$$w = \prod_i w_i, \tag{5.6}$$

where w_i represents the weighting factor according to each considered criteria.

5.4 Restricted optimization problem

The optimization problem consists of minimization of the target function. The different kinds of the minimizers mentioned in Sect. 3.1.3 can be used for solving of this kind of problems. However, from time to time, the specific efforts appear, when the approaches designed for the unrestricted minimization problem are necessary for the use in the minimization with restrictions. The current section is focused on the solution of these contradictions.

The typical minimization problem (3.1) taking into account the defined error function (5.5) is:

$$\boldsymbol{p} = \arg\min_{\boldsymbol{p}\in\mathbb{P}} \xi(\boldsymbol{p}), \tag{5.7}$$

where $\mathbb{P}$ is the unbounded space of the material parameters.

Within the mentioned definition the resulting vector of the parameters $\boldsymbol{p}$ corresponds to the minimum of Gauß function ξ. In general, the material parameters $\boldsymbol{p}$ are not restricted and can lay in the infinite space of parameters $\mathbb{P}$. In the current particular case, Gauß function ξ includes the information about the mechanical processes taking place in the material. Thereby, the material parameters must lay in bounded space $\mathbb{P}_*$, which corresponding the physical meaning of declared functions.

The replacement of the unrestricted optimization problem by the restricted one can be performed by the introduction of the following transition function:

$$\begin{aligned} &\widetilde{\boldsymbol{p}} = T(\boldsymbol{p}),\ \boldsymbol{p} \in \mathbb{P},\ \widetilde{\boldsymbol{p}} \in \mathbb{P}_* \\ &\boldsymbol{p} = \arg\min_{\boldsymbol{p}\in\mathbb{P}} \xi(\widetilde{\boldsymbol{p}}) \end{aligned} \tag{5.8}$$

The particular representations for the transition function T can be chosen in the different way. The main idea laying behind this function is the smooth transformation of parameters $\boldsymbol{p}$ on infinite interval to parameters $\widetilde{\boldsymbol{p}}$ in the limited interval. There are many different opportunities for the design of the function T. The various definitions of T considered in this work are given in Table 5.1. In the Table 5.1 $z^i = \frac{p^i_{\max}+p^i_{\min}}{2}$, $a^i = \frac{p^i_{\max}-p^i_{\min}}{2}$, α is a parameter,

Linear	$\widetilde{p}^i = p^i$, if $p^i \in [p^i_{\min}, p^i_{\max}]$ $\widetilde{p}^i = p^i_{\min}$, if $p^i < p^i_{\min}$ $\widetilde{p}^i = p^i_{\max}$, if $p^i > p^i_{\max}$
Tangential	$\widetilde{\boldsymbol{p}} = \widetilde{p}^i \boldsymbol{e}_i$, $\forall i \in L(\widetilde{\boldsymbol{p}})$, $\widetilde{p}^i = a^i \tanh\left(\alpha p^i\right) + z^i$
Exponential	$\widetilde{\boldsymbol{p}} = \widetilde{p}^i \boldsymbol{\theta}_i$, $\forall i \in L(\widetilde{\boldsymbol{p}})$, $\widetilde{p}^i = z^i + \operatorname{sgn}(p^i) a^i \left(1 - e^{-\lvert\alpha p^i\rvert}\right)$

Table 5.1: Transition functions

which can be used for the regulation of the smoothness of the transition, $\boldsymbol{\theta}^i$ is the basis of the parameters space.

The proposed linear definition of the transition function T is the simplest one, however it has the specific points $p^i = p^i_{\max}$ and $p^i = p^i_{\min}$, which lead to the discontinuity of the function's derivative. The above-mentioned feature of the linear transition functions is not desirable in cases, when the gradient-based minimization approaches are used. However, the application of the zero-order minimization algorithms makes the influence of the derivative insignificant.

The tangential and exponential definitions proposed in the Table 5.1, except the linear one, give the continuous smooth derivative of transition function, that not affects the smoothness of the Gauß function $\xi(T(\boldsymbol{p}))$. The considered transition functions used within the current research are shown in Fig. 5.4. The exponential transition function is used in this work, because it does not exhibit undesired features in the bounds like the linear function and representing the lower time-consumption with respect to the tangential transition function.

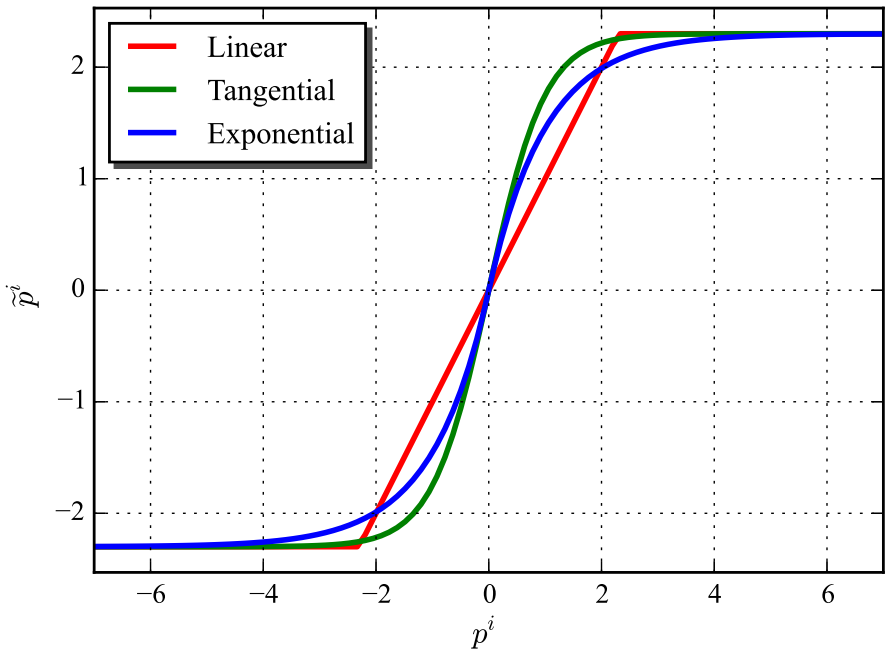

Figure 5.4: Transition functions

5.5 Extrapolation problem

The optimization-based identification step requires the determination of the error function for the specific loading conditions. In the case of the simulation of the material's behavior under the conditions observed in creep tests, tensile tests, LCF and TMF tests the evaluation of the error function can be performed through the full integration of the constitutive equations for the corresponding loading conditions. However, the above-mentioned approach is not useful for the identification of the fatigue damage model. Mainly, it is related to the necessity to compute the number of cycles to the rupture N_{A} as the representative measure constructing the error function in case of low-cycle fatigue damage. In the combination with the iterative optimization procedure and large number of LCF tests, the time-consuming integration of the constitutive equations becomes unrealistic. Therefore, the additional steps to reduce the computation costs must be considered.

The enchanted extrapolation approach is used in this work for the estimation of the number of cycles to the rupture. In particular, the extrapolation is available for the current type of constitutive model, because the simulation of the LCF and TMF tests gives the power-law dependence of the damage parameter ω with time. The resulting growth of the damage parameter for the

LCF loading conditions at T =0.519T_m and ε_A = 0.474ε_n is shown in Fig. 5.5.

Thereby, the accumulation of damage in the cases of LCF and TMF loading profiles exhibits the asymptotic trend to the power-law function, which in term of current notations can be represented as follows:

$$\ln\left[\frac{\omega_{i+1}}{\omega_i}\right] = k \ln\left[\frac{i+1}{i}\right], \tag{5.9}$$

where ω_i and ω_{i+1} are accumulated damages at i^{th} and $(i+1)^{\mathrm{th}}$ cycles, respectively, k is the effective damage growth rate. Equation 5.9 is derived taking into account linearity of power-law functions in a double logarithmic scale. The effective damage growth rate k can be determined through differentiation of the expression (5.9):

$$k = \frac{\mathrm{d}(\ln(\omega))}{\mathrm{d}(\ln(N))} = \frac{N}{\omega}\frac{\mathrm{d}\omega}{\mathrm{d}N}, \; k \neq \mathrm{const} \tag{5.10}$$

The resulting effective damage growth rate for the LCF loads at T =0.519T_m and ε_A = 0.474ε_n is shown in Fig. 5.6. The asymptotic behavior of the damage allows us to avoid the integration of the constitutive equations until the rupture will be reached. However, the rate of the tendency of the da-

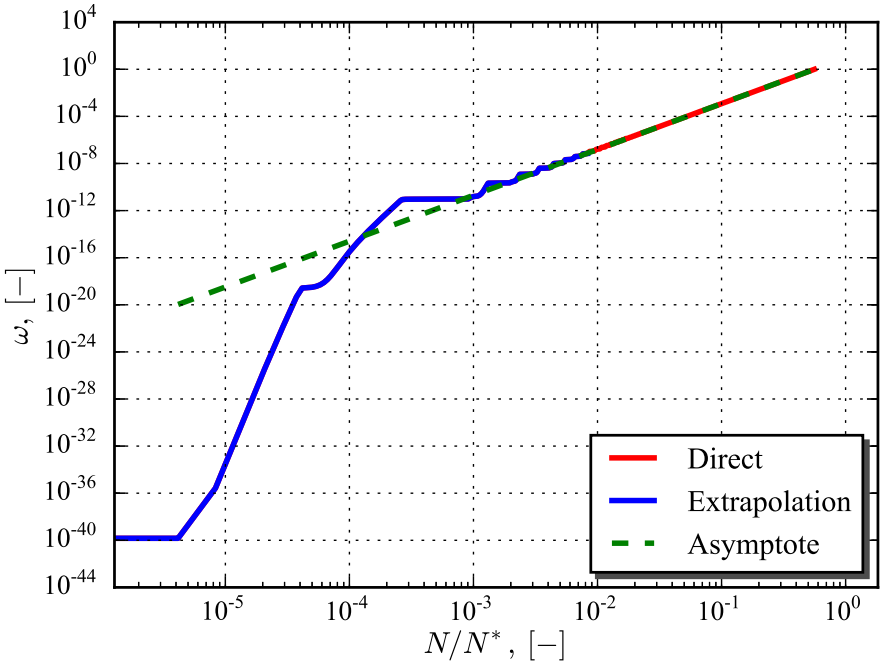

Figure 5.5: The creep-fatigue damage in the LCF test simulation: comparison of the direct integration and extrapolation

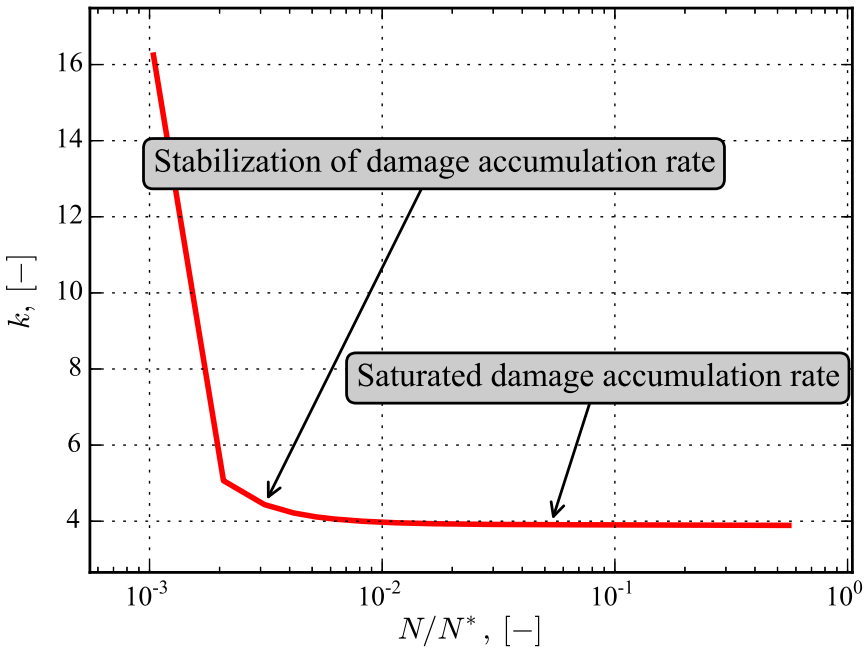

Figure 5.6: Change of effective damage accumulation rate k

mage parameter to the asymptote is such, that it requires the direct simulation of several cycles of loading in order to reach the accuracy criteria:

$$|(k_{i+1} - k_i)/k_i| < \eta,$$

where k_i and k_{i+1} are the effective damage rates computed for the i^{th} and $(i+1)^{\text{th}}$ cycles, respectively, $\eta = 0.01$ provides the accuracy of extrapolation $\approx 99\%$. The proposed enchanted extrapolation scheme leads to the average 100 times reduction of the computation time.

5.6 Secondary identification of the inelastic material properties

On the current step the primary identification of the constitutive model for the inelastic material properties must be finished, and the structure of the functions and guess values of the material parameters must be determined. The step is focused on the further calibration of the constitutive model according to the complete set of the available experimental data related to the inelastic material behavior. Below, the secondary identification includes the

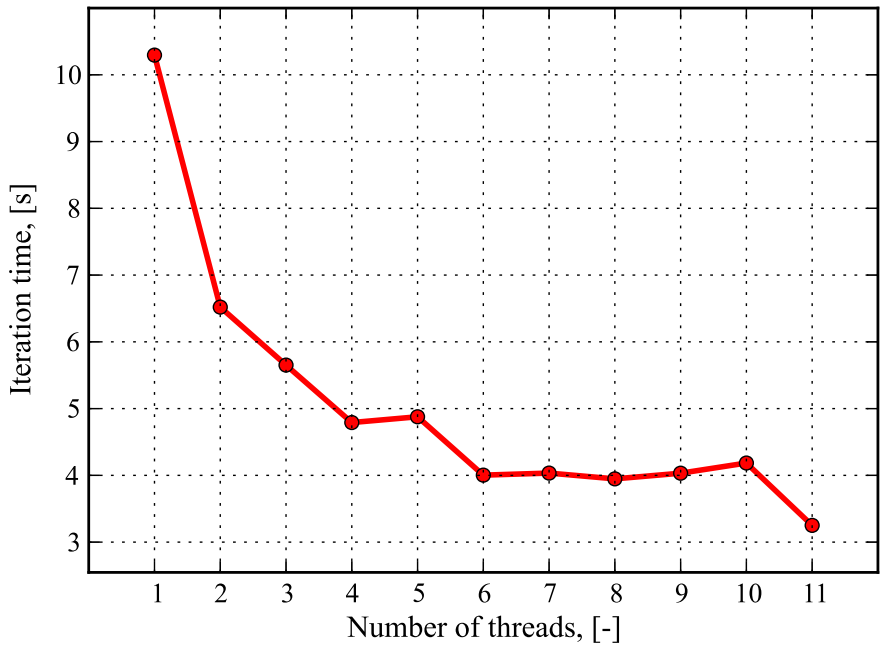

Figure 5.7: The influence of the multiprocessing on the computation time

creep tests, tensile tests, considering the inelastic response in the LCF and TMF tests. Complete list of the used experimental data is given in Table 5.2.

The experimental data from the creep tests and tensile tests can be used within the secondary identification step in the processed format, which includes only information about the initial and steady inelastic strain rates at the different loading conditions. The above-mentioned approach allows us to avoid the simulation of these tests that saves the computational time spent on the identification. However, the evaluation of the error requires the complete simulation of the material behavior for the LCF and TMF loading profiles of the loads, which are most time-consuming part of computation of the error function.

In addition, the application of the experimental data corresponding to the saturated material regime requires to simulate the several cycles of the LCF and TMF tests. Thereby, the saturation of the constitutive model is considered in order to determine the interruption conditions for the integration procedures. On practice, the saturation of the model response for the TMF and LCF loading profiles reaches at the third - fourth cycle.

The simulation of several loading cycles within the each type of test induces the strong necessity for the consideration of the possibilities for increase of efficiency of the algorithm. In particular, the computation of the

error function within the each iteration of the minimization algorithm can be performed by use of the parallel computing tools. Application of the multi-threading computing allows us to reach the significant reduction the time of parameters search. However, the parallel computation gives good results only upto the certain number of computational threads. Moreover, excessive parallelization leads to increase of the computation time. The approximate effect of the parallelization computed for the modern eight-cores computer is shown in Fig. 5.7.

The resulting steady and initial inelastic strain rates are shown in Fig. 5.8a and in Fig. 5.8b, respectively. In particular for the initial inelastic strain rates in except to the primary identification (see Fig. 4.5), the experimental data for the low temperature T =0.359T_{m} from LCF and TMF tests were used for secondary identification of the constitutive model.

The changes in the inelastic strain rate functions lead to the changes in the hardening saturation function (4.15), which is shown in Fig. 5.9a. The hardening rate function is also calibrated in the secondary identification stage according to all available kinds of the experimental data. Within the frame of the similar structure of the hardening rate function, the resultant temperature dependence of the hardening rate μ_{h} is determined as shown in Fig. 5.9b.

Tests	Testing conditions	Weights	Details
Creep tests	$T=0.359T_{\mathrm{m}}$, $\sigma=3.88\sigma_{\mathrm{n}}$	(1,1)	Only initial and steady inelastic strain rates are used. The weights are chosen according to the quality of experimental data and the purpose of the model.
	$T=0.359T_{\mathrm{m}}$, $\sigma=4\sigma_{\mathrm{n}}$	(0.5,0.5)	
	$T=0.359T_{\mathrm{m}}$, $\sigma=4.45\sigma_{\mathrm{n}}$	(0,0)	
	$T=0.359T_{\mathrm{m}}$, $\sigma=4.91\sigma_{\mathrm{n}}$	(0,0)	
	$T=0.466T_{\mathrm{m}}$, $\sigma=0.57\sigma_{\mathrm{n}}$	(0.5,0.5)	
	$T=0.466T_{\mathrm{m}}$, $\sigma=0.68\sigma_{\mathrm{n}}$	(0.5,0.5)	
	$T=0.466T_{\mathrm{m}}$, $\sigma=0.8\sigma_{\mathrm{n}}$	(0.5,0.5)	
	$T=0.466T_{\mathrm{m}}$, $\sigma=1.43\sigma_{\mathrm{n}}$	(0,0.5)	
	$T=0.466T_{\mathrm{m}}$, $\sigma=1.71\sigma_{\mathrm{n}}$	(0,0)	
	$T=0.519T_{\mathrm{m}}$, $\sigma=0.23\sigma_{\mathrm{n}}$	(0.5,0.5)	
	$T=0.519T_{\mathrm{m}}$, $\sigma=0.29\sigma_{\mathrm{n}}$	(0.5,0.5)	
	$T=0.519T_{\mathrm{m}}$, $\sigma=0.37\sigma_{\mathrm{n}}$	(0.5,0.5)	
	$T=0.519T_{\mathrm{m}}$, $\sigma=0.46\sigma_{\mathrm{n}}$	(0.5,0.5)	
	$T=0.573T_{\mathrm{m}}$, $\sigma=7.99\cdot10^{-2}\sigma_{\mathrm{n}}$	(0.5,0.5)	
	$T=0.573T_{\mathrm{m}}$, $\sigma=0.11\sigma_{\mathrm{n}}$	(0.5,0.5)	
	$T=0.573T_{\mathrm{m}}$, $\sigma=0.17\sigma_{\mathrm{n}}$	(0.5,0.5)	
Tensile tests ($\dot{\varepsilon}=3.6\mathrm{h}^{-1}$)	$T=0.159T_{\mathrm{m}}$	0.1	The initial and steady inelastic strain rates computed from tensile tests data are used in the identification. The weights are chosen according to the operating temperature.
	$T=0.199T_{\mathrm{m}}$	0.5	
	$T=0.253T_{\mathrm{m}}$	0.9	
	$T=0.359T_{\mathrm{m}}$	0.9	
	$T=0.413T_{\mathrm{m}}$	0.9	
	$T=0.466T_{\mathrm{m}}$	0.9	
	$T=0.519T_{\mathrm{m}}$	0.9	
	$T=0.573T_{\mathrm{m}}$	0.5	
LCF tests ($\dot{\varepsilon}=3.6\mathrm{h}^{-1}$)	$T=0.253T_{\mathrm{m}}$, $\varepsilon_{\mathrm{A}}=0.79\varepsilon_{\mathrm{n}}$, $N=1$	0.5	The constitutive model is integrated for the saw-type loading profile. The comparison of obtained results is performed for the few loading cycles and for the saturated regime. The weights are chosen according to the quality of experimental data and operating temperature.
	$T=0.359T_{\mathrm{m}}$, $\varepsilon_{\mathrm{A}}=0.79\varepsilon_{\mathrm{n}}$, $N=1$	0.9	
	$T=0.413T_{\mathrm{m}}$, $\varepsilon_{\mathrm{A}}=0.79\varepsilon_{\mathrm{n}}$, $N=1$	0.9	
	$T=0.519T_{\mathrm{m}}$, $\varepsilon_{\mathrm{A}}=0.632\varepsilon_{\mathrm{n}}$, $N=1$	0.9	
	$T=0.573T_{\mathrm{m}}$, $\varepsilon_{\mathrm{A}}=0.632\varepsilon_{\mathrm{n}}$, $N=1$	0.5	
	$T=0.253T_{\mathrm{m}}$, $\varepsilon_{\mathrm{A}}=0.79\varepsilon_{\mathrm{n}}$, $N=N_{\mathrm{A}}/2$	0.5	
	$T=0.359T_{\mathrm{m}}$, $\varepsilon_{\mathrm{A}}=0.79\varepsilon_{\mathrm{n}}$, $N=N_{\mathrm{A}}/2$	0.9	
	$T=0.413T_{\mathrm{m}}$, $\varepsilon_{\mathrm{A}}=0.79\varepsilon_{\mathrm{n}}$, $N=N_{\mathrm{A}}/2$	0.9	
	$T=0.519T_{\mathrm{m}}$, $\varepsilon_{\mathrm{A}}=0.632\varepsilon_{\mathrm{n}}$, $N=N_{\mathrm{A}}/2$	0.9	
	$T=0.573T_{\mathrm{m}}$, $\varepsilon_{\mathrm{A}}=0.632\varepsilon_{\mathrm{n}}$, $N=N_{\mathrm{A}}/2$	0.5	
TMF tests	Direct loading profiles: Probes 3,4 Inverse loading profiles: Probe 2	1	The constitutive model is integrated for the TMF loading profiles. The comparison of obtained results is performed for the few loading cycles and saturated regime.

Table 5.2: The experimental data used in the secondary identification of the inelastic material properties

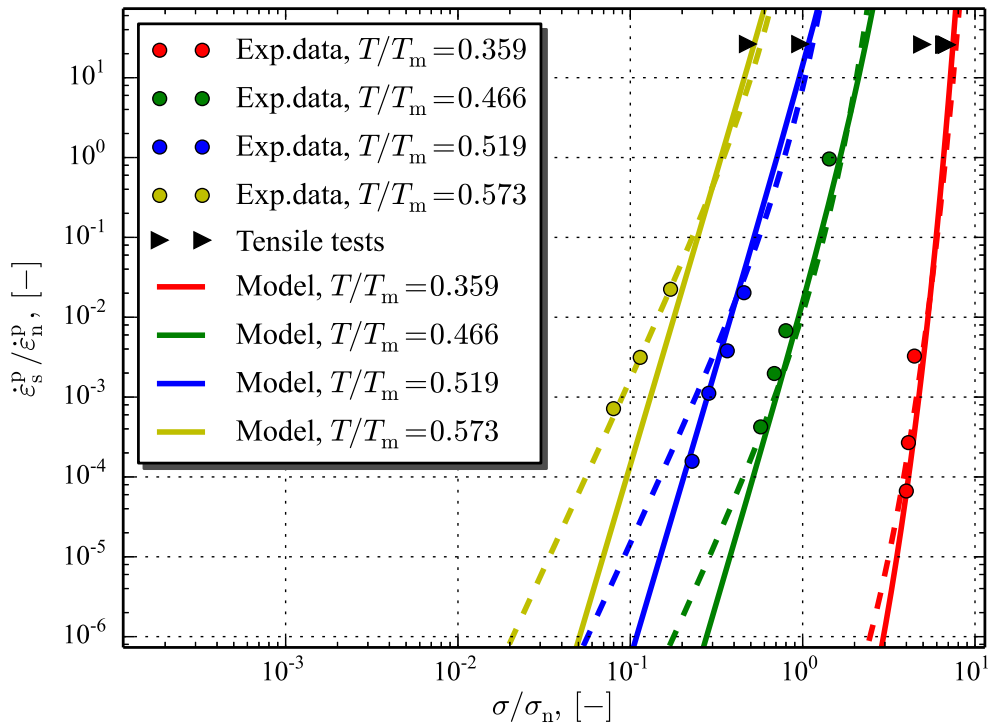

(a)

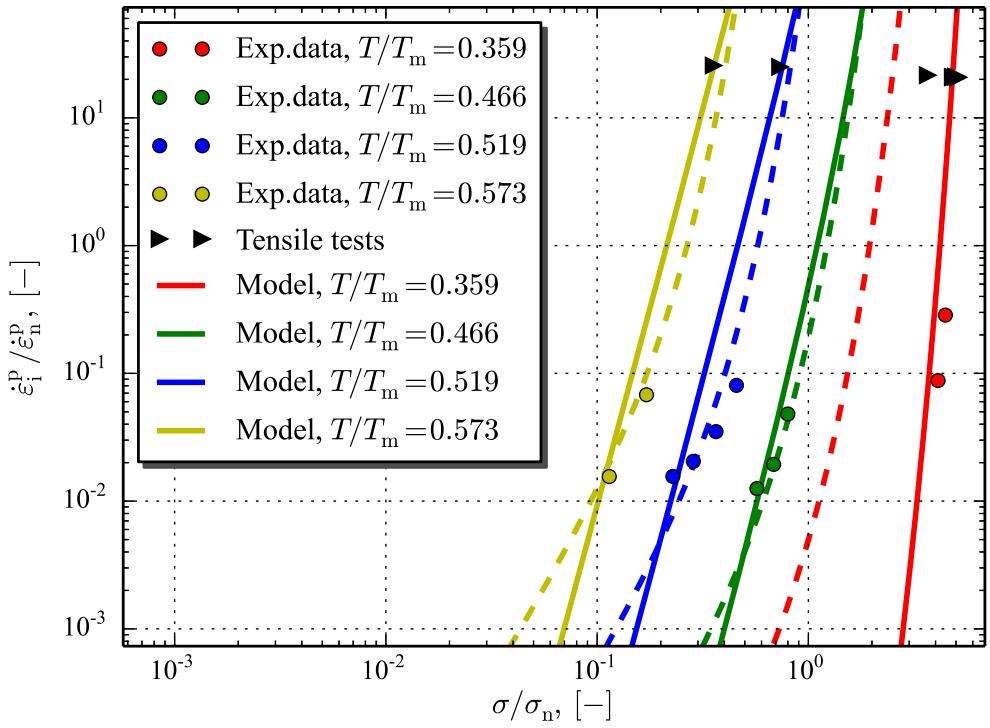

(b)

Figure 5.8: Identified inelastic strain rates: **(a)** steady, **(b)** initial. Dashed lines are the primary identification, solid lines are the secondary identification

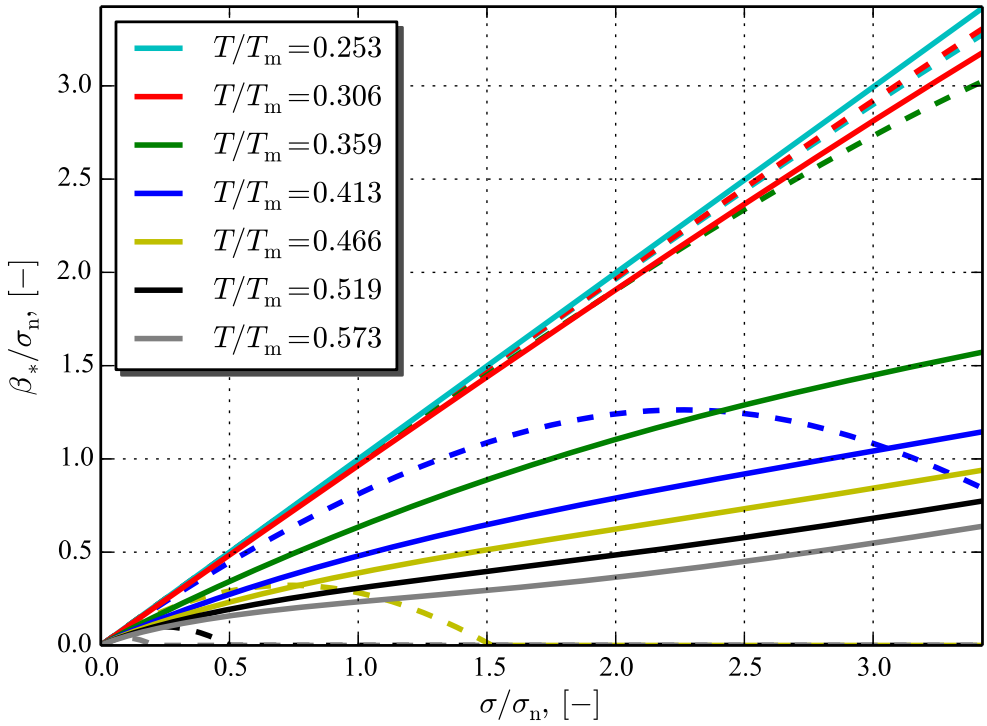

(a)

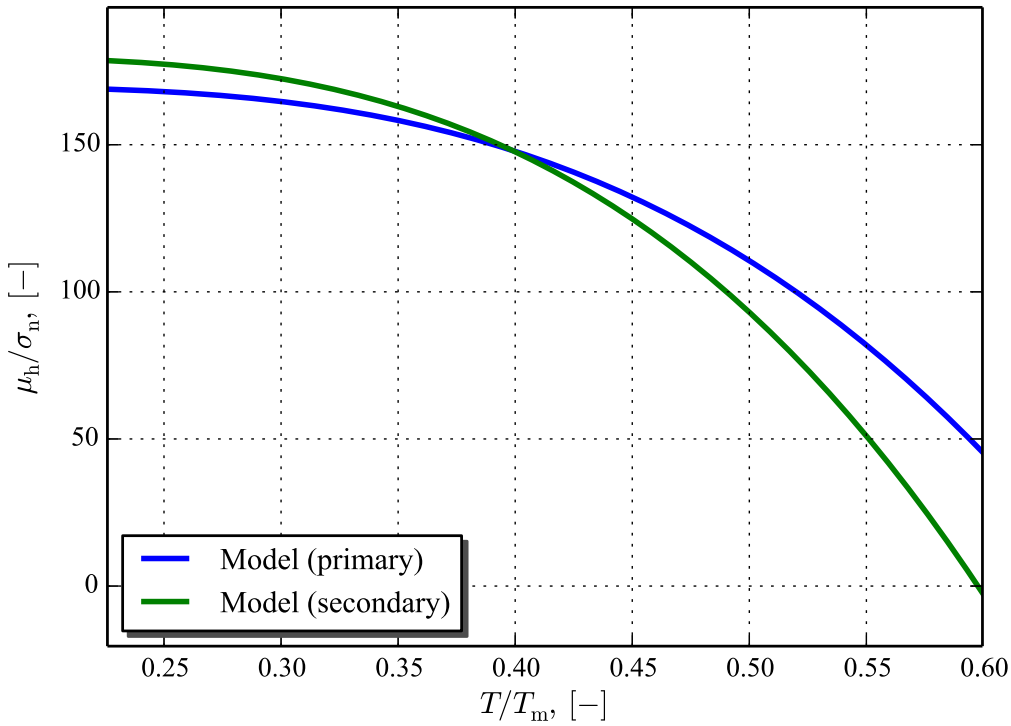

(b)

Figure 5.9: Determined hardening functions: **(a)** hardening saturation function (dashed lines are the primary identification, solid lines are the secondary identification), **(b)** hardening rate function

5.7 Identification of creep-fatigue damage

The current section is focused on the identification of the complete creep-fatigue model based on the identified creep damage evolution equation (4.21) and estimated guess of the parameters used by the creep-fatigue damage evolution equation.

In general, the secondary identification of the creep-fatigue damage model is performed according to the scheme shown in Fig. 5.1. However, except the identification of the constitutive model for the inelastic material behavior (see Sect. 5.6), the current approach uses the extrapolation (see Sect. 5.5) for the estimation of the lifetime of the material at the LCF and TMF loads.

The results obtained after the identification are shown in Fig. 5.10. The identified constitutive model allows us to estimate the lifetime of the material under the LCF and TMF loads with factor two (dashed line). The solid line in Fig. 5.10 represents the direct correspondence of the experimental data to the simulated one. The circled experimental points are excluded from the identification, because the numbers of cycles to rupture in these particular case laying out of interval corresponding to the definition of the low-cycle fatigue. The thermo-mechanical fatigue tests used in the secondary identification of the creep-fatigue damage models are also represented in Fig. 5.10.

Temperature influence function

The resultant temperature influence function calibrated according to the available experimental data is shown in Fig. 5.11. The minimization of the error function leads to the change of the material parameters, and, therefore, to the significant increase of the values of S with respect to primary identification. However, the shape of temperature response function S is not changed.

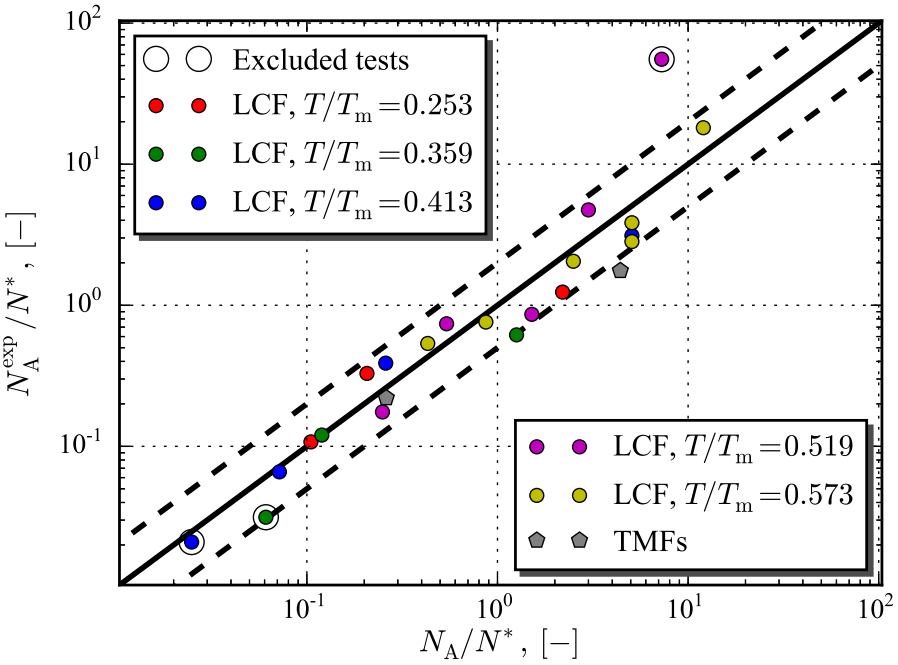

Figure 5.10: The correspondence of the estimated number of cycles to the rupture N_A to the experimental one N_A^{exp}

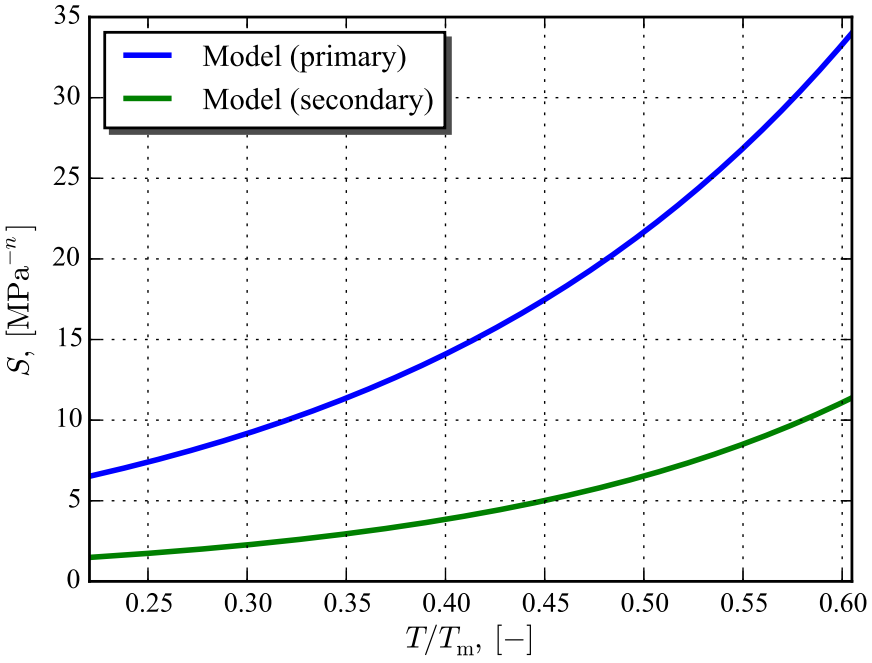

Figure 5.11: Secondary identification results for temperature response function S

5.8 Stiffness degradation function

When the identification of the constitutive model for the inelastic material behavior and creep-fatigue damage is finished, the stiffness degradation function used in the definition for the stress tensor (2.24) can be identified. Mainly, the stiffness degradation feature is required in the constitutive model only in the case, when the behavior of the material in the pre-rupture mode must be described. The above-mentioned mode is represented in the experimental data by the several cycles before the rupture with the significant reduction of stress amplitude. However, the contribution of the pre-rupture mode into the complete lifetime of the material is very low and reaches approximately 1% of the complete lifetime. Thereby, taking into account the accuracy of the experimental data and the accuracy of the fatigue damage model, the stiffness reduction can be neglected.

However, despite the above-mentioned statement, the stiffness reduction opportunity is introduce into the constitutive model in order to generalize its application for the wide class of the materials. The identification is based on the experimental data of the thermo-mechanical fatigue tests (see Fig. 3.9), which clearly shows the degradation of the stiffness at the last cycles of the test. The accumulated damage here is assumed to be $\omega \approx 1$, that corresponds to the rupture of the material. However, the influence of the damage parameter at the beginning and intermediate stage of the test is not observed in the experimental data. The stiffness reduction function must to reflect the above-mentioned feature.

The following expression for the stiffness degradation function is defined:

$$\kappa(\omega) = 1 - \omega^m, \tag{5.11}$$

where m is the parameter identified as $m = 20$. The stiffness degradation function $\kappa(\omega)$ is shown in Fig. 5.12. The simulated stress response according to the TMF loading profiles is shown in Fig. 5.13.

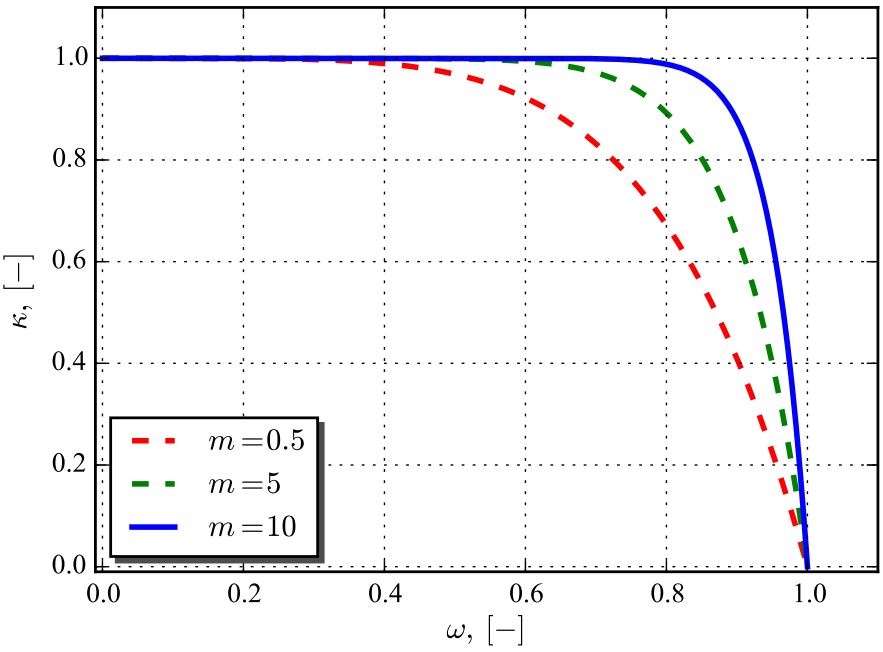

Figure 5.12: Stiffness degradation function κ with respect to the continuous damage parameter ω

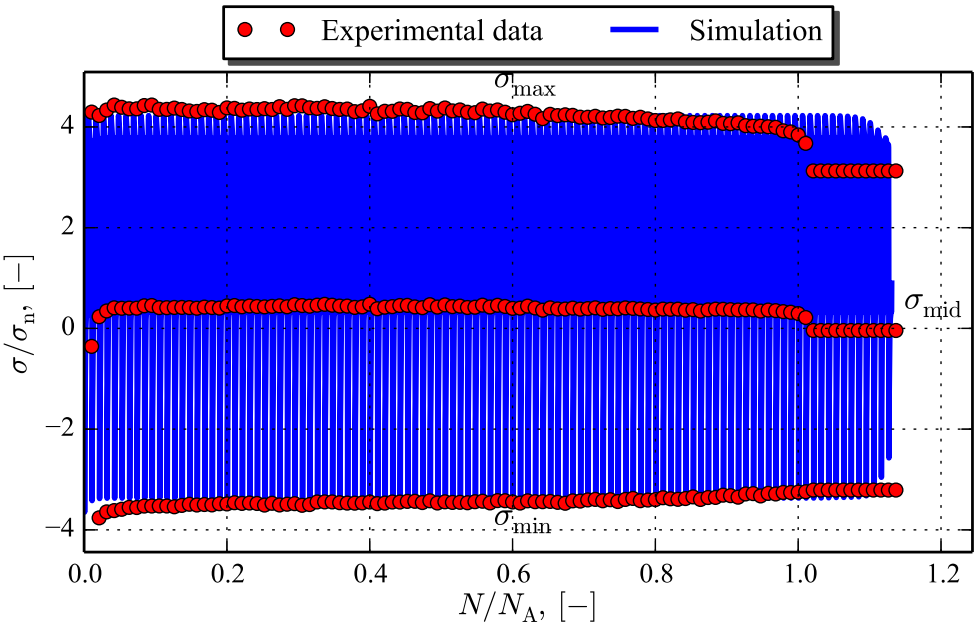

Figure 5.13: Simulated stress response in TMF test (WaTd4)

5.9 Summary

The current chapter is focused on the secondary identification of the constitutive model for the GJV cast iron. The identification is based on the conjugate-directional minimization approach proposed by [71]. The error functional consists of the parts computed for the different kinds on the experimental data. The secondary identification approach allows us to use the experimental data with complicated thermal and mechanical loading profiles, when the decomposition of the problem onto subproblems is not possible and complete system of constitutive equations must be integrated.

Within the framework of target material of current research, the unified constitutive model for large range of the loads is identified. The model is calibrated for simulation of the slow and fast inelastic material behavior (creep, plasticity), strain hardening effects and estimation of the lifetime of the material, which is normally a part of the risk analysis in the mechanical engineering. In particular, the lifetime analysis is based on the continuous creep-fatigue damage model, which can take into account the arbitrary loading regimes.

CHAPTER

6 Verification

Within the framework of the current chapter, several approaches are considered for the verification of the determined constitutive model. The starting point is the verification of the constitutive model for the inelastic material behavior. The mentioned stage of the verification includes the simulation of the inelastic behavior of the GJV material performed for the loading conditions corresponding to the creep tests, tensile tests, LCF tests, and TMF tests. The verification of the creep-fatigue damage model is based on the experimental data, which were not used within the identification procedures. In addition, the simplified form of the constitutive model derived for the uniaxial loading case is used. Finally, the equivalent measures introduced in the work are compared with the components of the stress and strain tensors corresponding to the uniaxial loading case.

6.1 Inelastic material behavior

The verification of the constitutive model is mainly performed by means of the direct integration the constitutive equations for the corresponding loading conditions. The verification of the constitutive model for the inelastic material behavior is based of the simulation of the material response under thermo-mechanical loads. The values of stress at the initial and steady loading cycles are used for the comparison of model prediction with the experimental data. It must be noted, that within the verification the experimental data from TMF tests, which were not used in the identification of the constitutive model, are utilized. The mentioned above set of the experimental data and prediction of

the model are shown in Fig. 6.1.

The comparison of the experimental and simulated stresses is performed for the first loading cycle $N = 1$ and for the cycle corresponding to the half of lifetime of the specimen. The stress response on the first loading cycle in the material corresponds to the non-saturated state of the material. The comparison of the results with the above-mentioned data allows us to check the accuracy of the constitutive model at the transient loading regimes, which are mainly governed by the tendency of the backstress value to saturate into some steady cycle. The simulation of the thermo-mechanical loads until the reaching of the steady cyclic stress response allows us to compare the obtained results with experimental data for $N = N_A/2$, and to verify the constitutive model for stabilized cycles. In practice, the current constitutive model exhibits the stabilization at the cycles $N = 3..6$. Therefore, the simulation up to the half of the lifetime of the material is not necessary.

The computed error functions used within the secondary identification step are shown in Fig. 6.2a and Fig. 6.2b. These functions were obtained by the substitution of the experimental and simulated values of stress into the specific error function (5.3). As presented in figure, the constitutive model exhibits the highest disagreement with the experimental values of stresses for the temperatures $T < 0.359 T_m$, that mainly related to the underestimation of the inelastic strain rates. The major reason for the inconsistency of the simulation with experiments within the current case is related to the low temperatures, and, therefore, to the presence of the rate-independent material behavior in the experiments, which, unfortunately, is described by the constitutive model with lower accuracy. However, the accuracy of the simulation within the mentioned regimes is still sufficient and comparable with the accuracy of TMF tests. In addition, the weight functions can be managed in order to compensate the disagreement of the constitutive model for mentioned range of the operation conditions.

In order to verify the constitutive model for the isothermal cyclic loads, the behavior of the material under the LCF loads was simulated. The simulations were performed for the highest strain amplitudes of the available experimental data at the temperatures $0.253 T_m$, $0.359 T_m$, $0.413 T_m$, $0.519 T_m$ and $0.573 T_m$. The quality assurance of the constitutive model within the current part of the verification is performed by the comparison of simulated stresses with the experimental values. The resulting and experimental hysteresis loops for the different testing temperatures are shown in Fig. 6.4. According to the presented results of simulations, the best correlation of the constitutive model with experimental data is reached for the temperatures

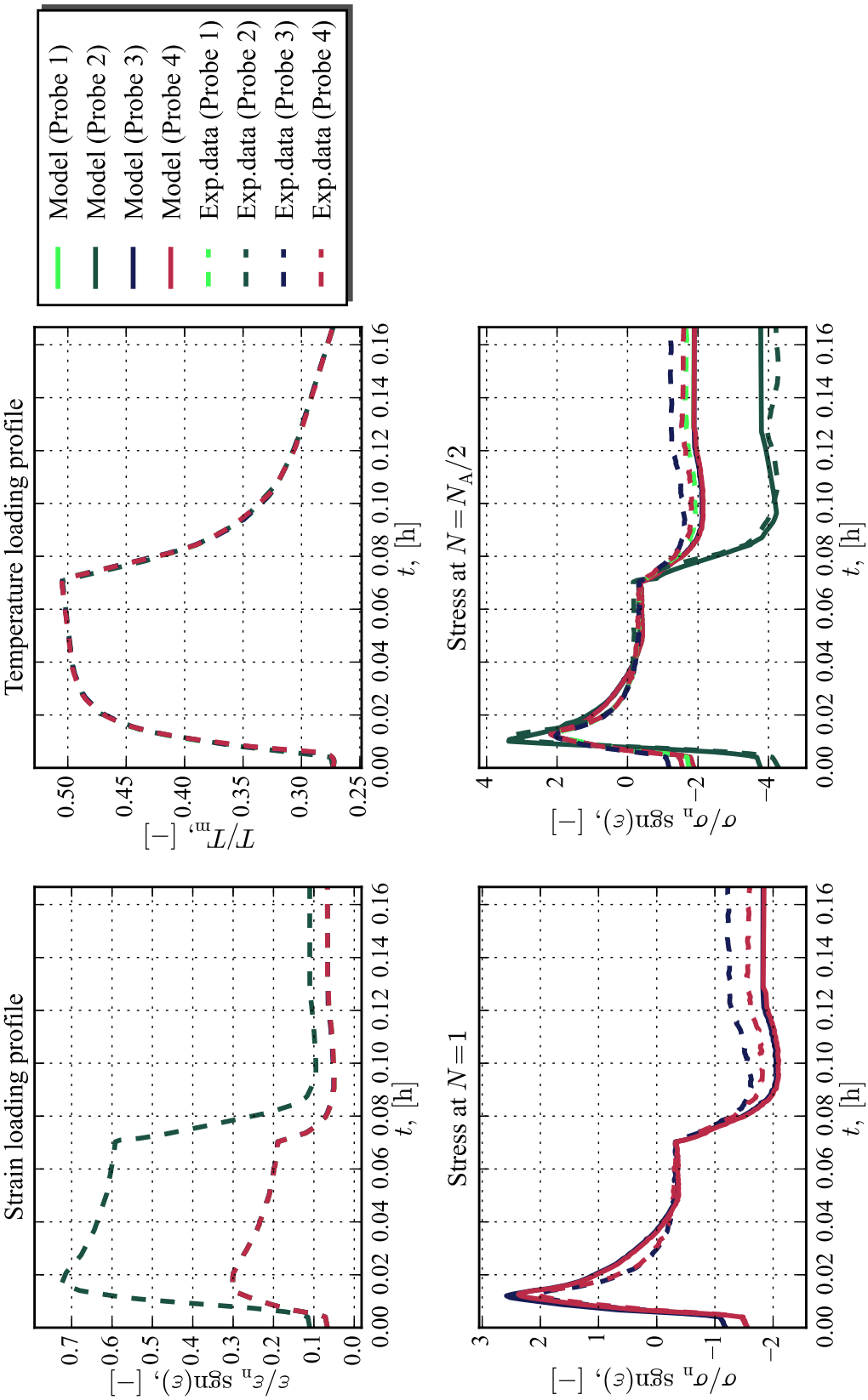

Figure 6.1: Simulation of the material behavior under thermo-mechanical loads

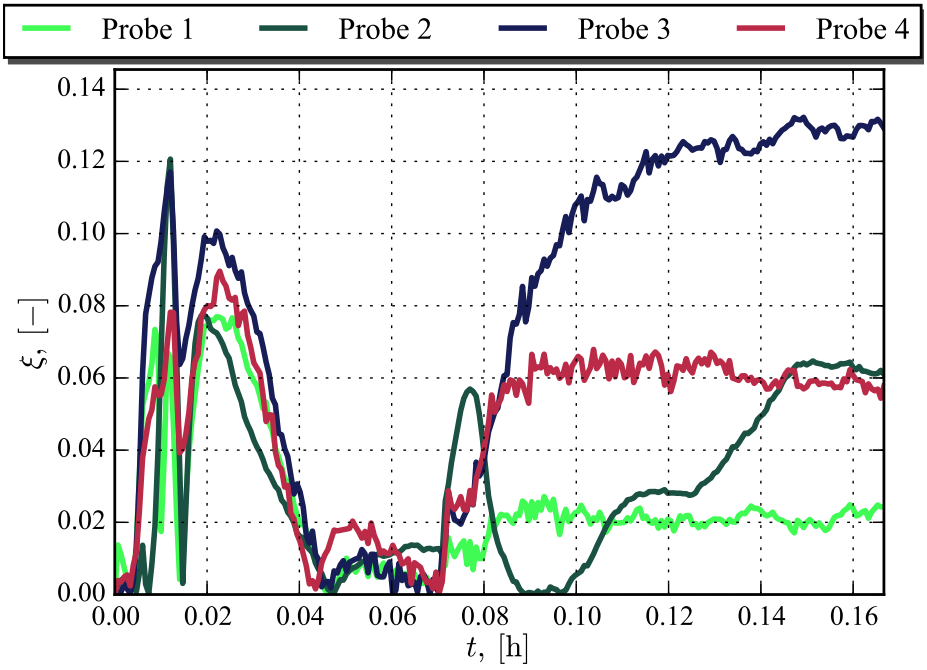

(a)

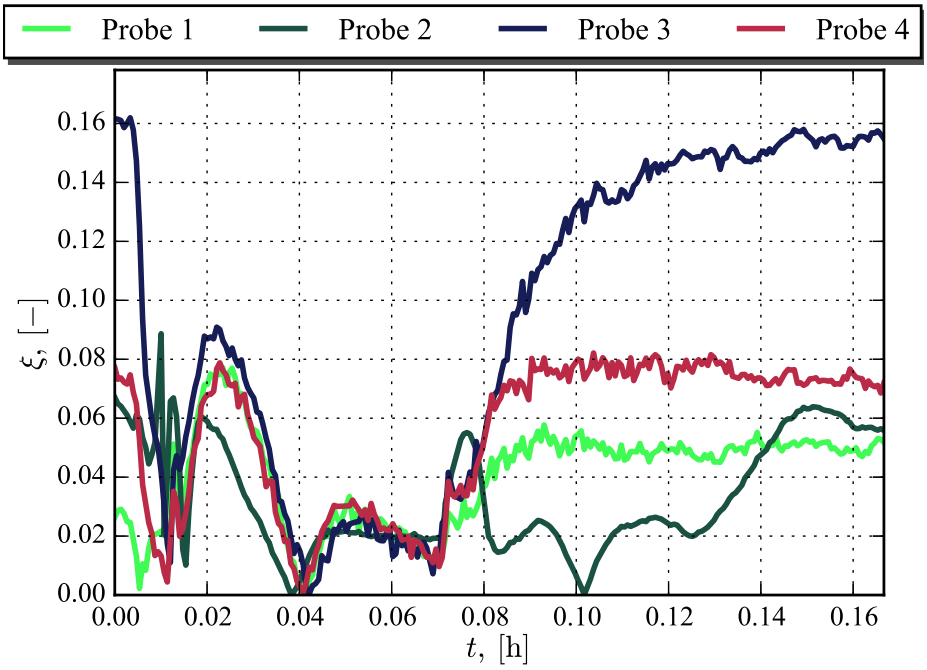

(b)

Figure 6.2: The error of the simulation of TMF test: **(a)** stress response at $N = 1$, **(b)** stress response at $N = N_A/2$

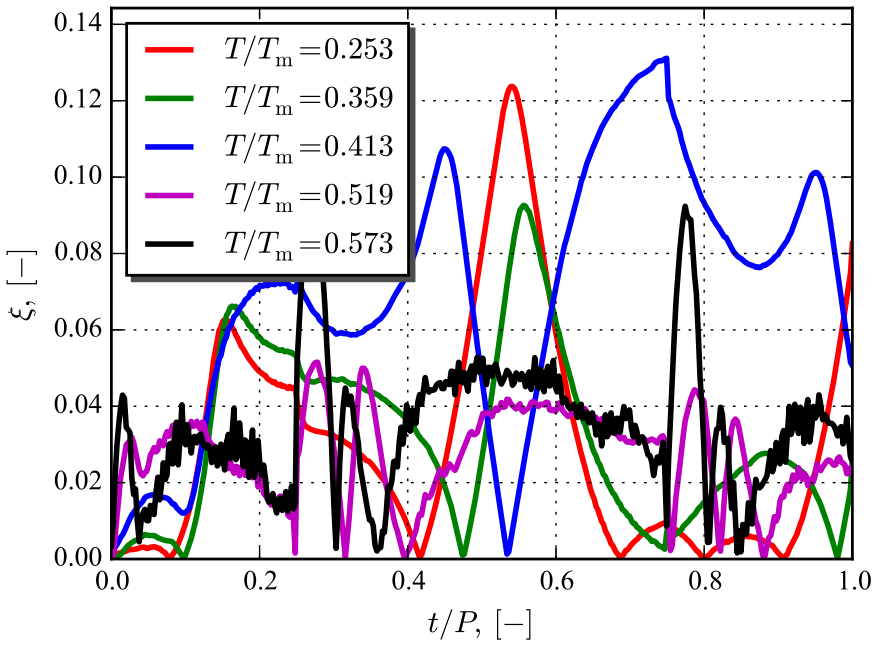

Figure 6.3: The error of the simulation of LCF tests (time axis is normalized by cycle periods P)

$0.253T_\mathrm{m}$, $0.359T_\mathrm{m}$, $0.519T_\mathrm{m}$ and $0.573T_\mathrm{m}$. However, the accuracy of stresses at temperature $0.413T_\mathrm{m}$ is lower.

The error values for the above-mentioned data evaluated according to (5.3) are shown in Fig. 6.3. The highest error values correspond to the simulation of the LCF test at temperature $0.413T_\mathrm{m}$. However, the maximal disagreement of the constitutive model with the experimental data is about 14%, that comparable with the assumed accuracy of the experimental data.

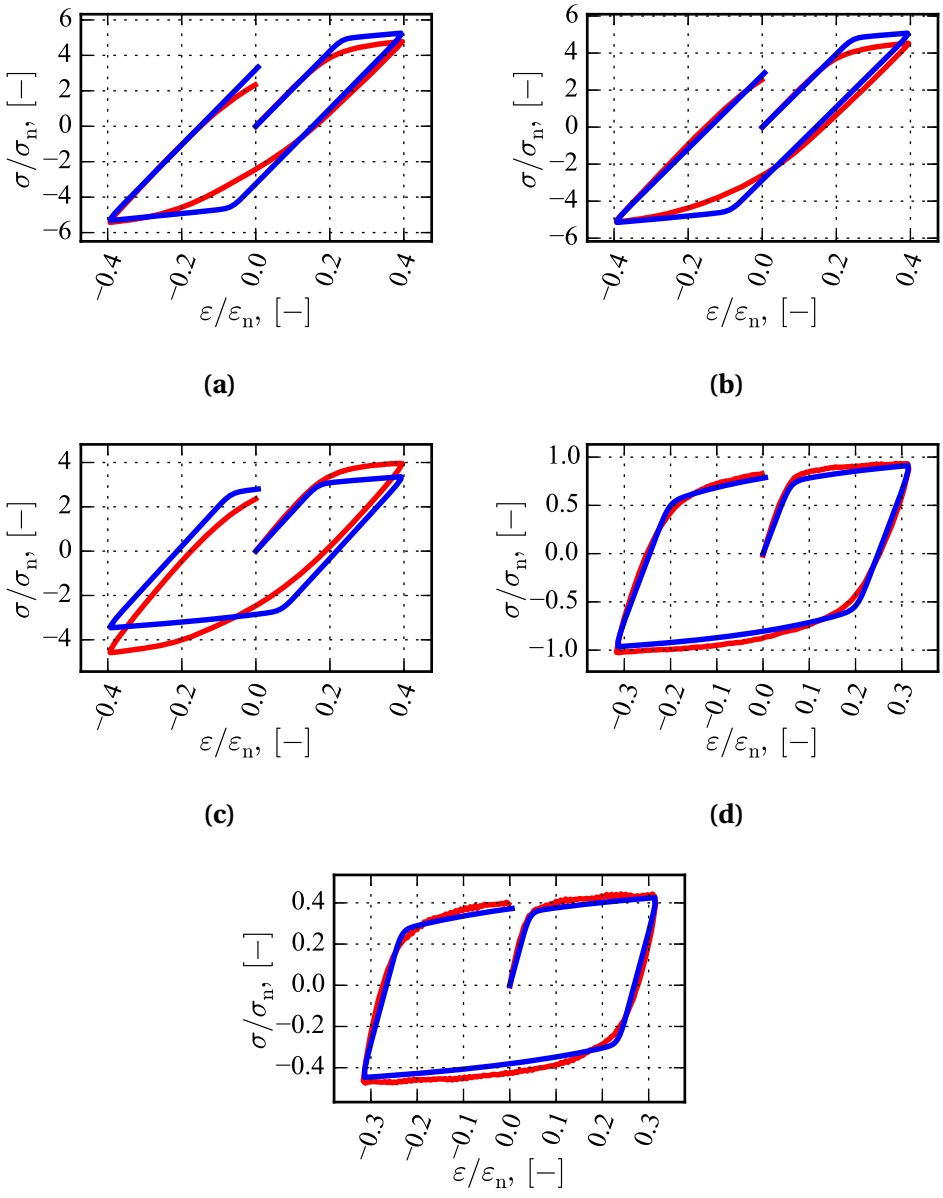

Figure 6.4: Simulation results of LCF tests at the different loading conditions (– experimental data, – prediction by model): **(a)** $T = 0.253\,T_\mathrm{m}$, $\varepsilon_\mathrm{A} = 0.79\varepsilon_\mathrm{n}$; **(b)** $T = 0.359\,T_\mathrm{m}$, $\varepsilon_\mathrm{A} = 0.79\varepsilon_\mathrm{n}$; **(c)** $T = 0.413\,T_\mathrm{m}$, $\varepsilon_\mathrm{A} = 0.79\varepsilon_\mathrm{n}$; **(d)** $T = 0.519\,T_\mathrm{m}$, $\varepsilon_\mathrm{A} = 0.632\varepsilon_\mathrm{n}$; **(e)** $T = 0.573\,T_\mathrm{m}$, $\varepsilon_\mathrm{A} = 0.632\varepsilon_\mathrm{n}$

6.2 Creep-fatigue damage

The verification of the creep-fatigue damage model is based on the complete integration of the constitutive equations until the rupture of the material. The rupture of sample is assumed if the damage variable ω reaches the value 0.97. Within the framework of the verification of the creep-fatigue damage model the experimental data from TMF and LCF tests are utilized. However, the experiments, which were not used within the identification, are essential within the verification procedures. Within the current part of the verification, the accuracy of the identified constitutive model is checked by the comparison of the experimental and estimated lifetime of the specimen.

According to Fig. 6.5 the identified constitutive model for creep-fatigue damage, which is developed within the frame of the current work, is able to predict the lifetime of GJV cast iron subjected to the thermo-mechanical loads with accuracy of factor 2. Taking into account that the current model is mainly focused on the prediction of the number of cycles to rupture for the interval $1.039N^* < N < 10.395N^*$, the accuracy of the constitutive model is sufficient within the framework of the requirements of the current research.

6.3 Accuracy of extrapolation

The extrapolation approach was used within the secondary identification step. Before the application of the approach, its accuracy was checked. This is accomplished by the comparison of the predicted lifetime of the material obtained by the extrapolation and after complete integration of the constitutive equation until the rupture state is reached. Obviously, the same vector of the material parameters was used within the extrapolation and the direct approach. However, the verification of the extrapolation approach presented within the framework of the current section is performed based on the resulting vector of the material parameters. The simulations are performed for the LCF and TMF loading profiles and shown in Fig. 6.6. The error of the extrapolation is computed by means of the following expression:

$$\xi = 1 - \frac{N_{\mathrm{A}}^{\mathrm{extr}}}{N_{\mathrm{A}}^{\mathrm{int}}},$$

where $N_{\mathrm{A}}^{\mathrm{extr}}$ is the extrapolated number of cycles to rupture, $N_{\mathrm{A}}^{\mathrm{int}}$ is the integrated one. The expression above allows us to compute the deviation of the extrapolated results with respect to the direct integration-based method, taking into account the sign of the deviation.

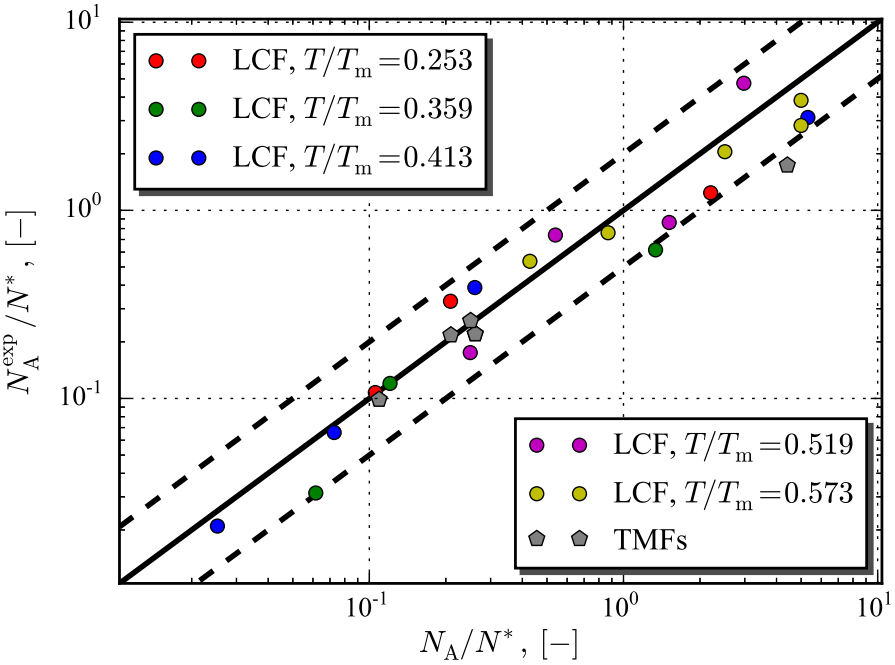

Figure 6.5: Verification of creep-fatigue damage model

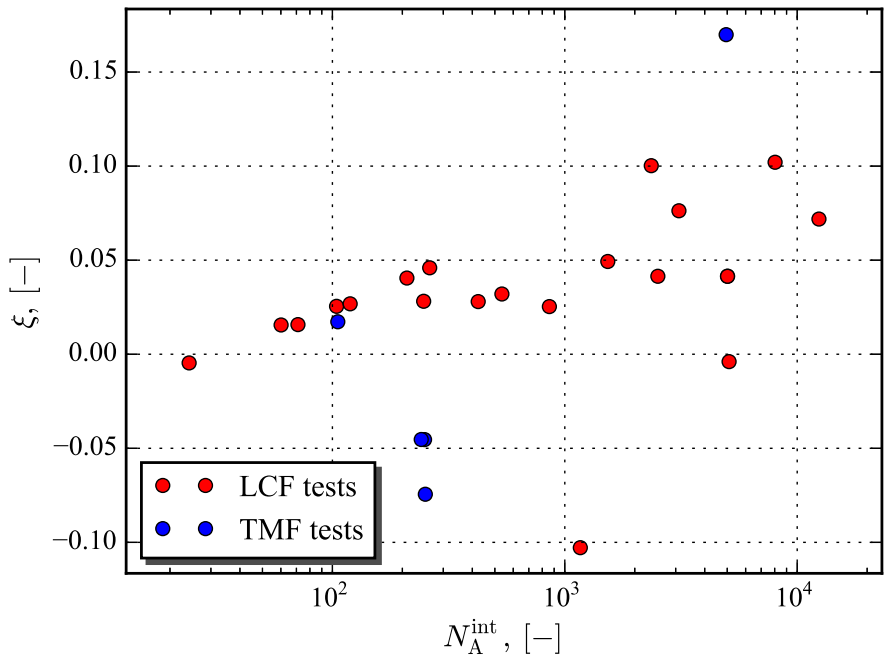

Figure 6.6: Verification of extrapolation approach

Tests	Testing conditions	N_A^{int}	N_A^{extr}	ξ
LCF tests ($\dot{\varepsilon} = 3.6\,h^{-1}$)	T =0.253T_m, ε_A =0.474ε_n	2.448N^*	2.203N^*	0.10023
	T =0.253T_m, ε_A =0.632ε_n	0.217N^*	0.208N^*	0.0405
	T =0.253T_m, ε_A =0.79ε_n	0.108N^*	0.105N^*	0.02547
	T =0.359T_m, ε_A =0.474ε_n	1.212N^*	1.337N^*	−0.10283
	T =0.359T_m, ε_A =0.632ε_n	0.124N^*	0.121N^*	0.02679
	T =0.359T_m, ε_A =0.79ε_n	$6.236\cdot10^{-2}N^*$	$6.133\cdot10^{-2}N^*$	0.01555
	T =0.413T_m, ε_A =0.316ε_n	5.293N^*	5.314N^*	−0.00393
	T =0.413T_m, ε_A =0.474ε_n	0.272N^*	0.26N^*	0.04594
	T =0.413T_m, ε_A =0.79ε_n	$7.379\cdot10^{-2}N^*$	$7.172\cdot10^{-2}N^*$	0.01575
	T =0.413T_m, ε_A =1.186ε_n	$2.493\cdot10^{-2}N^*$	$2.493\cdot10^{-2}N^*$	−0.00462
	T =0.519T_m, ε_A =0.158ε_n	8.35N^*	7.498N^*	0.10205
	T =0.519T_m, ε_A =0.238ε_n	3.22N^*	2.974N^*	0.07626
	T =0.519T_m, ε_A =0.316ε_n	1.591N^*	1.512N^*	0.0493
	T =0.519T_m, ε_A =0.474ε_n	0.557N^*	0.539N^*	0.03202
	T =0.519T_m, ε_A =0.632ε_n	0.256N^*	0.249N^*	0.02815
	T =0.573T_m, ε_A =0.158ε_n	12.894N^*	11.967N^*	0.07186
	T =0.573T_m, ε_A =0.238ε_n	5.212N^*	4.996N^*	0.04144
	T =0.573T_m, ε_A =0.316ε_n	2.613N^*	2.505N^*	0.04144
	T =0.573T_m, ε_A =0.474ε_n	0.892N^*	0.869N^*	0.02533
	T =0.573T_m, ε_A =0.632ε_n	0.44N^*	0.428N^*	0.02798
TMF tests	Probe 1	0.261N^*	0.28N^*	−0.07443
	Probe 2	5.141N^*	4.268N^*	0.16987
	Probe 3	0.259N^*	0.27N^*	−0.04538
	Probe 4	0.251N^*	0.262N^*	−0.04533
	Probe 5	0.109N^*	0.107N^*	0.01725

Table 6.1: Verification of the extrapolation approach

In general, the extrapolation of the number of cycles to the rupture exhibits the trend to underestimate the lifetime predicted by the complete integration of the constitutive model. Within the the interval $N \in (10^2, 10^4)$, where the rupture is assumed to be induced by the low-cycle fatigue damage. The extrapolation exhibits an underestimation of the lifetime of approx $4-5\%$, which is low if the general accuracy of the constitutive model is taken into account.

The detailed results of the verification of the extrapolation approach are given in Table 6.1. As mentioned above, a major number of the results exhibits the underestimation of $4-5\%$. However, there are exceptional cases of the loads, when the error of the extrapolation is higher. The general growing tendency of the extrapolation error allows us to conclude that the accuracy of the estimation in the interval belonging to the high-cycle fatigue may not be sufficient and, therefore, the above-mentioned extrapolation approach in this

case can not be used in the current formulation. However, within the framework of the constitutive modeling of the low-cycle fatigue of cast irons, the accuracy of the extrapolation is sufficient.

6.4 Verification of the equivalent values

The application of the constitutive model within the industrial-oriented simulations requires the three-dimensional formulation of the constitutive model. Therefore, the constitutive model formulated in terms of scalars must be verified for the general three-dimensional cases of the mechanical loads. For that purpose, the three-dimensional problem of the rod deformation is solved. The loading profiles used in the simulation are corresponding to TMF test (Probe 1).

The representative values, which must be verified within the constitutive model, are the equivalent von Mises stress σ_{vM}, the equivalent von Mises plastic strain $\varepsilon^{\mathrm{p}}_{\mathrm{vM}}$, and the equivalent mechanical strain $\varepsilon_{\mathrm{eq}}$. The resulting equivalent von Mises stress and equivalent plastic strain are shown in Fig. 6.7a and in Fig. 6.7b, respectively. The equivalent values exhibit a good correlation with the scalar variables used in the formulation of the constitutive model for the uniaxial stress state.

The equivalent strains, computed according to (4.26), are shown in Fig. 6.7c. They exhibit a good correlation of the uniaxial strain values used in the simplified constitutive model for the uniaxial loading cases and the equivalent strain values used by the complete constitutive model utilized in the general formulation, respectively.

6.5 Summary

The current chapter is focused on the verification of the identified constitutive model. The verification includes the check of the constitutive model for the inelastic material behavior, the prediction of the lifetime of the material and the check of the equivalent values used in the model.

The part of the constitutive model focused on the description of the inelastic behavior of the GJV cast iron is verified based on the experimental data of TMF tests (Sect. 6.1), which were not used in the identification of the constitutive model. The response in stresses are used as the representative measures for the estimation of the quality of the identification. The maximum deviation of simulation results compared to experimental data is obtained for

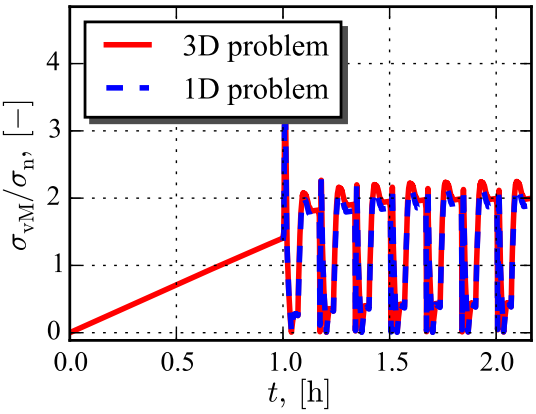

(a)

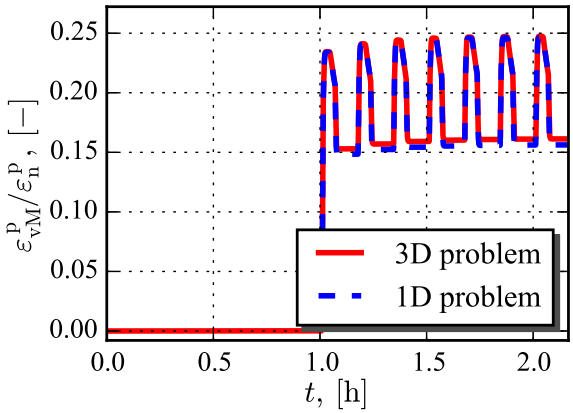

(b)

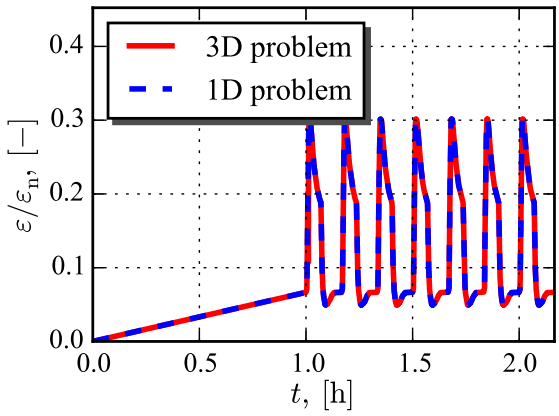

(c)

Figure 6.7: Verification of equivalent values used in three-dimensional formulation of the constitutive model: **(a)** equivalent von Mises stress σ_{vM}, **(b)** equivalent von Mises inelastic strain $\varepsilon^{\mathrm{p}}_{\mathrm{vM}}$, **(c)** equivalent mechanical strain $\varepsilon_{\mathrm{eq}}$

the low-temperature regimes. The peak value of the error is 16%. This disagreement is comparable with the scatter of the results in the different TMF tests under similar loading conditions.

The part of the constitutive model describing the creep-fatigue damage is verified by the comparison of the estimated lifetime of the material with the experimental one for similar loading conditions (Sect. 6.2). The verification includes experimental data from LCF and TMF tests. Mainly, the constitutive model for the creep-fatigue damage satisfies the accuracy requirements for the range of the cycles to rupture $10^2 < N_\mathrm{A} < 10^4$ corresponding to low-cycle fatigue damage within the GJV material, and allows us to estimate the lifetime of the material with accuracy factor of 2.

The accuracy of the extrapolation approach used in the identification of the creep-fatigue damage model is checked through the comparison of the estimated number of cycles to rupture obtained by the complete integration of the constitutive equations with the extrapolated results (Sect. 6.3). Mainly, the developed extrapolation approach within the range of low-cycle fatigue exhibits an underestimation of the lifetime of $4-5\%$. Taking into account general accuracy of the material's lifetime prediction, the obtained accuracy of the extrapolation is sufficient not only for the identification of the constitutive model, but also for the application in the industrial-oriented simulations.

In order to check the correspondence of the uniaxial and the three-dimensional formulations of the constitutive model and to check its realization in program code, the equivalent values of stress σ_vM, strain ε_eq and inelastic strain $\varepsilon^\mathrm{p}_\mathrm{vM}$ are compared with the scalars utilized in the uniaxial model (Sect. 6.4). The obtained results indicate that the constitutive model is correctly utilized inside the finite element code.

In general, the identified constitutive model exhibits the sufficient quality in the description of the inelastic behavior and in the estimation of the lifetime of the GJV cast iron.

CHAPTER

7 Conclusions

7.1 Summary

Within the current work, the step-by-step identification approach for the formulation of constitutive models for cast irons was developed. The identified constitutive model includes the elastic and inelastic material behavior, creep damage, fatigue damage and creep-fatigue damage interaction. One of the ideas followed within the work was to split the general identification problem into sub-problems of less dimensions, which were solved by means of simple and representative identification approaches and simplify the identification of advanced constitutive models for mechanical engineers.

Before the identification problem, continuum mechanics relations were discussed (Chapt. 2). According to the target class of materials, infinitesimal strains were assumed. The strain tensor takes into account three parts including the elastic, thermal and inelastic contributions into the deformation process. The elastic part within the framework of current materials was assumed to be physically linear for the undamaged state. The increase of damage above 0.9 leads to strong nonlinearity of elastic material properties. In order to describe the contribution of the thermal expansion, the linear isotropic constitutive relation for thermal strains was used. The constitutive model used for the inelastic behavior of the material is based on Odqvist flow rule [50, 60]. The kinematic hardening is introduced by model of Frederick and Armstrong [19] and implemented by means of active stress principle [39, 50]. The creep damage is included into the material model according to Kachanov-Rabotnov effective square principle [25, 75]. In order to predict the lifetime of the material during cyclic loading, the continuum fatigue damage model was considered

and the non-linear creep-fatigue damage rule was introduced. In general, the formulation of the sketch for the constitutive model includes the postulated material-independent part and material-dependent functions requiring further identification procedures.

Within Chapt. 3 the identification problem was presented in a generalized way and in particular form for target class of cast irons. Within this chapter the useful identification approaches were introduced. Additionally, the set of experimental data for GJV cast iron was presented.

The complete identification problem has been split into the primary (see Chapt. 4) and secondary identification stages (see Chapt. 5). The primary step is focused on the determination of the material-dependent functions of the constitutive model and the preliminary estimation of the vector of material parameters. This identification step requires experimental data which may show the natural processes taking place in the material in explicit form. However, the approach is not completely limited by the abovementioned requirement because in some cases the processing and recalculation of the experimental data with respect to the determined part of the constitutive model allows us to obtain the evaluated experimental values for the implicit processes, i.e. hardening, damage, etc. In particular, the primary identification step includes the following items:

1) The identification of the function for Young's modulus according to available experimental data.
   Within the framework of current works, the elastic material properties were given by the discreet values of Young's modulus with respect to temperature. The influence of the damage at this stage was neglected.

2) The identification of the inelastic behavior of the material.
   Within the current step of identification, the concept of the initial and steady inelastic strain rates was introduced. The identification of the initial and steady inelastic strain rates utilized the experimental data from the primary and secondary stages of creep curves and tensile tests. The measurement scheme for representative values of the inelastic strain rates were introduced. The response functions of stress and temperature were determined within the current step of the identification.

3) The identification of the hardening saturation and hardening rate functions.
   The identified functions for initial and steady inelastic strain rates allow us to determine the hardening saturation function β_* analytically.

The hardening rate function μ_h was determined by means of the decomposition of the experimental data from the creep tests according to the identified functions for the initial and steady inelastic strain rates and hardening saturation function. In addition, the semi-analytical approach for the identification of the hardening saturation and hardening rate for the specific loading conditions was developed.

4) The identification of the creep damage function.
The procedure used the experimental value of the inelastic strains at the rupture moment. The identification is focused on the determination of the inelastic rupture strain function ε_p^* with respect to temperature and stress loads.

5) The identification of the structure and guess of the material parameters for the fatigue damage evolution equation.
The primary identification was based on the idealized isothermal cycle with saw-type kinematic loads. The fatigue damage evolution law was integrated for the single loading cycle and the increment of the fatigue damage was obtained.

6) The creep-fatigue damage interaction model was described.
The introduced function was proposed in order to represent by the constitutive model the damaging processes taking place at the slow creep-like regimes and fast cyclic loads.

Finally, the primary identification step gave the complete constitutive model of the material including the elastic, inelastic and damage properties. The application of the constitutive model at the current stage of development was limited only on the loads observed in the creep tests and LCF tests. The application of the constitutive model for the simulation of the thermo-mechanical behavior of the material is not recommended.

The secondary identification step was developed in order to include the experimental data into the identification process, which were no used in the primary identification. This data are mainly belong to TMF tests. The secondary identification step was based on the numerical optimization approach. In particular, the following features and mechanisms were developed within the secondary identification step:

1) The introduced weight functions allows us to involve into the identification additional features to the constitutive model, i.e. restrictions in the loading ranges, assurance of the experimental data, major regimes of the loads in design, etc.

2) The enchanted extrapolation algorithm was developed in order to reduce the computation cost during the simulation of the lifetime of the material at certain loads.

3) The developed optimization-based identification algorithm includes the facilities for the multiprocessing during the computation of the error functional ξ, which significantly increases efficiency of the algorithm.

4) The different forms of error functions were considered. The estimated errors of the experimental data were taken into account.

5) The facility of the transformation of the restricted optimization problem into an unrestricted optimization problem was considered.

The constitutive model obtained after the secondary identification step can be used for a range of the loading conditions, which was assigned by the weights functions and available experimental data. It must be mentioned, that the secondary identification is a time-consuming. However, the contribution of the "hand work" within the current step is significantly lower then in the primary identification step, and the major consumption of the approach is due to the machinery time. For instance, in case of GJV cast iron, whose complete constitutive model has 20 parameters, the comparison of the time-consumption of the secondary identification step to the primary step is about 3/2.

The work is finalized by the verification procedures (see Chapt. 6), that is necessary for the estimation of the quality of the obtained constitutive model. The verification includes the following steps:

1) Verification of the extrapolation approach used within the secondary identification.

2) Simulation of the TMF tests which were not used within the identification.

   a) Verification of the constitutive model for the inelastic material behavior. The simulation of the stress response during TMF loading cycle and comparing with the experimentally observed stresses.

   b) Verification of the creep-fatigue damage model. The numerical estimation of the time to the rupture and its comparison with the experimentally measured lifetime of specimen are performed.

3) Verification of the equivalents used in the formulation of the constitutive model for the three-dimensional loading case.

7.2 Restrictions

The developed identification algorithm is valid for the materials which exhibit the linear the elastic material properties, work at small deformations, and, do not represent the significant softening behavior. The flow rule introduced in the constitutive model is sufficient for description of the isotropic creep behavior and includes Kachanov-Rabotnov type of creep damage. The creep and fatigue damage models proposed within the current work are valid for the estimation of the isotropic creep-fatigue damage in the material.

It must be mentioned, that the identification scheme do not require the significant modification in case of the extension of the constitutive model for the anisotropic elasticity.

7.3 Outlook

The further development of the presented identification technique can be continued in different directions. The structure of the research is shown in Fig. 7.1.

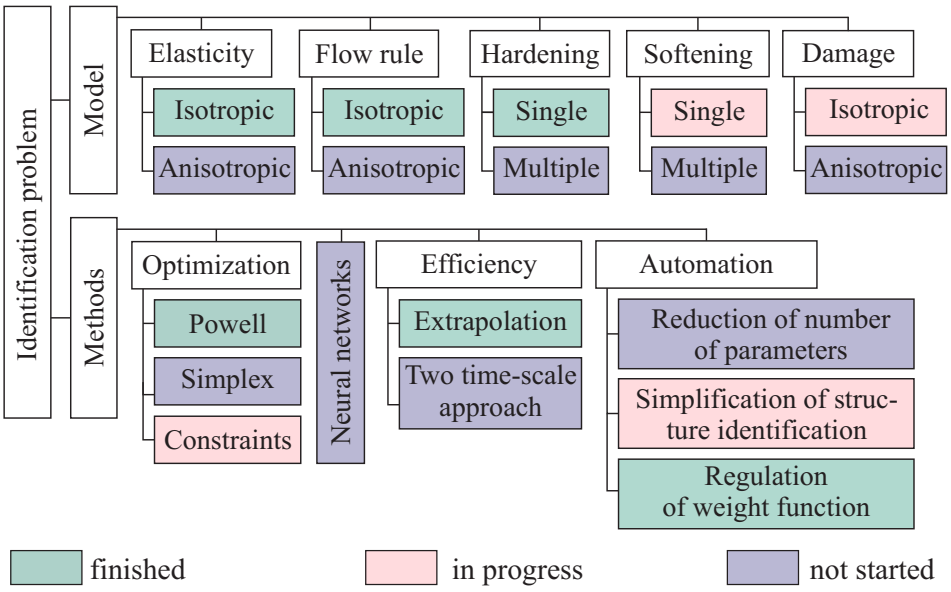

Figure 7.1: Research scheme of the identification problem

As presented in Fig. 7.1, the research includes two main parts belonging to the phenomenological structure of the constitutive model and methodology utilized within the identification problem. The structure of the constitutive model identified in the current work is restricted for a limited num-

ber of cases. The changes in the structure of the constitutive model can lead to the necessity to modify the primary identification scheme. For example, the elastic properties are formulated as temperature-dependent functions and affected by the damage on the final stage of cycling before the failure. The consideration of the anisotropic elasticity in this case requires the additional development of the primary identification step. The inelastic flow rule is formulated for the isotropic creep and switching to the anisotropic creep model requires to consider a modified inelastic flow rule [50]. The changes of the phenomenological structure of the constitutive model (e.g. including of anisotropic creep-fatigue damage model, including multiple hardening functions, introduction of the softening mechanisms) necessarily leads to the need to change the primary identification step, and, therefore, requires to development of corresponding identification strategy.

The application of the optimization-based identification is time-consuming and, despite the flexibility, is not completely suitable for the identification of the constitutive model for the fatigue damage. Therefore, the perspective directions of the development of the approach is the replacement of the conjugate-directional Powell's method [72] by the Simplex method [53], or even the complete replacing of an optimization by a neural network [88]. Besides the mentioned facilities, the enchanted extrapolation scheme may be replaced by two time-scales approach [15], whose application in the estimation of the lifetime of the material supposedly leads to a $5-50$ times decrease of the computational time.

Finally, the simplification of the identification scheme for the use and its realization in software with a unified user interface is one of the perspective directions of current research. The simple, fast and convenient automation of the developed identification strategy is an actual problem, whose solution is attractive and useful for industrial mechanical engineers.

Bibliography

[1] M. Abdel-Karim and N. Ohno. Kinematic hardening model suitable for ratchetting with steady-state. *International Journal of Plasticity*, 16(3): 225 – 240, 2000.

[2] J. Aktaa and B. Schinke. The influence of the hardening state on time dependent damage and its consideration in a unified damage model. *Fatigue and Fracture of Engineering Materials*, 19(9):1143 – 1151, 1996.

[3] J. Aktaa and R. Schmitt. Creep fatigue lifetime prediction rules for ferritic martensitic steels. Technical report, Forschungszentrum Karlsruhe, FZKA 6931, Karlsruhe, 2004.

[4] H. Altenbach. *Kontinuumsmechanik: Einführung in die materialunabhängigen und materialabhängigen Gleichungen*. Springer, Heidelberg, 2012.

[5] A.L. Araujo, M. Soares, and M.J. de Freitas. Characterization of material parameters of composite plate specimens using optimization and experimental vibrational data. *Composites Part B: Engineering*, 27(2):185–191, 1996.

[6] S. Bargmann and M. Ekh. Microscopic temperature field prediction during adiabatic loading using gradient extended crystal plasticity. *International Journal of Solids and Structures*, 50(6):899 – 906, 2013.

[7] J.F. Besseling and E. van der Giessen. *Mathematical Modelling of Inelastic Deformation*. Chapman & Hall, London, 1994.

[8] J. Betten. *Creep Mechanics*. Springer, Berlin, 2005.

[9] E.W. Billington. The Poynting-Swift effect in relation to initial and post-yield deformation. *International Journal of Solids and Structures*, 21(4): 355 – 372, 1985.

[10] J.T. Boyle and J. Spence. *Stress Analysis for Creep*. Butterworth, London, 1983.

[11] R.H. Byrd, P. Lu, J. Nocedal, and C. Zhu. A limited memory algorithm for bound constrained optimization. *SIAM Journal on Scientific Computing*, 16(5):1190–1208, 1995.

[12] J.-L. Chaboche. Continuum damage mechanics: Part I - general concepts. *Journal of Applied Mechanics, Transactions ASME*, 55:59 – 64, 1988.

[13] B.M. Chaparro, S. Thuillier, L.F. Menezes, P.-Y. Manach, and J.V. Fernandes. Material parameters identification: Gradient-based, genetic and hybrid optimization algorithms. *Computational Materials Science*, 44(2): 339 – 346, 2008.

[14] J.E. Dennis and R.B. Schnabel. *Numerical Methods for Unconstrained Optimization and Nonlinear Equations*. Prentice Hall, Eaglewood Cliffs, New Jersey, 1983.

[15] A. Devulder, D. Aubry, and G. Puel. Two-time scale fatigue modelling: application to damage. *Computational Mechanics*, 45(6):637 – 646, 2010.

[16] P. Eickhoff. *System Identification - Parameter and System Estimation*. Wiley, New York, 1974.

[17] J.D. Embury and D.J. Lloyd. On the Bailey-Orowan for steady state creep. *Scripta Metallurgica*, 3(11):821 – 825, 1969.

[18] H.E. Evans. Mechanisms of creep fracture. *Elsevier Applied Science Publishers Ltd.*, pages 319–319, 1984.

[19] C.O. Frederick and P.J. Armstrong. A mathematical representation of the multiaxial Bauschinger effect. *Materials at High Temperatures*, 24(1):1 – 26, 2007.

[20] F. Garofalo. *Fundamentals of Creep and Creep-Rupture in Metals*. Mc Millan, New York, 1965.

[21] C.-S. Han, H. Gao, Y. Huang, and W.D. Nix. Mechanism-based strain gradient crystal plasticity. *Journal of the Mechanics and Physics of Solids*, 53 (5):1204 – 1222, 2005.

[22] S. Haykin. *Neural Networks: a Comprehensive Foundation*. Mc Millan, New Jersey, 1994.

[23] N. Huber. Anwendung neuronaler Netze bei nichtlinearen Problemen der Mechanik. *Wissenschaftliche BerichteForschungszentrum*, 2000.

[24] J.A. Hult. *Creep in Engineering Structures*. Blaisdell Publishing Company, Waltham, 1966.

[25] L.M. Kachanov. O vremeni razrusheniya v usloviyakh polzuchesti (on the time to rupture under creep conditions, (in Russ.). *Izv. AN SSSR. Otd. Tekh. Nauk. Mekhanika i mashinostroenie*, 8:26 – 31, 1958.

[26] L.M. Kachanov. *Introduction to Continuum Damage Mechanics*. Martinus Nijhoff, Dordrecht, 1986.

[27] M.E. Kassner and M.T. Pérez-Prado. *Fundamentals of Creep in Metals and Alloys*. Elsevier, Amsterdam, 2004.

[28] H. Kraus. *Creep Analysis*. John Wiley & Sons, New York, 1980.

[29] F. Laengler, T. Mao, H. Aleksanoglu, and A. Scholz. Phenomenological lifetime assessment for turbine housings of turbochargers. In *Proceedings of 9th International Conference on Multiaxial Fatigue & Fracture, 7th-9th June, 2010, Parma, Italy*, pages 283 – 291, Parma, 2010. (CD-ROM).

[30] J. Lemaitre. *A Course on Damage Mechanics*. Springer, Berlin, 1992.

[31] J. Lemaitre and J.-L. Chaboche. *Mechanics of Solid Materials*. Cambridge University Press, Cambridge, 1990.

[32] J. Lemaitre and R. Desmorat. *Engineering Damage Mechanics: Ductile, Creep, Fatigue and Brittle Failures*. Springer, Berlin, 2005.

[33] J. Lubliner. *Plasticity Theory*. Courier Dover Publications, 2008.

[34] A.I. Lurie. *Nonlinear Theory of Elasticity*. North-Holland, Dordrecht, 1990.

[35] A.I. Lurie. *Theory of Elasticity*. Foundation of Engineering Mechanics. Springer, Berlin, 2005.

[36] R. Mahnken. Identification of material parameters for constitutive equations. *Encyclopedia of Computational Mechanics*, pages 637 – 656, 2004.

[37] N.N. Malinin. *Prikladnaya teoriya plastichnosti i polzuchesti (Applied theory of plasticity and creep, in Russ.)*. Mashinostroenie, Moskva, 1975.

[38] N.N. Malinin. *Raschet na polzuchest' konstrukcionnykh elementov (Creep calculations of structural elements, inRuss.)*. Mashinostroenie, Moskva, 1981.

[39] N.N. Malinin and G.M. Khadjinsky. K postroeniyu teorii polzuchesti s anizotropnym uprochneniem (on the formulation of a creep theory with anisotropic hardening, in Russ.). *Izv. AN SSSR. Mekhanika tverdogo tela*, 3:148 – 152, 1969.

[40] N.N. Malinin and G.M. Khadjinsky. Theory of creep with anisotropic hardening. *International Journal of Mechanical Sciences*, 14:235 – 246, 1972.

[41] S.S. Manson. Interfaces between fatigue, creep, and fracture. *International Journal of Fracture Mechanics*, 2(1):327–327, 1966.

[42] W.S. McCulloch and W. Pitts. A logical calculus of the ideas immanent in nervous activity. *The Bulletin of Mathematical Biophysics*, 5(4):115 – 133, 1943.

[43] E. Melan and H. Parkus. *Wärmespannungen infolge stationärer Temperaturfelder*. Springer, Wien, 1953.

[44] C. Miehe, M. Hofacker, and F. Welschinger. A phase field model for rate-independent crack propagation: Robust algorithmic implementation based on operator splits. *Computer Methods in Applied Mechanics and Engineering*, 199(45):2765 – 2778, 2010.

[45] M.A. Miner. Cumulative damage in fatigue. *Journal of Applied Mechanics*, 12(3):159 – 164, 1945.

[46] S. Murakami. *Continuum Damage Mechanics: A Continuum Mechanics Approach to the Analysis of Damage and Fracture*. Solid Mechanics and Its Applications. Springer, Dordrecht, 2012.

[47] S. Murakami and N. Ohno. A continuum theory of creep and creep damage. In *Creep in structures*, pages 422–444. Springer, 1981.

[48] M. Nagode, F. Längler, and M. Hack. Damage operator based lifetime calculation under thermo-mechanical fatigue for application on ni-resist d-5s turbine housing of turbocharger. *Engineering Failure Analysis*, 18(6): 1565 – 1575, 2011.

[49] M. Nagode, F. Längler, and M. Hack. A time-dependent damage operator approach to thermo-mechanical fatigue of ni-resist d-5s. *International Journal of Fatigue*, 33(5):692 – 699, 2011.

[50] K. Naumenko and H. Altenbach. *Modelling of Creep for Structural Analysis*. Springer, Berlin et al., 2007.

[51] K. Naumenko, H. Altenbach, and A. Kutschke. A combined model for hardening, softening and damage processes in advanced heat resistant steels at elevated temperature. *International Journal of Damage Mechanics*, 20:578 – 597, 2011.

[52] K. Naumenko, A. Kutschke, Y. Kostenko, and Th. Rudolf. Multi-axial thermo-mechanical analysis of power plant components from 9-12%Cr steels at high temperature. *Engineering Fracture Mechanics*, 78:1657 – 1668, 2011.

[53] J.A. Nelder and R. Mead. A simplex method for function minimization. *The Computer Journal*, 7(4):308–313, 1965.

[54] R.W. Neu and H. Sehitoglu. Thermomechanical fatigue, oxidation, and creep: Part II. Life prediction. *Metallurgical and Materials Transactions A*, 20(9):1769 – 1783, 1989.

[55] F.H. Norton. *The creep of steel at high temperatures*. McGraw-Hill Book Company, Inc., New York, 1929.

[56] J.P. Norton. *An Introduction to Identification*. Academic Press, London, 1986.

[57] J.P. Norton. *An Introduction to Identification*. Courier Dover Publications, 2009.

[58] F.K.G. Odqvist. Applicability of the elastic analogue to creep problems of plates, membranes and beams. In N.J. Hoff, editor, *Creep in Structures*, pages 137 – 160. Springer, Berlin, 1962.

[59] F.K.G. Odqvist. *Mathematical Theory of Creep and Creep Rupture*. Oxford University Press, Oxford, 1974.

[60] F.K.G. Odqvist and J. Hult. *Kriechfestigkeit metallischer Werkstoffe*. Springer, Berlin, 1962.

[61] S.O. Ojediran and O. Ajaja. The Bailey-Orowan equation. *Journal of Materials Science*, 23(11):4037–4040, 1988.

[62] M.H.J. Paas. *Continuum damage mechanics with an application to fatigue*. PhD thesis, Technische Universität Einbhoven, Eindhoven, 1990.

[63] A. Palmgren. Die lebensdauer von kugellagern. *Zeitschrift des Vereins Deutscher Ingenieure*, 68(14):339 – 341, 1924.

[64] V.A. Palmov. *Fundamental Laws of Nature (in Russ.)*. Publishing House of Polytechnic University, Saint Petersburg, 2008.

[65] V.A. Palmov. *Elements of Tensor Algebra and Tensor Analysis (in Russ.)*. Publishing House of Polytechnic University, Saint Petersburg, 2008.

[66] K.M. Pedersen and N.S. Tiedje. Graphite nodule count and size distribution in thin-walled ductile cast iron. *Materials Characterization*, 59(8): 1111 – 1121, 2008.

[67] R.H.J. Peerlings, W.A.M. Brekelmans, R. de Borst, and M.G.D. Geers. Gradient-enhanced damage modelling of high-cycle fatigue. *International Journal for Numerical Methods In Engineering*, 49:1547 – 1569, 2000.

[68] I.J. Perrin and D.R. Hayhurst. Creep constitutive equations for a 0.5Cr-0.5Mo-0.25V ferritic steel in the temperature range 600-675°C. *The Journal of Strain Analysis for Engineering Design*, 31(4):299 – 314, 1994.

[69] I.J. Perrin and D.R. Hayhurst. Continuum damage mechanics analyses of type iv creep failure in ferritic steel crossweld specimens. *International Journal of Pressure Vessels and Piping*, 76(9):599 – 617, 1999.

[70] M.J.D. Powell. An efficient method for finding the minimum of a function of several variables without calculating derivatives. *The Computer Journal*, 7(2):155 – 162, 1964.

[71] M.J.D. Powell. A view of algorithms for optimization without derivatives. *Mathematics Today-Bulletin of the Institute of Mathematics and its Applications*, 43(5):170–174, 2007.

[72] P.C. Powell. *Engineering with Fiber-reinforced Laminates*. Chapman & Hall, London, 1994.

[73] L. Prandtl. Ein Gedankenmodell zur kinetischen Theorie der festen Körper. *ZAMM-Journal of Applied Mathematics and Mechanics/Zeitschrift für Angewandte Mathematik und Mechanik*, 8(2):85 – 106, 1928.

[74] W.H. Press, B.P. Flannery, S.A. Teukolsky, and W.T. Vetterling. *Numerical recipes*. Cambridge university press Cambridge, Hong Kong, 1990.

[75] Y.N. Rabotnov. O mechanizme dlitel'nogo razrusheniya (a mechanism of the long term fracture, in Russ.). *Voprosy prochnosti materialov i konstruktsii, AN SSSR*, pages 5 – 7, 1959.

[76] Y.N. Rabotnov. *Creep Problems in Structural Members*. North-Holland, Amsterdam, 1969.

[77] E. Robinson. Effect of temperature variation on the long-time rupture strength of steels. *Transactions ASME*, 74(5):777 – 781, 1952.

[78] H. Sehitoglu. Thermo-mechanical fatigue life prediction methods. *Advances in Fatigue Lifetime Predictive Techniques, ASTM STP*, 1122:47 – 76, 1992.

[79] J. Skrzypek and A. Ganczarski. *Modelling of Material Damage and Failure of Structures*. Foundation of Engineering Mechanics. Springer, Berlin, 1998.

[80] C. Sommitsch, R. Sievert, T. Wlanis, B. Günther, and V. Wieser. Modelling of creep-fatigue in containers during aluminium and copper extrusion. *Computational Materials Science*, 39:55 – 64, 2007.

[81] S. Straub. *Verformungsverhalten und Mikrostruktur warmfester martensitischer 12%-Chromstähle*. PhD thesis, Universität Erlangen-Nürnberg, Fortschr.-Ber. VDI Reihe 5, Nr. 405, Düsseldorf, 1995.

[82] B. Svendsen and S. Bargmann. On the continuum thermodynamic rate variational formulation of models for extended crystal plasticity at large deformation. *Journal of the Mechanics and Physics of Solids*, 58(9):1253 – 1271, 2010.

[83] C.A. Truesdell and W. Noll. *Handbuch der Physik*. Springer, 1965.

[84] R. von Mises. Mechanik der plastischen Formänderung von Kristallen. *ZAMM*, 8(3):161 – 185, 1928.

[85] K. Wiencek, T. Skowronek, and B. Khatemi. Graphite particle size distribution in nodular cast iron. *Metallurgy and Foundry Engineering*, 31: 167–173, 2005.

[86] M.H. Wright. Direct search methods: Once scorned, now respectable. *Pitman Research Notes in Mathematics Series*, pages 191–208, 1996.

[87] S.J. Wright and J. Nocedal. *Numerical Optimization*, volume 2. Springer, New York, 1999.

[88] S. Yoshimura, A. Matsuda, and G. Yagawa. New regularization by transformation for neural network based inverse analyses and its application to structure identification. *International Journal for Numerical Methods in Engineering*, 39(23):3953 – 3968, 1996.

[89] C. Zhu, R.H. Byrd, P. Lu, and J. Nocedal. Algorithm 778: L-BFGS-B: Fortran subroutines for large-scale bound-constrained optimization. *ACM Transactions on Mathematical Software (TOMS)*, 23(4):550–560, 1997.

[90] W.Z. Zhuang and N.S. Swansson. Thermo-mechanical fatigue life prediction: A critical review. Technical report, DTIC Document, 1998.

Curriculum vitae

Personal data

Name, Surname:	Ievdokymov, Mykola
Date of Birth:	10 September 1985
Place of Birth:	Izvarino
Marital status:	married
Nationality:	ukrainian

School

1992-1999	School, Krasnodon
1999-2003	School, Ordzhonikidze

Study

2003-2007	Bachelor of Science in Mechanics, National Technical University "Kharkiv Polytechnic Institute", Kharkiv, Ukraine
2007-2009	Master of Science in Mechanics, National Technical University "Kharkiv Polytechnic Institute", Kharkiv, Ukraine
2009-2011	PhD Student in Technical Mechanics Department Martin-Luther University, Halle(Saale), Germany
2011-2015	PhD Student in Technical Mechanics Department Otto-von-Guericke University, Magdeburg, Germany

Magdeburg, May 11, 2015 Mykola Ievdokymov

Personal publications

[1] M. Ievdokymov, H. Altenbach, and V.A. Eremeyev. On the impact on a plate made of hyperelastic foam. In *Proceedings of the 3rd International Conference on Nonlinear Dynamics*, pages 236 – 241, Kharkov, 2010.

[2] M. Ievdokymov, H. Altenbach, and V.A. Eremeyev. Collapse criteria of foam cells under various loading. In *Proceedings in Applied Mathematics and Mechanics*, volume 11, pages 365 – 366, Graz, 2011.

[3] M. Ievdokymov, V.A. Eremeyev, and H. Altenbach. Modeling of packaging behavior in closed-cell aluminum foam. *PAMM*, 14(1):241 – 242, 2014.

[4] F. Längler, K. Naumenko, H. Altenbach, and M. Ievdokymov. A unified constitutive model for the thermo-mechanical fatigue analysis of turbochargers. In *CanCNSM 2013. - Montre'al, insges. 6 S.Kongress: CanCNSM*, Montre'al, Canada, 2013.

[5] F. Längler, K. Naumenko, H. Altenbach, and M. Ievdokymov. A constitutive model for inelastic behavior of casting materials under thermo-mechanical loading. *The Journal of Strain Analysis for Engineering Design*, page 0309324714522034, 2014.